TAMPEREEN TEKNILLINEN YLIOPISTO
TAMPERE UNIVERSITY OF TECHNOLOGY

SAMULI KOSTAMO

CONFIGURATOR TOOL FOR THE PRELIMINARY DESIGN OF AN ELECTROSTATIC PRECIPITATOR CASING

Master of Science thesis

Examiner: Assoc. Prof. Sami Pajunen
Examiner and topic approved by the Faculty Council of the Faculty of Engineering Sciences on 04.01.2017

ABSTRACT

SAMULI KOSTAMO: Configurator tool for the preliminary design of an electrostatic precipitator casing.
Tampere University of technology
Master of Science Thesis, 92 pages, 4 Appendix pages
January 2017
Master's Degree Programme in Mechanical Engineering
Major: Machine Design and Product Development
Examiner: Associate Professor Sami Pajunen

Keywords: Configurator, finite-element-method, stiffness method, limit state design, Eurocode, Electrostatic precipitator

In this thesis, we develop an easy-to-use configurator tool for an electrostatic precipitator (ESP) casing structure. Since the emergence of computers, numerous design software applications have been developed to aid with design calculations and to automate the design process. The software used for structural design usually focuses on either of the following: Estimating the structure's response to loading via some numerical method and then comparing the internal loading to load limits provided by standards. Determining the loading conditions present based on location data and standards. Applications capable of both estimating the loading and then evaluating the structure's response are rare and usually very product-specific.

The loading acting on the ESP casing structure was analyzed via the approaches provided in the Eurocodes. These approaches were addressed on such level, that their intricacy meets the requirements of preliminary design phase. A mathematical model of the structure was formulated to suit the selected platform with its complexness and this model was further developed to a finite element model to evaluate the structure's response to loading via stiffness matrix approach. The mathematical tools for solving the linear systems, such as Cholesky and LU -decompositions, were addressed to provide an overview of the configurator tool's solving algorithm and it was found, both theoretically and in practice, that Cholesky factorization is drastically more efficient than direct inverse when solving sets of linear equations.

The project resulted in a configurator tool for the ESP casing primary support structures, capable of evaluating casing's loading conditions without excessive knowledge requirements from the user. The tool analyzes the structure's response to loading and either selects required profiles based on maximum allowed utility ratio or checks the structure's durability with user-provided profile selections. The tool utilizes finite element method based on beam elements, solves the set of linear equations efficiently and analyzes the utility of the structure based on the requirements set by Eurocodes. The dimensioning results were extensively benchmarked against commercial software with only minute deviation. Additionally, the selections made by the configurator were compared to those made by a structural engineer by looking at old projects. The selections proved to be very similar even when the tool was used with limited knowledge of the design rationale behind the existing products and thus the approach and execution was proven effective.

TIIVISTELMÄ

SAMULI KOSTAMO: Konfiguraattorityökalu sähkösuodattimen kammion alustavaan suunnitteluun.
Tampereen teknillinen yliopisto
Diplomityö, 92 sivua, 4 liitesivua
Tammikuu 2017
Konetekniikan Diplomi-Insinöörin koulutusohjelma
Pääaine: Koneensuunnittelu ja tuotekehitys
Tarkastaja: Associate Professor Sami Pajunen

Avainsanat: Konfiguraattori, elementtimenetelmä, jäykkyysmenetelmä, rajatilamitoitus, Eurokoodi, sähkösuodatin

Tämä diplomityö keskittyy kehittämään helppokäyttöistä konfiguraattoria sähkösuodattimen kammion suunnitteluun. Erilaisia ohjelmistotyökaluja suunnittelun avuksi ja sen automatisointiin on kehitetty läpi modernin tietotekniikan historian. Rakennesuunnittelussa käytettävät ohjelmat keskittyvät yleensä toiseen kahdesta ongelmasta: Rakenteen kuormitusvasteen ratkaiseminen jonkin numeerisen menetelmän avulla, ja rakenteen sisäisten kuormien vertaaminen standardista saataviin suunnittelukuormien rajoihin. Rakenteeseen kohdistuvan kuormitustilan arviointi standardin asettamien ohjeiden avulla. Sovellukset, jotka kykenevät sekä arvioimaan rakenteen kuormituksen, että rakenteen vasteen tälle kuormitukselle ovat yleensä harvinaisia ja tuotekohtaisia.

Sähkösuodattimen rakenteeseen kohdistuvat kuormat arvioidaan Eurokoodien esittämillä menetelmillä niin, että kuormien esitystarkkuus on alustavaan suunnitteluun sopivalla tasolla. Rakenteen analysointia varten luodaan matemaattinen malli, joka on monimutkaisuudeltaan käytettävälle ohjelmisto-alustalle sopiva. Tästä mallista kehitetään jäykkyysmenetelmään perustuva palkkielementtimalli rakenteen sisäisten kuormien selvittämistä varten. Elementtimenetelmään liittyvien lineaaristen yhtälöryhmien ratkaisemiseksi sovelletaan LU-hajotelmaa ja sen erityismuotoa Choleskyn hajotelmaa. Choleskyn hajotelma osoittautuu sekä teoriassa, että käytännössä merkittävästi inverssiä tehokkaammaksi tavaksi ratkaista lineaarinen yhtälöryhmä.

Diplomityöprojektin tuloksena syntyy konfiguraattorityökalu sähkösuodattimen kammion kannatinrakenteen suunnittelun tueksi. Työkalu kykenee arvioimaan rakenteeseen kohdistuvat kuormat asettamatta kuitenkaan liiallisia osaamisvaatimuksia käyttäjälle. Työkalu arvioi rakenteen vasteen tälle kuormitukselle ja joko valitsee sopivat kannatinprofiilit tai tarkistaa käyttäjän tekemät profiilivalinnat. Työkalu hyödyntää elementtimenetelmää ratkaisten yhtälöryhmän tehokkaasti ja arvioi rakenteen osien kestävyyden Eurokoodissa määriteltyjen rajojen perusteella. Elementtiratkaisijaa vertaillaan kaupallisiin työkaluihin ja huomataan tulosten poikkeavan toisistaan vain merkityksettömän vähän. Työkalun tekemiä valintoja vertaillaan olemassa oleviin rakenteisiin ja siten valintoihin, jotka on tehnyt rakennesuunnittelija. Työkalun tekemät valinnat osoittautuvat hyvin samanlaisiksi siitä huolimatta, että laskenta suoritetaan puutteellisilla tiedoilla alkuperäisessä suunnittelussa käytetyistä lähtötiedoista. Tarkastelun nojalla voidaan todeta, että valittu laskentamenetelmä tuottaa käytännössä hyviä tuloksia, jotka vastaavat hyvin sekä kaupallisia ohjelmistoja, että vanhoja projekteja.

PREFACE

As the author of this thesis I would like to thank Valmet Technologies for providing me an interesting task exceeding my original skill level and therefore allowing me to develop myself within this project. Secondly, I would like to thank Kari Pehkonen, the owner and facilitator of this thesis project for his strive for continuous improvement and development ultimately resulting in the assignment for this thesis. Thirdly I would like to thank Sami Pajunen for his aid in making this thesis represent the pinnacle of my academic studies. Last but not least, I would like to thank my beloved wife Annika, for supporting me throughout this entire project and tirelessly believing in me even when I doubted myself the most.

Samuli Kostamo

Tampere, February 2017

CONTENTS

1. INTRODUCTION 1
2. ELECTROSTATIC PRECIPITATOR 3
2.1 General operating principle 3
2.2 Structure and design scope 4
3. THEORETICAL BACKGROUND 8
3.1 Statically indeterminate structures 8
3.1.1 Mathematical model 11
3.1.2 Finite element model 12
3.1.3 Constraints and error 17
3.2 Linear systems 20
4. CALCULATION 26
4.1 Limit state design 26
4.1.1 Serviceability and ultimate limit states 26
4.1.2 Cross-section classification 29
4.1.3 Definition of load limits 33
4.1.4 Multiaxial loading 37
4.2 Load types 39
4.2.1 Temperature 39
4.2.2 Self-weight 41
4.2.3 Wind load 42
4.2.4 Snow load 49
4.2.5 Seismic load 50
4.2.6 Live load 54
4.2.7 Imperfection load 55
5. DIMENSIONING TOOL 57
5.1 Configurators in general 57
5.2 Tool functionality 58
5.2.1 Geometry generation 59
5.2.2 Cross-section properties 62
5.2.3 Loading 63
5.2.4 Calculation options 67
5.2.5 FEM-Solver 69
5.2.6 Solver algorithm 70
5.2.7 Results 71
5.3 Algorithms 74
5.4 Validation and verification 78
5.4.1 Finite element model accuracy 78
5.4.2 Result consistency 83
5.4.3 Solve time 85
6. CONCLUSIONS 87

7. DISCUSSION AND FUTURE WORK....88
8. REFERENCES....91
APPENDIX A – CHOLESKY DECOMPOSITION ALGORITHM IN VISUAL BASIC FOR APPLICATIONS (VBA) 94
APPENDIX B – THE LINEAR SUBSTITUTION ALGORITHM IN VISUAL BASIC FOR APPLICATIONS (VBA) 95
APPENDIX C: DETAILS ABOUT THE FEM BENCHMARKING....96
APPENDIX D – MAXIMUM ERROR OF INTERNAL LOAD VALUES COMPARED TO RESPECTIVE RESISTANCE VALUE....97

LIST OF SYMBOLS AND ABBREVIATIONS

A hierarchy of bolded letters is used in this thesis to distinguish scalars, vectors and matrices without the need of indexing notation. Matrices and vectors are represented with bolded variables such as $\boldsymbol{v}$ and $\boldsymbol{V}$.

$a_{ij}^{<1>}$	Matrix element changed by a row operation.
$\overline{\lambda}_w$	Modified web slenderness.
h_w	Beam web height.
χ_w	Contribution of the web to shear resistance.
A_{Ed}	Design value of seismic load.
A_e	Element cross section area.
A_{eff}	Effective area. Used with CSC 4 beams to account for reduced load bearing capacity due to local buckling.
A_{ref}	Reference area.
A_{tot}	Total cross-section area.
A_v	Shear area of a cross-section. Estimation of the cross-section area capable of carrying shear load.
E_d	Effect of loading.
E_e	Elastic modulus. If presented with a subscript, the subscript is used to distinguish element specific values from each other.
F_{fr}	Frictional wind load resultant.
$F_{w,e}$	External wind pressure resultant
$F_{w,i}$	Internal wind pressure resultant.
G_k	Characteristic value of permanent load.
G_{kinf}	Upper limit of permanent load.
G_{ksup}	Lower limit of permanent load.
H_i	Horizontal sway imperfection load.
I_e	Second moment of area (moment of inertia of plane area). An attribute of a planar cross-section used to reflect how its points are distributed with regard to axis n in element e.
I_v	Wind turbulence intensity
$M_{N,Rd}$	Resistance for bending reduced for excessive axial load.
M_{Rd}	Design resistance for bending moment.
$M_{b,Rd}$	Design resistance for buckling.
$M_{c,Rd}$	Bending moment design resistance in compression.
$M_{c,el,Rd}$	Elastic design resistance for bending.
$M_{c,pl,Rd}$	Plastic design resistance for bending.
M_e	Elastic moment. Bending moment required for yield limit to be exceeded.
M_p	Plastic moment. Bending moment required for ultimate limit to be exceeded.
N_{Ed}	Design value for axial load.
N_{Rd}	Design resistance for axial load.
N_{cr}	The critical buckling load.
Q_k	Characteristic value of variable load.
T_1	The first vibration mode of a structure.

T_B, T_C, T_D	The attribute values used for defining the response spectra (type 1 and type 2)
T_s	System temperature
V_{Ed}	Design value for shear load.
V_{Rd}	Design resistance for shear load.
$V_{bf,Rd}$	Design value for flange shear-buckling resistance.
$V_{bw,Rd}$	Design value for web shear-buckling resistance.
$V_{el,Rd}$	Design value for elastic shear resistance.
$V_{pl,Rd}$	Design value for plastic shear resistance.
W_{eff}	Effective section modulus. See A_{eff}
W_{el}	Elastic section modulus of a cross-section.
W_{pl}	Plastic section modulus of a cross-section.
a_g	Horizontal ground acceleration. See PGA.
a_{gv}	Vertical ground acceleration. See PGA
a_{ij}, u_{ij}, l_{ij}	Elements of the decomposition matrices.
b_s	Cross section width.
c_{dir}	Directional coefficient. Used to account for directional deviation in wind speeds. Suggested value 1.
c_{se}	Snow load exposure coefficient
c_e	Wind exposure coefficient.
c_{esl}	Accidental snow load coefficient, rec. value 2.
$c_{pe,1}$	External wind pressure coefficient for areas smaller or equal to 1 m^2
$c_{pe,10}$	External wind pressure coefficient for areas larger or equal to 10 m^2
c_{pe}	External pressure coefficient.
$c_r(z)$	Terrain roughness coefficient at a height z above ground.
$c_s c_d$	Structural factor that takes into account the non-simultaneous occurrence of peak winds on the surfaces c_s and the effect of structure vibration due to turbulence c_d.
c_{season}	Coefficient to account for seasonal deviation in wind speeds. Suggested value 1.
$f_{i,i}$	Global force vector component, indexes are used to distinguish different DOFs and nodes from each other.
$f_{in\,n}$	Element internal load acting towards the nth degree of freedom.
f_n	Force acting towards the nth degree of freedom.
$f_{p,T}$	Proportional limit in elevated temperature
f_p	Proportional limit
$f_{y,T}$	Yield strength in elevated temperature
f_y	Effective yield strength.
$f_{y4,T}$	Yield strength in elevated temperature for welded or hot rolled section of section class 4
f_{yr}	Yield limit reduced for excessive shear load.
$k_{11}..k_{66}$	6-DOF beam element's stiffness matrix's components.
k_r	Terrain factor.
l_e	Element length.
m_c	The number of columns in a row.
q_b	Basic wind velocity pressure.
q_n	Displacement towards the nth degree of freedom.

q_p	Peak velocity pressure. Includes both the basic velocity pressure q_b and the turbulence intensity I_v.
r_s	Radius between the section parts; flange and web.
s_k	Characteristic value of snow load at given location.
t_f	Beam flange thickness.
t_w	Beam web thickness.
$v_{b,0}$	Fundamental basic wind velocity.
v_b	Basic wind velocity.
$v_m(z)$	Mean wind velocity at a height z above ground.
w_1	Element of the vector **w.**
x_1, x_2, y_1, y_2	Element node coordinates.
z_0	The obstacle length value. Used when calculating terrain roughness coefficient.
z_e	Reference height for wind loading.
z_{max}	Limit of structure height for Eurocode; 200 m.
z_{min}	Minimum height value.
$\boldsymbol{A}^{(k)}$	Intermediate product matrix of LU-decomposition.
$\boldsymbol{F_G}$	Global force vector.
$\boldsymbol{K_G}$	Global stiffness matrix.
$\hat{\boldsymbol{L}}$	Lower triangular matrix before reorientation.
$\boldsymbol{L}_1$	First intermediate result of a sequential decomposition algorithm.
$\boldsymbol{L}_k$	kth intermediate result of a sequential decomposition algorithm.
$\boldsymbol{Q_G}$	Global displacement vector.
$\boldsymbol{e}_1^T$	Unit vector.
$\boldsymbol{f_{e,ext}}$	Element external node loads.
$\boldsymbol{f_e}$	Element force vector.
$\boldsymbol{k_e}$	Element local stiffness matrix.
$\boldsymbol{k_{rot}}$	Rotated local stiffness matrix.
$\boldsymbol{q_e}$	Element local displacement vector.
$\boldsymbol{r_e}$	Orientation matrix to rotate local coordinate system based matrices to global coordinates and back.
Ψ_0	Combination factor.
Ψ_1	Frequent representation factor.
Ψ_2	Quasi-permanent representation factor.
α_h	The reduction factor for height for sway imperfections.
α_{flange}	Factor describing the loading state of the flange.
α_{web}	Factor describing the loading state of the web.
γ_{M0}	The safety factor for cross-section durability regardless of the CSC.
γ_{M1}	The safety factor for member stability.
γ_{M2}	The safety factor for resistance against tension fracture.
γ_{Sd}	Partial safety factor for uncertainty of loads and effects.
γ_g	Partial safety factor for permanent actions.
$\overline{\lambda}$	Non-dimensional slenderness.
μ_i	Snow load shape factor.
ρ_w	Air density.
A	Accidental action.
CSC	Cross-section class of a beam member. Describes the members susceptibility for local buckling.
ESP	Electrostatic precipitator.

FEM	Finite element method.
FLOP	Floating point operation. Used to measure required computational resources.
G	Permanent action.
LFA	Lateral force analysis. Method for analyzing seismic loading.
LU-decomposition	Division of a matrix A to upper triangular and lower triangular matrix.
PGA	Peak ground acceleration. The acceleration caused by seismic action.
Q	Variable action.
SFS	Suomen Standardisoimisliitto, Finnish Standards Association.
ΔL	Change in length.
DOF	Degree of freedom.
L	Length, general.
NA	National Annex. Area dependent additions or alterations of the Eurocode.
S	Soil factor.
a	Geometric factor used for reducing bending resistance for excessive axial load.
c	Effective are of a flange.
d	Round section diameter.
l	Directional cosine.
m	Directional cosine.
q	Seismic behavior factor.
t	Round section thickness.
$\boldsymbol{A}$	General matrix used for explaining the LU-decomposition.
$\boldsymbol{H}$	Hermitian matrix.
$\boldsymbol{I}$	Identity matrix.
$\boldsymbol{L}$	Lower triangular matrix with ones on the diagonal.
$\boldsymbol{U}$	Upper triangular matrix.
$\boldsymbol{w}$	Intermediate vector used for forward and backward substitution process.
$\boldsymbol{z}$	Non-zero column vector.
ε	Factor to account for material selection when defining the CSC of a section. See CSC.
η	Factor used when defining section's susceptibility for shear buckling.
μ	Stiffness coefficient used when calculating the critical buckling load.
χ	Reduction factor for buckling resistance.
ϕ	The global initial sway imperfection factor.

1. INTRODUCTION

The purpose of this study was to design and develop a configurator tool to assist with the preliminary design process of an electrostatic precipitator (ESP) for Valmet Technologies. Valmet is a globally operating Finnish company with over 200 years of history in the fields of technology, pulp and paper and automation. The company today is a result of numerous mergers and company acquisitions and ultimately the demerging of Metso and Valmet into individual companies. The company's core business lines are pulp and energy business line, paper business line, automation business line and service. Each business line has its core offerings and the electrostatic precipitators are part of the offering of the pulp and energy business line.

The goal for the thesis project was to create an easy-to-use, excel-based design tool with minimal required input. The tool could autonomously perform dimensioning calculations for an ESP's casing in arbitrary dimensions and loading conditions. The tool would provide the user with utility ratios of all the user-determined profile selections under loading combinations determined according to the Eurocodes. Alternatively, the tool would allow the user to define limits for utility ratios and then select the profiles to be used in accordance to them. On the other hand, the tool would provide evaluation of the casing mass as a byproduct of the dimensioning calculations. Since the pricing is based mostly on the structure mass and the casing includes majority of the whole structure mass, this tool would have the potential to decrease the risk of incorrect pricing and the time consumed when calculating the offering price. When designing a structure of such large size, the importance of assuring structural integrity is of greater concern. Therefore, the tool should provide the designer with standard dimensioning details in order to provide a possibility to backtrack the calculations.

From a novelty point-of-view, this tool combines two commonly distinct functions to a product specific application. Configurators varying in the degree of intricacy of decision making as well as their application have been around since the modern computers became popular. Similarly, the main reason finite element method became popular is its suitability for analyzing complex structures via relatively simple repetitive operations. Automating the loading case evaluation and combining it with a system capable of optimizing structure profile selection for a case specific approach like this is always a product specific task. Therefore, the tool created is likely to be first of its kind within this exact scope.

The driver for the project was the urge to standardize and develop the design process of the ESP. The automated approach on the preliminary design phases saves time and frees recourses for more urgent tasks and speeds up the early phases of the design process. The

readily available dimension information provides valuable recourse for both mechanical design department and the sales department. Bidding process is based on the mass of the structure; thus, correct evaluation of mass will provide increased agility in the offering phase.

The different user-groups of the tool with varying knowledge levels bring a challenging aspect to the development project, since whereas accurate dimensioning information is needed, simultaneously the user interface would have to be accessible for everyone. The fact that the tool has to be easily accessible and thus preferably based on on-hand tools such as MS Excel limits the realm of calculation approaches.

The report is arranged so, that Chapter 2 provides an overview of the ESP as a product. The basics of the normal operation of the system are covered along with the main functions. Chapter 2 also covers the components of the ESP and structural members that are of interest in the scope of this thesis. Chapter 3 covers the theoretical side of the approaches used for the dimensioning calculations such as the finite element method and linear equation solving. Chapter 4 provides a view on the Eurocode's approach on structural design of structures like the ESP. The modelling process for different load types is presented and the principles used when dimensioning the casing members are illustrated with examples. In Chapter 5, after a brief overview on industrial configurators, the actual dimensioning tool is introduced. The basic functionality, inputs, outputs and operations are discussed along with the approaches used when performing different design tasks. Ultimately in the end of chapter 5, benchmarking results are presented along with discussion on their accuracy and the sources of deviation. Chapter 6 contains the conclusions on the overall thesis project and in Chapter 7, the project and its results are discussed with future work possibilities.

2. ELECTROSTATIC PRECIPITATOR

Electrostatic precipitator (ESP) is a device commonly used in processing industry and energy industry to remove particles or liquid droplets from flue gas. The particle separation is achieved using electrostatic force. This chapter gives an overview of the operating principle of the system, the considered casing structure and the design scope.

2.1 General operating principle

The two most common types of ESP are so-called parallel-plate ESPs and tubular ESPs of which only the first is considered within the scope of this thesis. Regardless of the ESP and process type, the basic operating principle of the precipitator is following: In the first phase, the flue gas from preceding process flows through the inlet nozzle and inlet diffuser screen to reach evenly distributed flow of gas over the whole chamber. The gas passes the first row of high voltage emission electrodes. The high DC-voltage, usually between 10 and 110 kV, causes the gas to ionize via corona discharges. The charged particles now drift towards the collecting plates of opposing charge (ground potential) and stick to the plates where their charge is again neutralized [1]. If, however, the particles arrive the chamber negatively charged, they stick to the emission electrodes due to opposed charges. The emission and collection electrode principle is shown in Figure 1 to support the understanding of the concept of the ESP. Here the red color is used to indicate parts with positive potential and the turquoise color to indicate ground potential.

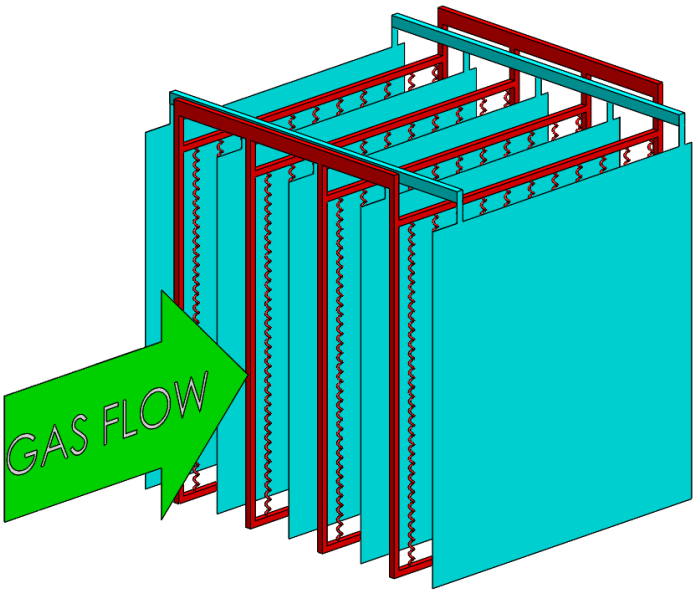

Figure 1: Emitting electrodes and collecting plates

The ash particles congregate on both the emission electrodes and collecting plates. The congregated ash is mechanically removed with a motor driven rapping system. The rapping hammers vibrate the collecting plate stacks and emission frames in order to separate the dust from the charged parts. The particles fall to the bottom of the chamber to be conveyed outside. Because the scope of this thesis project is limited to the casing structure, the bottom hopper structure is not discussed in detail. A general structure of an ESP is shown in Figure 2.

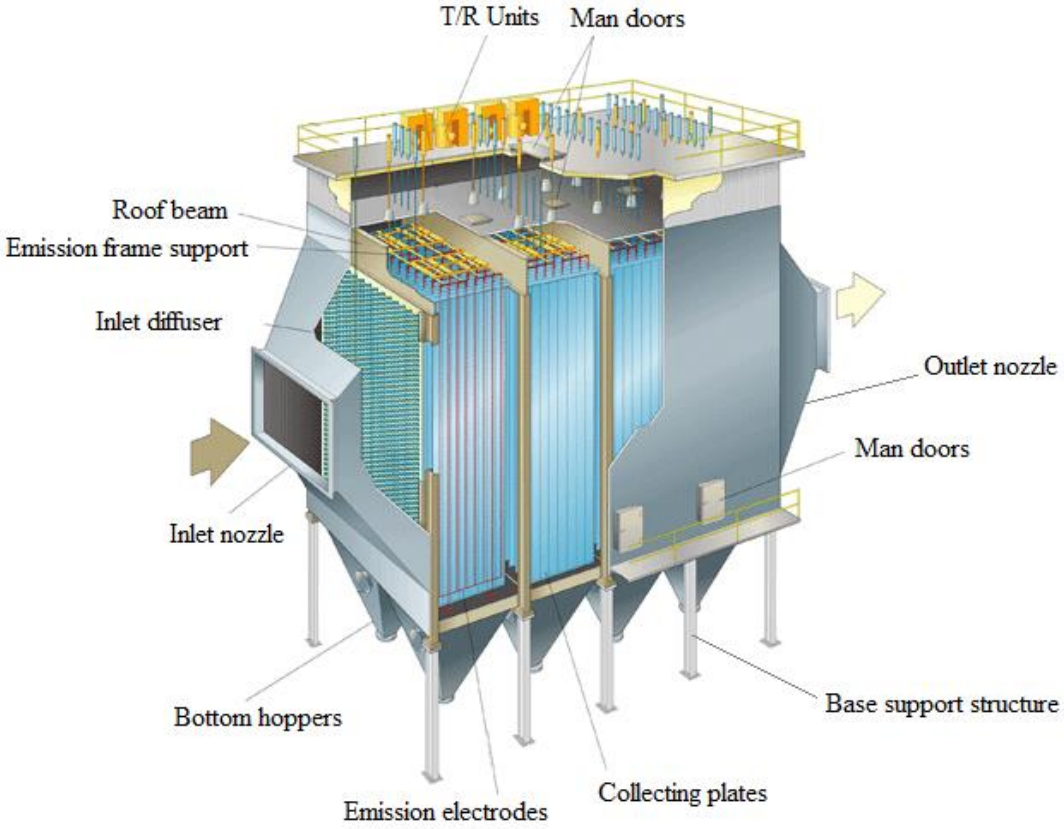

Figure 2: ESP general structure

As seen in Figure 2, the ESP chamber consists of multiple sub-chambers called fields. These fields are commonly labelled with letters A, B, C.., with A being the first field. The number of fields in ESPs vary depending on the use-case. Each field has its own separate emitting system and collecting system.

2.2 Structure and design scope

This chapter provides an overview on the ESP casing structure and the extent at which the structure is considered within this thesis. Parts or subassemblies that are not directly in relation with the casing are omitted and their effects on the casing design process is considered meaningless. Additionally, even though the configuration of the base structure (See Figure 3) has an effect on the casing's response to external loading, that effect is

neglected. This is done because estimating the rigidity of the casing base structure would require specific information of its stiffness properties and configuration. During the preliminary phases, this information is not yet available. The dimensioning error related to the assumption of infinitely rigid base is discussed in detail Chapter 3.1.3. Different parts are classified as primary support structures, secondary support structures and non-structural elements. This thesis focuses solely on designing the primary support structure, thus parts from different classes are discussed on a general level.

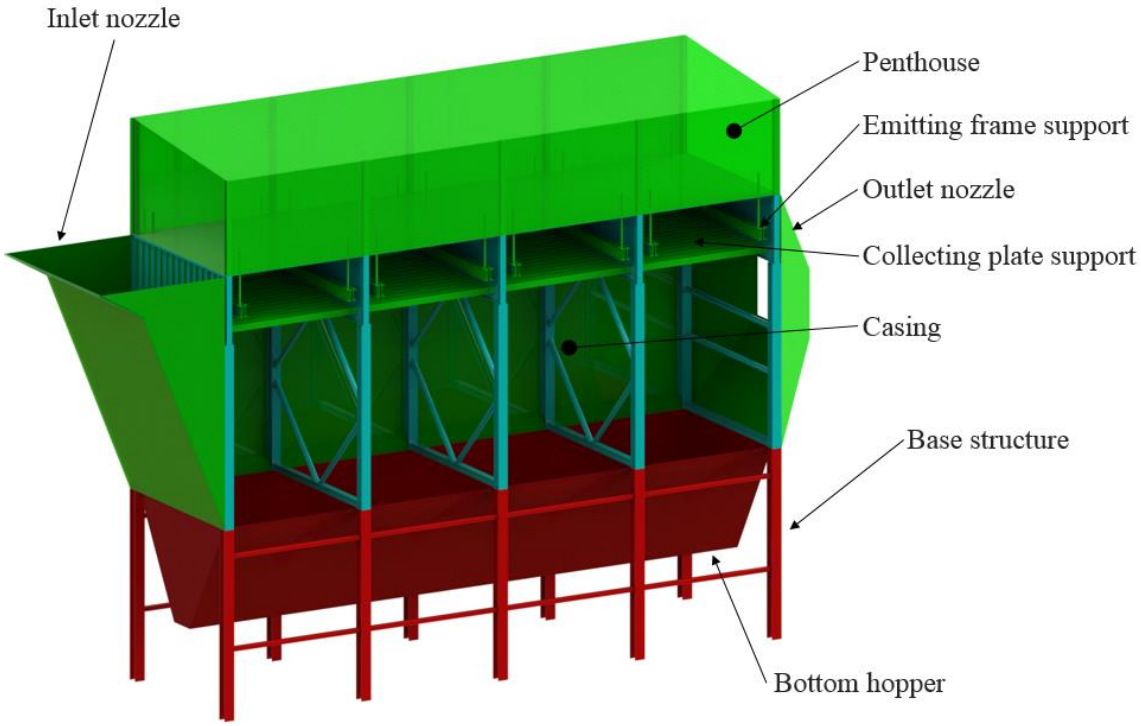

Figure 3: ESP's primary and secondary support structures

Mock-up model of the ESP's support structures is presented in Figure 3 with included secondary support structures colored green and omitted base support structures mentioned earlier colored red with the bottom hopper. The primary support structures are colored turquoise and shown in detail in Figure 4. The model lacks all the additional bracings included in the secondary support structures, such as wall plate stiffeners and roof stiffeners to improve clarity. All the non-structural elements are also omitted.

The non-structural elements of an ESP casing are considered only for their dead weight. This class consist of the emitting and collecting systems, rapping equipment, insulation, diffuser screens, baffle plates, electrical equipment and service platforms. The size of the dead weight is dependent of the design choices made prior to the casing design, which are done according to the customer needs.

The secondary support structures class consists of the structure parts transferring loads to the primary support structure. These parts include collecting plate and emission frame supports, hot walls and roofing, plate stiffeners, penthouse structure as well as inlet and

outlet nozzle structures. These structures have individual dead-weight properties but they also act as load-transferring elements for imposed loading such as live load, wind and snow. The size of the load acting on a secondary structural member, such as wall, is considered proportional to the area of the member in question. The response of these elements is considered infinitely rigid, so that all the loads are carried by the primary support structure. The durability or adequacy of any of the secondary support structures is not assessed within this thesis.

As mentioned earlier, dimensioning the primary support structure is the focus of this thesis as well as the primary task of the design tool. The primary support structure consists of portals situated at the ends of each field thus separating them from each other. The portals act as frames with rigid corner connections and they are analyzed separately on a 2-dimensional plane normal to the gas flow direction. Depending on the selected configuration, the inside of each 2-D frame is supported with series of stiffeners acting as a truss. See Figure 4 for an example of a single portal frame.

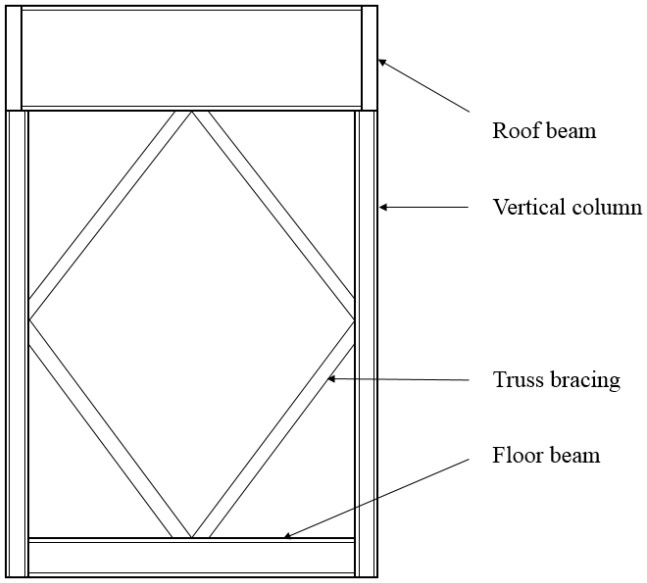

Figure 4: Example of a portal frame and inner truss

As shown in Figure 4, the portal frame consists of vertical columns, floor beam, roof beam and the inner truss. Vertical columns and inner truss profiles are the focus of the dimensioning task. These profiles are usually rolled sections and thus their dimensions are based on standard beam profiles. The roof beam is a relatively slender welded I-section and its geometry is standardized based on the amount of space needed between the hot roofing and collecting plates. The floor beam is either a standard hot-rolled profile or a custom welded I-section similar to the roof beam. The selection is based on need, and the welded section is needed only when there are truss braces connected to the floor beam. It becomes clear later, that the approach we select for the calculation model restricts us from explicitly analyzing the floor beam stresses when there are no bracings connected directly to it, because then the only loading it is opposed to is its own mass.

Aside from restricting the dimensioning calculation to the primary support structure pictured above, we limit the analysis to consider only the resistances of the members themselves. What this means, is that we assume all the connections to have the same load bearing capacity as the connecting members and thus no reduction in resistance considered within beam connections. The Eurocode [2] allows the neglecting of connections for the analysis of structure's internal load distribution and global deformation if the connections are considered stiff. As mentioned earlier, all the supports are considered infinitely rigid due to the unavailability of accurate rigidity-data of the base.

Another important remark of the dimensioning tool functionality is that when the tool is looking for optimal solution for the structure, we limit the design variables to the vertical columns and inner truss bracings only. This is done because these profiles are standard sections and therefore iterating can be done by changing only one global variable (the profile selection) at a time and thus the iteration only consists of altering two design variables. Selecting the welded sections used for the roof beam and occasionally for the floor beam would increase the amount of design variables drastically. The welded sections are considered for their durability to make sure that their loading does not exceed their durability.

Additionally, the scope of the dimensioning tool being developed is also affected by the mathematical approximations made within the development phase. The limitations caused by the mathematical approach are addressed in more detail after the approaches themselves have been covered. See Chapter 3.1.3.

3. THEORETICAL BACKGROUND

Traditionally, the preliminary design of structures like the casing frame have been carried out with more or less simplified models. Simplifications could include methods like considering the corner connections as joints or splitting the structures into smaller sections and neglecting some of the resulting force reactions to make the calculation procedure easier. Generally, all the simplifications are made in order to achieve a model of the structure that is statically determinate, which it rarely actually is.

Usually these kinds of simplifications result in calculation results that are within the limits of their application. Structural design of such robust industrial structures usually includes safety factors large enough to cope with the lack of accuracy. The advantage we gain when using simplified methods is obvious: we get results much faster. This approach, however, is not very suitable when considering dimensioning configurators or arbitrary dimensioning tasks like the one included in the scope of this thesis.

When structural systems increase in complexity, the analytic approaches for solving them become equally complex and system-specific. Furthermore, when carrying out structural analysis with a computer, the solving methods must be systematic and efficient. For the design of these increasingly complex arbitrary structures, approximate numerical methods have been developed in order to enable the use of computation in design. The numerical approach for structural analysis is generally labelled as Finite Element Method (FEM). [3]

This chapter is focused on the mathematical approaches utilized for the dimensioning tool, so that formulation of the mathematical model describing structure's response to loading is discussed in Chapter 3.1. Solving the model is discussed in Chapter 3.2.

3.1 Statically indeterminate structures

For statically determinate structures such as simple cantilever beams or pin-jointed trusses, the distribution of external load to the supports and members can be determined via static equilibrium approach. A structure is considered statically determinate when the number of unknown member forces and reactions is equal to the number of equilibrium equations available. For example, when considering a planar structure in two dimensions, the number of available equilibrium equations is 3; horizontal equilibrium, vertical equilibrium and rotational equilibrium. The approach would now involve constraining the sum of reaction forces at supports to be equal to the external loads in every direction and in every point in the system. However, when the number of unknowns exceeds the number of these equations, the structure is considered statically indeterminate or hyperstatic.

[4]. Structures can be statically indeterminate either internally, externally or both. Examples of statically indeterminate planar structures are presented in Figure 5.

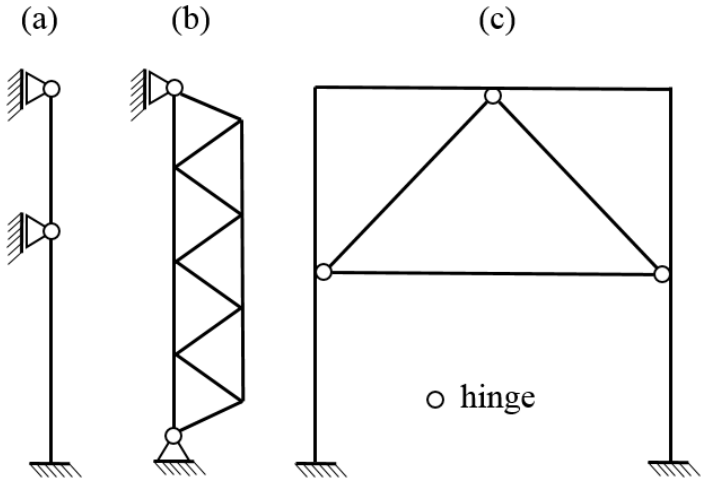

Figure 5: Statically indeterminate structures

The beam labelled (a) is considered externally statically indeterminate since the number of unknown external force reactions (5) exceeds the number of available equilibrium equations (3). The end-jointed frame structure labelled (b) is externally statically determinate but internally statically indeterminate due to excess internal member forces. Note that the internal member connections in (b) are not considered pin-jointed but stiff. Ultimately, the frame-truss-combination labelled (c) is considered both internally and externally statically indeterminate. The situation in case (c) represents the portal frames of an ESP structure presented in Figure 4 and thus solving the internally and externally statically indeterminate structures will be the focus of this chapter.

As the structure increases in number of support members the mathematical model of its behavior increases in complexity. If we were to analyze such a structure as a material continuum (continuous system), the mathematical model would be very case specific and solving the response of the system would be based on the solution of differential equations. Solving the system as a continuum is possible for only relatively simple structures and even then, employment of numerical methods is required for predicting the system response. [5]

In order to reduce the complexity of the structural system's mathematical model we must discretize it. The approach of dividing a continuous system into discrete, finite parts is generally called the finite element method (FEM). Depending on context in literature, the term finite element method is used ambiguously to also refer to direct stiffness matrix method in structural analysis. In this thesis, FEM refers to the discretization procedure and stiffness matrix method is considered separately.

Bathe [5] describes the general process of achieving finite element solution for a physical system as presented in Figure 6. This procedure accurately represents the route taken within the development process of the dimensioning tool as well as the route the dimensioning tool follows as it analyses the structure.

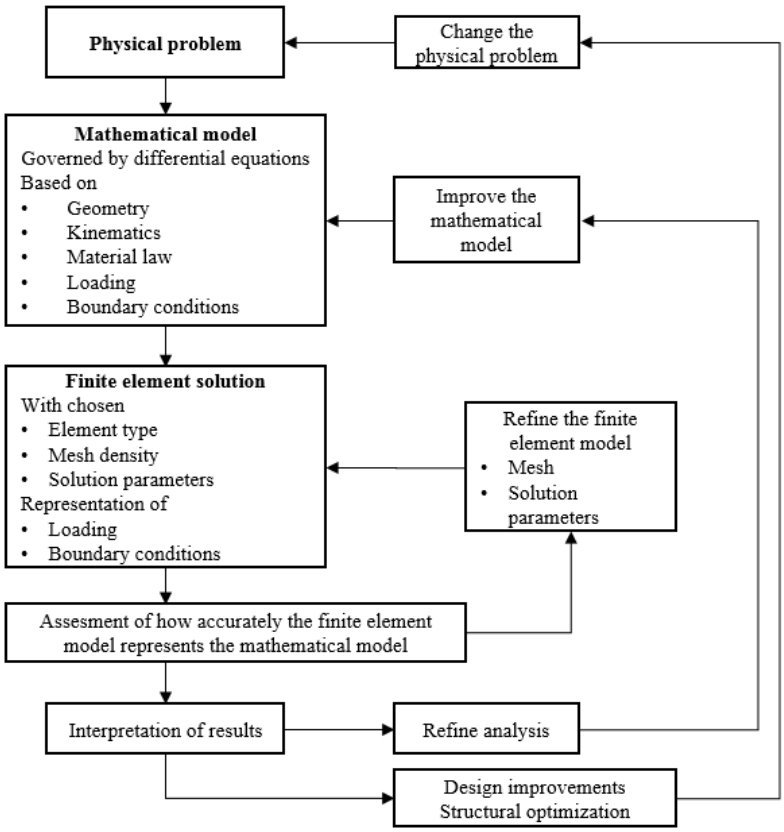

Figure 6: General workflow of finite element method

As mentioned before, the FEM-model of the system is an approximate representation of the mathematical model and its accuracy is naturally dependent on number of factors. Both the mathematical model and FEM model must be selected according to the nature of the system, since the FEM solution only yields reliable results within the realm of constraining assumptions made. As an example, we could consider a system with elements made of material with non-linear stress-strain curve. If this system is analyzed with a model assuming the behavior linear, the results are not reliable. More examples of restraining selections made within the generation of the FEM model in this project are discussed later in Chapter 3.1.3.

The workflow presented in Figure 6 starts with the formulation of a mathematical model of the physical system, an ESP casing in this case. We start by making assumptions on the geometry of the system. Geometry, in this context refers to the relation of different structural elements as well as the geometry of the individual members. The geometry is directly related to the kinematic properties of the system, for example the behavior of the connections between members. Selected material law dictates how the system and its

parts behave as a whole and individually, for example whether the material response is homogenous in all directions or not. Boundary conditions in this context refer to the assumptions one makes of the system's behavior. The boundary conditions should be considered thoroughly in order to ensure that the model represents the physical system. Loading is another influential part of mathematical model generation and it is addressed separately in detail in chapter 4.2. The mathematical model of an ESP casing used is considered in the following sub-chapter 3.1.1.

3.1.1 Mathematical model

In general, all the selections made while formulating the mathematical model of a physical system should be of equally approximate nature. At this phase, we must emphasize the fact that the intended use for the tool being developed is the preliminary design phase. Thus, the uncertain nature of relations and properties of different design parameters yields a relatively large error and ultimately this renders intricate mathematical models useless. This should not however lead to any kind of neglecting of already existing data we have of the physical system.

The mathematical model (or mechanical idealization) of the system is based on 2-dimensional truss-braced frames considered separately of each other. This is the main approximation used in the analysis, as the structure itself is obviously 3-dimensional. The selection of such approach is based on the requirement of creating dimensioning tool using only moderate amount of computational resources, since the platform we are working with (MS Excel) cannot carry out complex numerical procedures. For simplicity's sake, these frames could be considered only for the most loaded one, since the same profiles are used among the others as well. This however leads to a problem of explicitly showing which frame is the critical among all the loading combinations and limit-states (see Chapter 4.1.1). This leads to a situation where analyzing all the frames separately yields an easier and more comprehensive results, and is thus the approach selected. The effect of the penthouse structure is considered separately with a similar approach to the casing structure and the penthouse base loads is later added as point loads and moments to each of the casing portals.

Each of the frames is considered to be fixed to the environment from the low ends of the vertical columns and all the distribution of loading is based on the size proportions of the surrounding chambers. What this means is that each portal frame carries half of the loading imposed to each of its conjoining fields. Additionally, the portal frames at each end of the casing structure need to be accounted for additional loads caused by the equipment and secondary structures, such as nozzles and diffusers situated there.

3.1.2 Finite element model

In this chapter, we focus on formulating the finite element model specifically based on the stiffness matrix method. The stiffness matrix method is the traditional approach when carrying out a computer-aided analysis of building structures [4]. This is likely due to the fact, that stiffness method can be applied to a large variety of different types of structures regardless of their static determinacy and the methods' easy scalability via repetition of simple operations.

The finite element model is generated directly based on the mathematical model selected in the earlier chapter. The mathematical model divides the whole casing structure into individual portal frames and the finite element model furthermore divides these frames into elements. For this division we use beam elements. This requires the idealization of the frames and their parts as 1-dimensional entities with homogenous stiffness properties. How these properties are evaluated in different directions depends largely on the selected theoretical approach. Probably the simplest of these approaches is the classical beam theory, which is based on the theory of linear elasticity and Hooke's law. This theory, also called Euler-Bernoulli beam theory is used to connect the behavior of the beam member's deflection curve and its loading state. Euler-Bernoulli beam theory also includes a kinematic assumption that material points on the normal of the deflection curve remain on the normal during deformation. In other words, the beam is considered infinitely rigid in its own plane and thus the cross-section itself remains undeformed under loading [5]

Each of the elements of the structure are given independent stiffness properties in relation to their cross-section and global orientation. When considering elements in planar systems, a beam element has a specific response (stiffness) to loads in every direction. This response can be described with series of equations considering all the degrees of freedom. When the orientation and cross-section properties of these equations are concatenated to a matrix form it results in the so-called stiffness matrix of the element in question. If we expand the system from single degree of freedom to multiple, we can generalize following: For each degree of freedom there exists a force f_n and deflections $q_1 .. q_n$ which are tied to each other via the stiffness properties of the whole structure.

As an example for the definition of the stiffness properties of an element we consider a simple homogenous beam element with length of l_e and forces f_1 and f_2 acting on its ends resulting in axial end-displacements q_1 and q_2. For homogenous beam, the elastic modulus E_e and cross-section area A_e are constant over the whole length. See Figure 7.

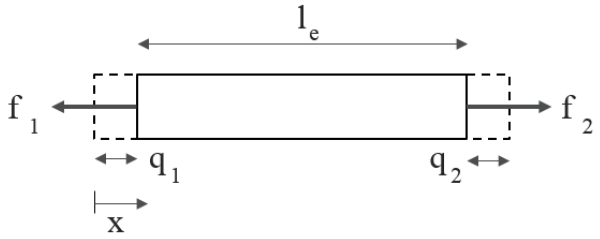

Figure 7: Basic one-dimensional element

Now we can write following Equation (1) based on Hooke's law $\sigma = E\varepsilon$ and the definitions for normal stress $\sigma = F/A$ and strain $\varepsilon = \Delta L/L$

$$\frac{f_1 - f_2}{A_e} = \frac{E_e q_1 - E_e q_2}{l_e} \tag{1}$$

If we now solve for the forces acting on the ends of the element we get

$$\begin{cases} f_1 = \frac{E_e A_e}{l_e} q_1 - \frac{E_e A_e}{l_e} q_2 \\ f_2 = -\frac{E_e A_e}{l_e} q_1 + \frac{E_e A_e}{l_e} q_2. \end{cases} \tag{2}$$

Now we can present the equations in a matrix form as follows

$$\underbrace{\begin{bmatrix} f_1 \\ f_2 \end{bmatrix}}_{\boldsymbol{f_e}} = \underbrace{\frac{E_e A_e}{l_e} \begin{bmatrix} 1 & -1 \\ -1 & 1 \end{bmatrix}}_{\boldsymbol{k_e}} \underbrace{\begin{bmatrix} q_1 \\ q_2 \end{bmatrix}}_{\boldsymbol{q_e}} \tag{3}$$

where the connection between local forces ($\boldsymbol{f_e}$) and displacements ($\boldsymbol{q_e}$) is called the local stiffness matrix of the element $\boldsymbol{k_e}$. This type of element can be used with structures with only axial deformation of elements, such as trusses. In similar fashion, we can consider a so-called Euler-Bernoulli beam element, which in turn includes end-displacements perpendicular to the axial direction as well as rotation. This element includes resistance for bending and shear, and the formulation is based on the beam's deflection curve's equation and beam's strain energy. The in-depth description of the formulation of the stiffness matrices is omitted to stay on an applicatory level (Available in [6]). Euler-Bernoulli beam alternative for Equation (3) is following:

$$\underbrace{\begin{bmatrix} f_1 \\ f_2 \\ f_3 \\ f_4 \end{bmatrix}}_{\boldsymbol{f_e}} = \underbrace{\frac{E_e I_e}{l_e^3} \begin{bmatrix} 12 & 6l_e & -12 & 6l_e \\ 6l_e & 4l_e^2 & -6l_e & 2l_e^2 \\ -12 & -6l_e & 12 & -6l_e \\ 6l_e & 2l_e^2 & -6l_e & 4l_e^2 \end{bmatrix}}_{\boldsymbol{k_e}} \underbrace{\begin{bmatrix} q_1 \\ q_2 \\ q_3 \\ q_4 \end{bmatrix}}_{\boldsymbol{q_e}} \tag{4}$$

where I_e is the second moment of inertia, f_1, f_3, q_1 and q_3 represent the node forces and displacements perpendicular to the normal axis and f_2, f_4, q_2 and q_4 represent the moments and rotations on each element end.

The presented elements are suitable for 2-dimensional structures comprising of pin-jointed trusses or frame structures with only non-axial loading. Incorporating more degrees of freedom becomes necessary when considering frame structures in multiaxial loading, because in these cases the elements are opposed to loading in all the general directions; axial, shear and bending. For structures requiring inspection of all the general loading directions, we can directly merge the two local stiffness matrices presented as parts of Equations (3) and (4) to create a so-called 6 degree-of-freedom (DOF) beam element. This yields the following 6 degree-of-freedom beam-element stiffness matrix shown in Equation (5):

$$\boldsymbol{k}_e = \begin{bmatrix} \frac{E_e A_e}{l_e} & 0 & 0 & -\frac{E_e A_e}{l_e} & 0 & 0 \\ 0 & \frac{12E_e I_e}{l_e^3} & \frac{6E_e I_e}{l_e^2} & 0 & -\frac{12E_e I_e}{l_e^3} & \frac{6E_e I_e}{l_e^2} \\ 0 & \frac{6E_e I_e}{l_e^2} & \frac{4E_e I_e}{l_e} & 0 & -\frac{6E_e I_e}{l_e^2} & \frac{2E_e I_e}{l_e} \\ -\frac{E_e A_e}{l_e} & 0 & 0 & \frac{E_e A_e}{l_e} & 0 & 0 \\ 0 & -\frac{12E_e I_e}{l_e^3} & -\frac{6E_e I_e}{l_e^2} & 0 & \frac{12E_e I_e}{l_e^3} & -\frac{6E_e I_e}{l_e^2} \\ 0 & \frac{6E_e I_e}{l_e^2} & \frac{2E_e I_e}{l_e} & 0 & -\frac{6E_e I_e}{l_e^2} & \frac{4E_e I_e}{l_e} \end{bmatrix} \quad (5)$$

This approach leads to an assumption that there is no connection between the axial loading and the loading in other directions. Figure 8 describes the 6-DOF beam element and its numbering semantics.

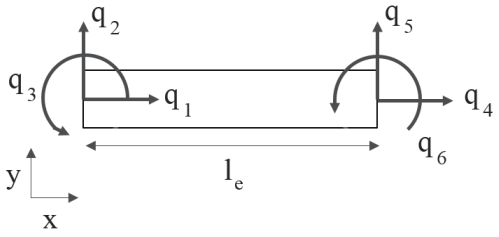

Figure 8: 6-DOF beam element and its indexing

The local stiffness matrices are defined separately for every element of the structure, after which they are merged to a global stiffness matrix. The merging is done per each local node's respective global node number. In other words, the local stiffness matrix cells representing global nodes shared by multiple elements are combined via summation. For

structures comprising of elements with misaligning local coordinate systems (such as the portal frame) the local stiffness matrices must be rotated to represent their global properties. A so-called rotation matrix is used to rotate the stiffness matrix coordinate system to the desired orientation as shown in Equation (7) [7]:

$$\boldsymbol{r_e} = \begin{bmatrix} l & m & 0 & 0 & 0 & 0 \\ -m & l & 0 & 0 & 0 & 0 \\ 0 & 0 & l & 0 & 0 & 0 \\ 0 & 0 & 0 & l & m & 0 \\ 0 & 0 & 0 & -m & l & 0 \\ 0 & 0 & 0 & 0 & 0 & 1 \end{bmatrix} \tag{6}$$

$$\boldsymbol{k_{rot}} = \boldsymbol{r_e^T k_e r_e} \tag{7}$$

where l and m represent the orientation of the element local coordinate system compared to the global coordinate system so, that $l = (x_2 - x_1)/l_e$ and $m = (y_2 - y_1)/l_e$. The resulting matrix $\boldsymbol{k_{rot}}$ is the newly re-orientated local stiffness matrix, $\boldsymbol{k_e}$ is the original local stiffness matrix. Ultimately, this results in a single stiffness matrix representing the whole system's response to each nodal force so that:

$$\boldsymbol{K_G} = \sum_{\boldsymbol{i}} \boldsymbol{k_{rot_i}} \tag{8}$$

where i is the number of elements and therefore the number of individual element stiffness matrices. We use the matrix $\boldsymbol{k_{rot}}$ to refer to the element stiffness matrices because $\boldsymbol{k_{rot}} = \boldsymbol{k_e}$ when the local and global coordinate systems align. However, the direct summation of the local stiffness matrices requires a reduction in the matrix elements. The global stiffness matrix must include non-zero values only in the cells corresponding to an element degree of freedom [8] s. 74. This means that stiffness properties of fixed nodes must be set to zero. Additionally, we need to remove these zeroed-out columns and cells from the global stiffness matrix in order to end up with a positive definite matrix, but this requirement is addressed in more detail in Chapter 3.2. The respective rows are also removed from the force vector and displacement vector, since fixed nodes do not move and forces acting on them have no effect.

As the global stiffness properties of the structure have been mathematically modelled with the global stiffness matrix $\boldsymbol{K_G}$, the loading state of the system is to be represented next. Within the stiffness matrix method, the loads acting on the structure globally or locally can only be applied on the global nodes towards global degrees of freedom. Each deflection direction has its respective force direction and they form a force-deflection pair with identical indexes.

If there are mid-element loads, like point loads or distributed loads they are broken down into equivalent node loads. The external loading is typically determined according to the

global coordinates, so no additional rotating is required prior to the combination. The global force vector is constructed via similar summation as the global stiffness matrix.

$$\boldsymbol{F_G} = \sum_{\boldsymbol{i}} \boldsymbol{f_{i,1}} + \boldsymbol{f_{i,2}} + \cdots + \boldsymbol{f_{i,n}} \tag{9}$$

where the index i represents the global degree of freedom and the index n is the number of global node-forces acting on the global node i. When the direct summation is opened, we get the following form of the Equation (9)

$$\boldsymbol{F_G} = \begin{bmatrix} f_{1,1} + f_{1,2} + f_{1,3} + \cdots + f_{1,n} \\ f_{2,1} + f_{2,2} + f_{2,3} + \cdots + f_{2,n} \\ f_{3,1} + f_{3,2} + f_{3,3} + \cdots + f_{3,n} \\ f_{4,1} + f_{4,2} + f_{4,3} + \cdots + f_{4,n} \\ \cdots \\ f_{i,1} + f_{i,2} + f_{i,3} + \cdots + f_{i,n} \end{bmatrix} \tag{10}$$

This results in a $1 \times n$ force vector $\boldsymbol{F_G}$. As mentioned before, the force vector is also reduced by removing the elements related to fixed degrees of freedom and thus ultimately the force vector will have the same number of rows as the global stiffness matrix. Now we can generalize as follows:

$$\boldsymbol{K_G Q_G} = \boldsymbol{F_G} \tag{11}$$

where $\boldsymbol{Q_G}$ is the global displacement vector containing all the nodal displacements $q_1, q_2, q_3 \ldots q_n$ of the finite element model. As stated before we assume that the response of the system is linear and therefore the equation can be solved directly based on the principle of superposition. The principle of superposition states that the net displacement at an arbitrary point inflicted by multiple forces is the sum of the displacements, which would have resulted from each individual load acting alone. The solution methodology for the matrix Equation (11) is presented in detail in Chapter 3.2 and is not discussed further in this chapter.

Now that the structure's global response is known, we can revert to the element level and solve the internal nodal forces of each element resulting from the displacements. This is done with the help of the element's local stiffness matrix, orientation matrix and local force vector. If we state the Equation (11) for a single element and use the Equation (7) to rotate the coordinate system we get:

$$\boldsymbol{f_e} = \boldsymbol{r_e^T k_e r_e q_e} - \boldsymbol{f_{e,ext}} \tag{12}$$

and for 6-DOF beam element we can write

$$\begin{bmatrix} f_{in1} \\ f_{in2} \\ f_{in3} \\ f_{in4} \\ f_{in5} \\ f_{in6} \end{bmatrix} = \boldsymbol{r_e^T} \begin{bmatrix} k_{11} & k_{12} & k_{13} & k_{14} & k_{15} & k_{16} \\ k_{12} & k_{22} & k_{23} & k_{24} & k_{25} & k_{26} \\ k_{13} & k_{23} & k_{33} & k_{34} & k_{35} & k_{36} \\ k_{14} & k_{24} & k_{34} & k_{44} & k_{45} & k_{46} \\ k_{15} & k_{25} & k_{35} & k_{45} & k_{55} & k_{56} \\ k_{16} & k_{26} & k_{36} & k_{46} & k_{56} & k_{66} \end{bmatrix} \boldsymbol{r_e} \begin{bmatrix} q_1 \\ q_2 \\ q_3 \\ q_4 \\ q_5 \\ q_6 \end{bmatrix} - \boldsymbol{f_{e,ext}}. \qquad (13)$$

Here the scalar components with the index in are used to emphasize the fact that the components represent internal loading. The additional $\boldsymbol{f_{e,ext}}$ vector represents the external nodal forces acting on the element if there are any. Generally, the equation states the local force vector of an element is a sum of the forces resulting from the deformation and external forces acting on the nodes of the element. As shown in Equation (13), the local stiffness matrix is not reduced for fixed degrees of freedom as the global stiffness matrix is prior to the solving procedure. Calculation-wise this means that we need to add the removed columns back to the global force vector $\boldsymbol{F_G}$ and global displacement vector $\boldsymbol{Q_G}$ in order to solve the element force vector. Ultimately the inclusion of the rows corresponding to the fixed DOFs allows us to solve the reaction forces on supports with the help of the equilibrium equations of the fixed nodes.

If need be, we could continue the calculation from the local element forces to calculate respective stresses and utilize a yield criterion (such as Von Mises) to evaluate the utility ratio of each element against yield strength or ultimate strength. This is however unnecessary since the Eurocode provides the limits of structure durability directly in maximum forces rather than stresses.

3.1.3 Constraints and error

In the previous chapter, we formulated the stiffness matrix method for solving the structure's response under loading. As mentioned in both Chapter 3.1.1 and Chapter 3.1.2 the mathematical model is a mechanical idealization of the structure and the finite element model is a discretization of the continuous system. All the assumptions made along the way restrict the realm of problems applicable for this approach. This chapter addresses the limitations originating from the assumptions and the error caused by the idealizations.

The mathematical model of the system is based on dividing the system in to 2-dimensional portal frames each analyzed individually. This approach leads to the first major constraint in the analysis: we have no way of determining structure's behavior in the transverse direction. The motivation behind this idealization is firstly the reduction in computational resources required when using planar structures and secondly the fact that majority of the transversal stiffness of the structure is based on the stiffness of the wall plates. Even though these plate-elements could be analyzed with the help of series of correctly formulated elements, the benefit could possibly turn out to be meaningless compared to the increase resource requirements. Furthermore, the ESP's geometry is usually

such that the side area is multiple times larger than the end-area and thus the imposed horizontal loading (wind and casing pressure) is much larger towards the side.

The 2-dimensional approach also makes it unpractical to estimate the global buckling of the portal frames, since the loss of stability occurs towards the omitted direction. Additionally, the fact that major parts of the structure are omitted from the analysis, results in an inability to consider the structure's behavior globally. In other words, we cannot estimate the structure's susceptibility to the loss of global stability without including the base structure to the analysis.

The mathematical approach we selected for the structural system limits the system's behavior to static response only, same applies to the load definitions. Dynamic attributes of the system can't be evaluated without including the inertial properties of the system. Analyzing the dynamic behavior of the system would again increase the computational resource requirements and therefore only static analysis is used. This selection has notable effect on analyzing the seismic response, since the seismic actions are dynamic by nature.

Another major constraint is the result of the assumption we make about the cross-section properties when defining the stiffness matrices. By assuming that A, E and I are constant, we limit ourselves to using beam sections with uniform cross-sections. Moreover, the FEM approach selected is applicable to systems with linear response only, which means that the material has to be linear. Typically, we can assume that steel materials behave linearly when loading is under the yield limit, thus E remains constant. Mechanically this means that the stress state of any of the structural members should not exceed the material's specific yield strength and the behavior of the material is ideal. Once the yield strength is exceeded, the relation is no longer linear and the stiffness matrix method in its linear form is no longer applicable. Temperature lowers the yield strength of a structure with a material specific rate, so high temperatures also pose a risk of error in calculation. Even though we are now limited to linear-elastic analysis of the structure's response, we can use plastic load limits where additional requirements are met. More about the load limits and their definition in 4.1.2.

What comes to the finite element model the derivation behind the Euler-Bernoulli beam theory and the formulation of the stiffness matrices leads to following restrictions concerning the system [9] [10]:

- Deflections must remain relatively small.
- Isotropic, linear elastic and homogenous material.
- Load components are linearly independent of each other.
    - Bending doesn't cause axial loading nor shear.
    - Shear deformation doesn't occur.

The requirement for the lack of shear deformation starts to affect accuracy as the slenderness of beam profiles increase.

The use of one-dimensional approximation of the otherwise 3-dimensional beam elements leads inevitably to an assumption of members connecting to each other at their centerlines. This is rarely the case when connecting members of different cross sections and this results in a geometric error. This error is illustrated with an ESP geometry-related example in Figure 9

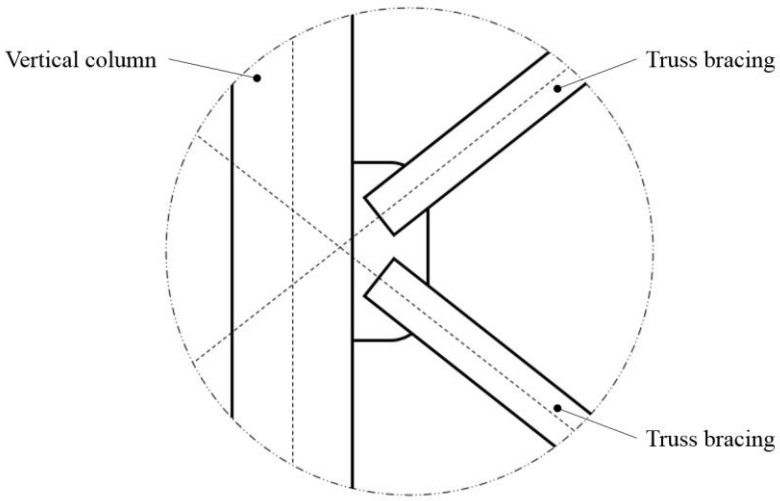

Figure 9: Detail view of the connection between the inner truss bracing and vertical column

It can be observed that the centerlines of the connected members do not intersect in one position as the finite element model assumes. This effect is amplified when as the centerline moves further from the connected edge of the member. As an example of this geometric error: If the roof beam elements were placed geometrically on the same height as the actual centerline of the roof beam, it would require an additional length of 1 meter to be added to the vertical column element interpretation and therefore a drastic geometrical error. The roof beam error is avoided by placing the vertical column elements first and considering the roof beam to begin from the top of the vertical columns. The same phenomenon happens on a smaller scale with the truss bracing connections shown in the Figure 9.

The base fixtures present in the system are considered infinitely rigid as mentioned in Chapter 2.2. The real structure is evidently not infinitely rigid, but due to unavailability of information it is impossible to evaluate the actual rigidity of the base structure. This assumption leads to over-estimations of force reactions on the base, but is thus a conservative method of analysis.

3.2 Linear systems

The problem of solving the set of linear equations by computing the inverse of the stiffness matrix is the fact that inversing a matrix is highly inefficient. This statement is addressed in the end of this chapter (see Figure 10). Moreover, the fact that the stiffness matrix is sparse increases the amount of unnecessary calculations carried out exponentially, since most of the relevant data resides near the diagonal of the matrix. Luckily, the set of linear equations can be computed via different methods proposed in literature by authors such as Bathe [5] & [8] and Zienkiewicz [11]. The most common approach is the so-called LU-decomposition, which is the matrix equivalent of the Gaussian elimination method. LU-decomposition divides the stiffness matrix into lower triangular matrix (L) and an upper diagonal matrix (U) [12]. In special cases, involving positive definite stiffness matrices LU-decomposition can be further developed in to a Cholesky decomposition. The generation of both of the decompositions mentioned is covered in this chapter along with the application of the Cholesky decomposition for solving the Equation (11).

As mentioned, LU-decomposition of a non-singular square matrix $\boldsymbol{A}$ refers to factorization of the matrix into upper triangular matrix $\boldsymbol{U}$ and lower triangular matrix $\boldsymbol{L}$ so that,

$$\boldsymbol{A} = \boldsymbol{L}\boldsymbol{U}. \tag{14}$$

An LU-decomposition is formulated by a sequence of row reductions, which generate 0s below the main diagonal in given column. The procedure is sequential and each step yields an intermediate product matrix $\boldsymbol{A}^{(k)}$ with increasing number of columns containing 0s below the main diagonal. Each step is equivalent to multiplication of the current matrix $\boldsymbol{A}^{(k-1)}$, by some matrix $\boldsymbol{L}_k$. Each $\boldsymbol{L}_k$ is non-singular. Equation (14) can be further denoted as

$$\begin{bmatrix} a_{11} & \dots & a_{1n} \\ \dots & \dots & \dots \\ a_{n1} & \dots & a_{nn} \end{bmatrix} = \begin{bmatrix} l_{11} & 0 & 0 \\ \dots & \dots & 0 \\ l_{n1} & \dots & l_{nn} \end{bmatrix} \begin{bmatrix} u_{11} & \dots & u_{1n} \\ 0 & \dots & \dots \\ 0 & 0 & u_{nn} \end{bmatrix} \tag{15}$$

Where a_{ij}, u_{ij}, l_{ij} represent the elements of each matrix on row i and column j. The sequential solution is generated by performing the following operations to each of the n columns. Given that, the first diagonal element of the non-singular square matrix $\boldsymbol{A}$ is non-zero, or $a_{11} \neq 0$, we select $\boldsymbol{L}_1$ so that it rotates the first column vector of $\boldsymbol{A}$ parallel to unit vector $\boldsymbol{e}_1$. This is done by multiplying the matrix $\boldsymbol{A}$ from the left side with matrix $\boldsymbol{L}_1$ so that

$$\boldsymbol{L}_1 = \boldsymbol{I} - \boldsymbol{l}_1\boldsymbol{e}_1^T = \begin{bmatrix} 1 & 0 & 0 & 0 & 0 \\ -l_{21} & 1 & 0 & 0 & 0 \\ -l_{31} & 0 & 1 & 0 & 0 \\ \dots & \dots & \dots & \dots & \dots \\ -l_{n1} & 0 & 0 & 0 & 1 \end{bmatrix} \tag{16}$$

where,

$$l_{i1} = \frac{a_{i1}}{a_{11}} \quad i = 2, \dots, n. \tag{17}$$

$$\boldsymbol{l}_1^T = [0 \quad l_{21} \quad l_{31} \quad \dots \quad l_{n1}]. \tag{18}$$

This yields the following intermediate result

$$\boldsymbol{L}_1\boldsymbol{A} = \begin{bmatrix} a_{11} & a_{12} & \dots & a_{1n} \\ 0 & a_{22}^{<1>} & \dots & a_{2n}^{<1>} \\ 0 & a_{32}^{<1>} & \dots & a_{3n}^{<1>} \\ 0 & a_{n2}^{<1>} & \dots & a_{nn}^{<1>} \end{bmatrix} \tag{19}$$

where $a_{ij}^{<1>}$ is used to distinguish, the elements changed by the multiplication from the original elements of matrix $\boldsymbol{A}$. For the k^{th} step, we can generalize the equations for the elimination procedure as shown in Equations (20) and (21).

$$\boldsymbol{L}_k = \boldsymbol{I} - \boldsymbol{l}_k\boldsymbol{e}_k^T \tag{20}$$

$$\boldsymbol{l}_k^T = [0 \quad 0 \quad \dots \quad l_{k+1k} \quad \dots \quad l_{nk}] \tag{21}$$

$$\boldsymbol{L}_k = \begin{bmatrix} 1 & 0 & \dots & 0 & \dots & 0 \\ 0 & 1 & \dots & 0 & \dots & 0 \\ 0 & \dots & & 1 & \dots & 0 \\ 0 & & & -l_{k+1\,k} & & \\ \dots & & & \dots & & \\ 0 & & & -l_{n\,k} & \dots & 1 \end{bmatrix}. \tag{22}$$

Eventually, when $k = n - 1$ and the last column is reached we obtain a result

$$\boldsymbol{L}_{n-1}\boldsymbol{L}_{n-2} \dots \boldsymbol{L}_1\boldsymbol{A} = \boldsymbol{U} \tag{23}$$

Where $\boldsymbol{U}$ is the upper triangular matrix of the LU-decomposition and since all the components of the matrix product $\boldsymbol{L}_{n-1}\boldsymbol{L}_{n-2} \dots \boldsymbol{L}_1$ are lower triangular matrices with 1s on the main diagonal, the product of these matrices ($\hat{\boldsymbol{L}}$) is also a lower triangular matrix with 1s on the main diagonal. We can now rearrange the equation to the form of equation (14) by computing the inverse of the $\hat{\boldsymbol{L}}$ matrix. This phase does not require an actual inverse but rather a rearrangement of the component matrices by multiplying the equation with the components of $\hat{\boldsymbol{L}}$ from the left as illustrated in equations (24) and (25):

$$\boldsymbol{A} = \boldsymbol{L}_1\boldsymbol{L}_2 \dots \boldsymbol{L}_{n-2}\boldsymbol{L}_{n-1}\boldsymbol{U} \tag{24}$$

$$\boldsymbol{L}_1\boldsymbol{L}_2 \dots \boldsymbol{L}_{n-2}\boldsymbol{L}_{n-1} = \boldsymbol{L} = \hat{\boldsymbol{L}}^{-1} = \boldsymbol{I} + \sum_{i=1}^{n-1} \boldsymbol{l}_i \boldsymbol{e}_i^T \tag{25}$$

This decomposition could now be used to solve the initial problem of $\boldsymbol{Ax} = \boldsymbol{b}$ but the decomposition can also be developed further if the matrix $\boldsymbol{A}$ in question is Hermitian positive-definite matrix. In this case the LU-decomposition can be simplified to Cholesky decomposition in order to reduce the recourses required by the calculation procedure. The theory for Cholesky decomposition states that for such matrix $\boldsymbol{A}$ there exists a unique lower triangular matrix $\boldsymbol{L}$, with real and positive elements at the diagonal, such that [13]

$$\boldsymbol{A} = \boldsymbol{L}\boldsymbol{L}^*. \tag{26}$$

Hermitian matrix is a complex square matrix, which is equal to its conjugate transpose. Since the conjugate transpose of any real matrix is equal to the transpose of the matrix in question, we can deduce that every symmetric real matrix is a Hermitian matrix. Hermitian real matrix $\boldsymbol{H}$ is positive-definite if and only if the scalar produced by multiplying the matrix from the left with the transpose of any non-zero column vector $\boldsymbol{z}^T$ and from the right with the column vector $\boldsymbol{z}$ is greater than zero. See equation (27).

$$\boldsymbol{z}^T\boldsymbol{H}\boldsymbol{z} \geq 0 \tag{27}$$

More generally this means, that the matrix $\boldsymbol{H}$ is invertible and all of the eigenvalues of matrix $\boldsymbol{H}$ are positive. Equation (27) is true for every non-singular matrix, which means that the factorization is applicable for every correctly formulated stiffness matrix. Cholesky factorization is based on the fact that every positive number has a positive square root. For symmetric positive-definite matrix, we can write [13]

$$\boldsymbol{H} = \boldsymbol{L}_1\boldsymbol{H}_1\boldsymbol{L}_1^T \tag{28}$$

where $\boldsymbol{L}_1$is lower-triangular matrix with strictly positive diagonal values. The algorithm of computing the Cholesky factorization is a modification of the Gaussian elimination used in the LU-factorization. For every element l_{jj} of matrix $\boldsymbol{L}$ for $j = 1, \dots, n$,

$$l_{jj} = \sqrt{h_{jj} - \sum_{k=1}^{j-1} l_{jk}^2} \tag{29}$$

and for $i = j + 1, \dots, n$,

$$l_{ij} = (h_{ij} - \sum_{k=1}^{j-1} l_{ik} l_{jk})/l_{jj}. \tag{30}$$

The Cholesky factorization can now be used to solve the linear system of equations $\boldsymbol{Ax} = \boldsymbol{b}$. Due to the fact that this decomposition is the one used with the calculation tool we change the matrix problem to the original finite element Equation (11) and use the approach to solve the displacement vector $\boldsymbol{Q_G}$. The initial problem is divided into two systems from which the unknown vector $\boldsymbol{Q_G}$ can be solved. The solution is reached by performing forward and backward substitutions ([14] p. 817). See equations (31) and (32).

$$\boldsymbol{L}w = \boldsymbol{F_G} \tag{31}$$

$$\boldsymbol{L}^T \boldsymbol{Q_G} = w \tag{32}$$

The equation (32) is called *forward substitution* due to the fact, that it can be computed by first solving the equation on the first row and then substituting the variable on the second row with the computed value and proceeding to next row. This method is illustrated in the equation (33) with a 4*4 $\boldsymbol{L}$ matrix:

$$\begin{bmatrix} l_{11} & 0 & 0 & 0 \\ l_{12} & l_{22} & 0 & 0 \\ l_{13} & l_{23} & l_{33} & 0 \\ l_{14} & l_{24} & l_{34} & l_{44} \end{bmatrix} \begin{bmatrix} w_1 \\ w_2 \\ w_3 \\ w_4 \end{bmatrix} = \begin{bmatrix} F_1 \\ F_2 \\ F_3 \\ F_4 \end{bmatrix} \tag{33}$$

which can be further denoted as shown in equations (34), (35) and generally in Equation (36)

$$w_1 = \frac{F_1}{l_{11}} \tag{34}$$

$$w_2 = \frac{F_2 - l_{12} w_1}{l_{22}} \tag{35}$$

$$w_j = \frac{F_j - \sum_{i=1}^{j-1} l_{ij} w_i}{l_{jj}} \tag{36}$$

Now that the intermediate vector $\boldsymbol{w}$ has been solved, we can continue to *backward substitution.* This phase is almost identical to the forward solution described earlier, the only difference being the order of calculation. This time we solve the Equation (36) starting from the last row. This ultimately results in solution for vector $\boldsymbol{Q_G}$ as shown in Equation (37).

$$Q_j = \frac{F_j - \sum_{i=1}^{j-1} l_{ji} Q_i}{l_{jj}} \tag{37}$$

As mentioned earlier, the main motivation for using the LU-decomposition is the reduction of required resources and thus increase in calculation speed. The resources required for computing a direct inverse for a matrix depend largely on the approach selected. Generally, direct inversion is considered highly inefficient and thus it is rarely used in computing. The decompositions provided in this chapter are much more suitable for inverting matrices, especially large ones, with the aid of a computer. The effectiveness of these approaches can be evaluated by comparing the floating-point operations (FLOPs) required for each of the approaches. FLOPs are used to quantify the amount of solving capacity required by a certain set of operations.

The Gaussian elimination (LU-decomposition) method for solving the linear system requires $2n^3/3 + 2n^2 \approx 2n^3/3$ FLOPs [15], where n is the order of the matrix. Furthermore, the Cholesky factorization requires only $2n^2 + n^3/3 \approx n^3/3$ due to the exploitation of the matrix symmetry [15]. This is only half of the FLOPs LU-decomposition requires. Both of the decompositions also have an ability of maintaining the sparse nature of the original matrix whereas direct inverse does not [16]. This is especially helpful when considering the memory usage of such calculation procedure.

As mentioned, the resources required for carrying out direct inverse and solving the set of linear equations directly depends on the selected inverse algorithm. Here the actual solving speeds were compared by using one approach for direct inverse (naïve Gauss-Jordan inverse) and the Cholesky factorization method for solving the same linear sets of equations with changing matrix order. The results are shown in Figure 10.

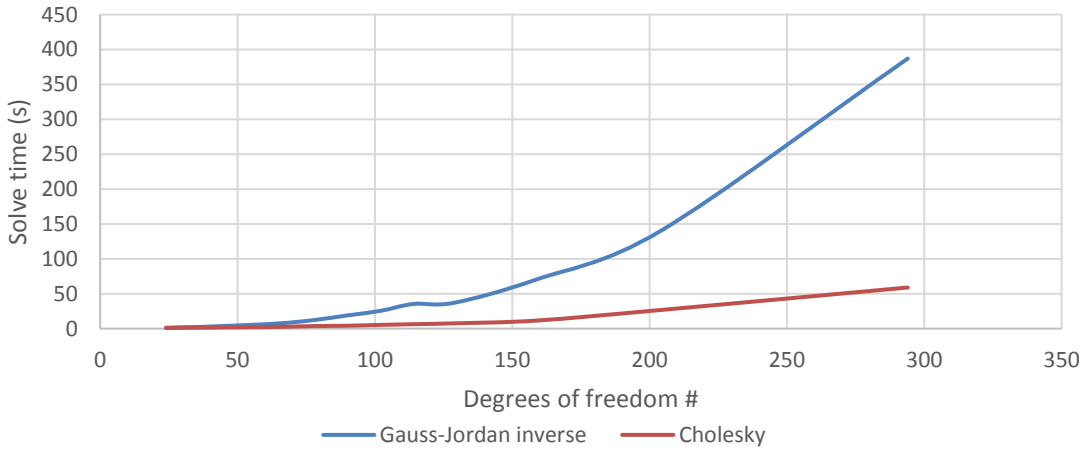

Figure 10: Cholesky decomposition and direct inverse solve time as a function of matrix order

It can be observed from Figure 10, that the solving speed difference starts to affect efficiency when the matrix order is in the hundreds. According to these results, the Cholesky factorization is far superior when solving a large number of linear equations. It is to be noted, that the solving speed is also affected by other operations taking place during the

normal operation of the dimensioning tool. Unfortunately, similar data comparing the effectiveness of direct inverse and LU-decomposition does not exist, since the solver was updated directly to utilize the Cholesky factorization. The commented VBA code for Cholesky algorithm is provided in Appendix A.

4. CALCULATION

This chapter covers the basic dimensioning approach used by the dimensioning tool including the general approach of limit state design and definition of load limits. Due to the general complexity of some of the loading types their formulation has been brought down to preliminary level thus leaving all special loading cases, such as extreme winds of unusual snow drifting outside the scope.

4.1 Limit state design

The approach of limit state design presented in the Eurocodes [17] and [2] is limited to analyzing the ultimate limit states and serviceability limit states of structures under static loading. Dynamic loading that can be assessed by using appropriate quasi-static equivalent forces and amplification factors is also considered applicable by this approach. As an example of such dynamic loads evaluated using their static equivalents: wind pressure and seismic actions. All the load calculations are presented at the same level of intricacy as they are utilized in the design tool.

4.1.1 Serviceability and ultimate limit states

The approach of limit states divides the structure and its loading system into different states according to the loading type and the structure's response. The main steps of this approach used mostly when designing buildings or other large constructions are presented in the Eurocode [17] as follows:

- Determine the different loads acting on the structure (see Chapter 4.2)
- Classify the loads into permanent actions, variable actions and accidental actions.
- Determine the design resistances and geometry of different structural elements.
- Carry out linear-elastic analysis and compare the resulting forces with different load combinations on the design values to get utility ratios.
- Ultimately it is required that no limit state is exceeded within the structure under loading.

The limit states are divided according to the response they precede. Serviceability limit state is the loading state after which the structure stops serving its purpose or where user comfort, normal functioning or appearance of the structure is affected negatively. Ultimate limit state is the state preceding local or global collapsing of the structure and therefore poses a risk to human safety. These situations usually include structure tipping over, fracture induced mechanisms and fatigue damage. The limit state dimensioning is to be based on the use of adequate limit states and loading models. It is to be shown, that no

limit state is exceeded for loading combinations, material properties or geometrical data. This also must include identifying the critical load cases. It should be noted, that limit state consists of both level of loading and limits for response. When it is required that serviceability limit state remains un-exceeded, it usually means that, for example, deflections remain within limits at certain points of structure. For the primary casing structure, the most influential loading state is ultimate limit state and therefore this state is the primary focus in this chapter. The serviceability limit state is however also considered, because deflection limits may be placed as additional requirements for the structure.

The loads are divided into classes and labelled according to their type. These classes are permanent actions (labelled with G), variable actions (Q) and accidental actions (A). The distribution of different actions within these classes depends largely on the situation. For example, snow loads and seismic loads can be considered accidental or an imposed depending on the location of the structure. Permanent actions are represented with either the single characteristic load value G_k, if fluctuation in the magnitude is minimal or as upper and lower limits G_{ksup} and G_{kinf} if the fluctuation is too large to ignore. This is the case when the permanent actions have positive effect on some loading combinations and negative on others. Variable actions should be determined as upper and lower limits between which the loading value should recede. If the statistical distribution is not known, the variable actions can also be presented with a single nominal value.

The loading combinations are defined separately for both of the limit states. The combinations are used in an attempt to capture the most critical loading situation taking place during the lifetime of the structure. The Eurocode [17] requires the different limit state loading limits to be compared to the internal loading taking place during all the different combinations of loads.

Combinations are to be considered for both the serviceability limit state and ultimate limit state. The limit state in question dictates the partition of different loads to be expected to occur simultaneously. The Eurocode [18] states that load combination used when considering serviceability limit state should consist of the characteristic values of dead weight and primary imposed load, which is likely to be either the wind load or the inner pressure in this case. Additionally, the secondary imposed loads are considered by using combination factors defined in their respective standards. Combination factors are addressed in more detail later in this chapter. At this phase, it is to be noted that prestressing loads are omitted from the equation formulation, since there are no prestressed members in the considered structure. The serviceability limit state load combination used to evaluate the effects of loading can be expressed as shown in Equation (38) ([17] p. 76):

$$E_d = E\{G_{k,j}; \Psi_{1,1} Q_{k,1}; \Psi_{2,i} Q_{k,i}\} \tag{38}$$

where E_d represents the effects of loading, G_k represents the characteristic value of permanent actions such as dead weight, Ψ_1 is the frequent factor of a variable action, Ψ_2 is

the quasi-permanent factor of variable action and $Q_{k,i}$ represents the characteristic value of ith variable action. In other words, the serviceability limit state is analyzed by using characteristic values of permanent loads (and prestressing loads) and then multiplying the primary variable load with frequent combination factor and secondary variable loads with the long-term affect factor. The latter subscript indexing refers to the number of the load of that type in question, when loads are numbered according to the effect of their severity.

Additionally, the ultimate limit state against internal failure or excessive deformation can be expressed as shown in Equation (39) ([17] p. 72):

$$E_d = \gamma_{Sd} E\{\gamma_{g,j} G_{k,j}; \gamma_{q,1} \Psi_{0,1} Q_{k,1}; \gamma_{q,i} \Psi_{0,i} Q_{k,i}\} \quad (39)$$

where γ_{Sd} is a partial safety factor representing the uncertainty associated with the loads or their effects, γ_g is a partial safety factor for permanent actions, and Ψ_0 is the combination factor of a variable action. In other words, the load combination used for determining effects of loading in ultimate limit states consists of permanent and variable actions multiplied with a safety factor to account for unfavorable deviation in the load values. Additionally, the variable actions are multiplied with combination factor because they are not likely to coexist all at their maximum value. While the standard ultimately requires the ultimate limit states for loss of global equilibrium, geotechnical stability and fatigue to be analyzed we focus only on the internal durability of the structure. The combinations for evaluating global static stability and the stability of the ground are omitted because they are outside the scope.

Ultimately, when considering seismic actions, it is to be done separately so that the effects are considered with the combination presented in Equation (40)

$$E_d = E\{G_{k,j}; A_{Ed}; \Psi_{2,i} Q_{k,i}\} \quad (40)$$

where A_{Ed} represents the design value of the seismic action, thus meaning that the seismic load is considered the primary variable load and all the other variable loads are added using combination factors.

As mentioned earlier the primary casing supports are of more interest when evaluating their ultimate durability. Eurocode [17] states that the serviceability limit state can be omitted from analysis if it can be shown that fulfillment of ultimate limit state requirements also fulfills the requirements for structure usability. Usability is commonly related to limits set for deflections so that deflected structure does not infer with the structure's functionality. In the case of ESP casing, the primary support structure maintains its proper functionality if its structural integrity is not compromised and thus we only focus primarily on the ultimate limit state.

The combination factor, frequent factor and quasi-permanent factor are defined separately for all the variable load types. The factors shown in Table 1 are given in the Eurocodes ([17] p. 80 and [19] p. 22).

Table 1: Variable load representation factors

Load type	Ψ_0	Ψ_1	Ψ_2
Live load on roof	0,7	0,5	0,3
Snow load when structure elevation > 1000 m	0,7	0,5	0,2
Snow load when structure elevation < 1000 m	0,5	0,2	0
Wind load	0,6	0,2	0
Internal temperature load	0,6	0,5	0

The reduction in temperature is not used within the ESP casing calculation, since the inner temperature is usually well known and only deviates a little. Along with the factors describing the coexistence of variable loads, the ultimate limit state combination described earlier included partial safety factors. The values used are listed in Table 2 [17].

Table 2: Partial safety factors

Favorable permanent actions γ_g	1
Unfavorable permanent actions γ_g	1,15
Unfavorable leading variable action $\gamma_{q,1}$	1,5
Unfavorable accompanying variable action $\gamma_{q,i}$	1,5
Favorable variable action $\gamma_{q,i}$	0

Along with the representation factors for accounting for load coexistence and safety factors for ultimate limit state, there are additional reliability and consequence factors to be taken into account when defining the load values and design resistances. These factors and their formulation are omitted due to the fact that the tool is designed to allow the user to define the multipliers for each of the load types independently. The recommended multipliers for ultimate limit state shown in earlier tables are supplied for the user by default.

4.1.2 Cross-section classification

Cross-section classification divides cross-sections into classes (CSCs) according to the extent the local buckling reduces the section member's durability [20]. In other words, members with low tendency for local buckling can reach their nominal load limit and then collapse via the formation of a plastic hinge. Furthermore, members with high tendency for local buckling lose their stability before such nominal load values are reached and collapse to a direction normal to their plane.

CSCs are determined separately for all the cross sections and cross section parts in the structure. The classification depends on the stress state and the width-to-thickness-ratio of the compressed parts of the cross section. The classification's relation to the stress state of the section links the cross-section classification to the loading. Therefore, the CSC of a member may change when its compressive loading (combination of bending moment and normal force) changes. The different CSC are described as follows [20] [18]

- Class 1 cross-section can form a plastic hinge with the rotation capacity from plastic analysis without reduction of the resistance.
- Class 2 cross-section can develop a moment resistance according to plastic analysis, but local buckling limits its rotation capacity.
- Class 3 cross-section might reach its yield strength at some points near the compressed edge, but local buckling tends to prevent the development of plastic moment resistance.
- Class 4 cross section will buckle before yield stress is reached in the cross section.

This classification needs to be considered when determining the durability of the structure members. If the cross-section falls into classes 1 or 2, its design resistance may be calculated according to plastic range, since it is able to develop plastic moment resistance. If the CSC of a member or its part is 3 or 4, the elastic range is used when calculating the design resistance values and additionally extra measures are taken to account for the susceptibility to buckling of a section belonging to CSC 4. These extra measures for resistance calculation are discussed in Chapter 4.1.3. Generally, CSC of 4 usually occurs only with welded sections, since rolled section dimensions are selected in a such manner, that CSC over 3 is never reached.

For all the cross-section classes, a linear-elastic analysis is suitable for determining the load carrying capacity. Furthermore, the cross-section-class of the beam elements of a beam member may vary, due to their different loading states. As a simplification, one is allowed to consider the whole beam to be of the same cross-section-class as the section part with the highest class. If parts of the cross-section fall into different classes, the whole cross-section may be considered according to the higher CSC [20]. The calculation excel doesn't, in fact, homogenize the whole beam section but rather bases the CSC of each individual element to its actual loading conditions. Some simplifications are however made when defining the CSC of a beam element. If the web and the flanges are of different cross-section class, the element in question is considered to belong to the higher class.

The effect of the cross-section class on the beam member's behavior under loading is illustrated in Figure 11.

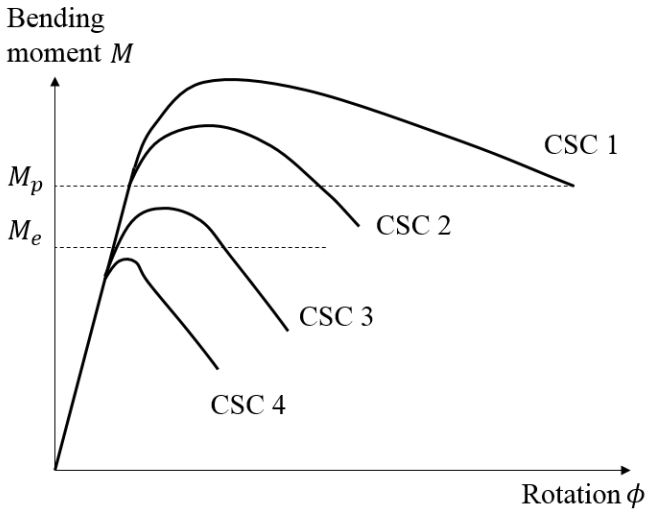

Figure 11: Illustration of the behavior of different CSC under loading

As seen from the above illustration, CSC 1 and 2 reach the plastic resistance area, but the CSC 1 beam reaches larger rotation before fracture. CSC 3 beam reaches the elastic resistance but CSC 4 beam doesn't. The evaluation of the cross-section class of a beam member under loading is based on the loading state of the member and the section dimensions. The standard supplies limits related to ratios of cross-sectional dimensions and the loading state. In Figure 12, the cross-section dimensions required for determining the CSC of the profiles used in the ESP casing are displayed.

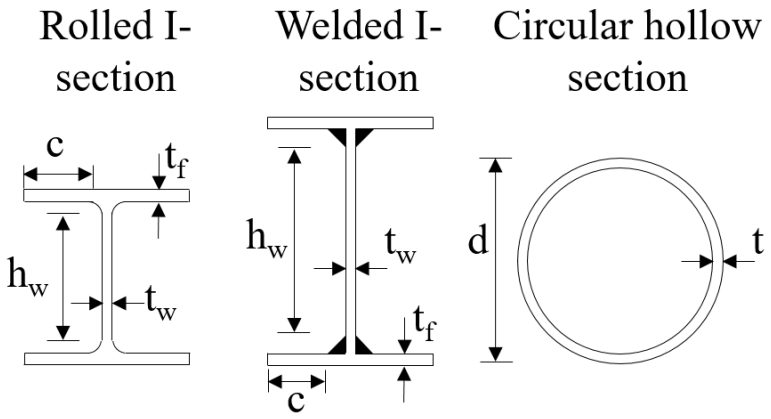

Figure 12: Section dimensions regarding the cross-section classification

In addition to the dimensions, we need to account for the section material and the type of the loading the section is opposed to. Two factors are defined for this purpose. See Equation (41) [2] for the material factor and equations (42) and (43) ([20] p. 119) for the loading type factor.

$$\varepsilon = \sqrt{\frac{235MPa}{f_y}} \tag{41}$$

$$\alpha_{web} = 0.5 + \frac{0.5 \cdot N_{Ed}}{t_w h_w f_y / \gamma_{M0}} \tag{42}$$

$$\alpha_{flange} = 0.5 + \frac{0.5 \cdot N_{Ed}}{t_f c f_y / \gamma_{M0}} \tag{43}$$

where f_y is yield strength of the material used, γ_{M0} is partial safety factor addressed more accurately later in Chapter 4.1.3 and N_{Ed} is the axial loading acting on the element. Now the cross-section class can be selected for web according to Table 3 and for flanges and circular tubes according to Table 4. [21]:

Table 3: CSC limits for web

CSC	Condition	Limit
1	$\alpha > 0.5$	$\frac{h_w}{t_w} \leq \frac{396\varepsilon}{13\alpha - 1}$
	$\alpha \leq 0.5$	$\frac{h_w}{t_w} \leq \frac{36\varepsilon}{\alpha}$
2	$\alpha > 0.5$	$\frac{h_w}{t_w} \leq \frac{456\varepsilon}{13\alpha - 1}$
	$\alpha \leq 0.5$	$\frac{h_w}{t_w} \leq \frac{41.5\varepsilon}{\alpha}$
3	$\psi > -1$	$\frac{h_w}{t_w} \leq \frac{42\varepsilon}{0.67 + 0.33\,\psi}$
	$\psi \leq -1$	$\frac{h_w}{t_w} \leq 62\varepsilon(1 - \psi)\sqrt{-\psi}$

Table 4: CSC limits for flanges and circular tubes

CSC	Limit for flange	Limit for tube
1	$\frac{c}{t_f} \leq 9\varepsilon$	$\frac{d}{t} \leq 50\varepsilon^2$
2	$\frac{c}{t_f} \leq 10\varepsilon$	$\frac{d}{t} \leq 70\varepsilon^2$
3	$\frac{c}{t_f} \leq 14\varepsilon$	$\frac{d}{t} \leq 90\varepsilon^2$

The limits for web CSC are defined for combined compression and bending due to the formulation of the limits. If alpha is 1, then the loading state is pure compression and if alpha is 0.5 the loading state is pure bending. The limits for flanges are determined for compression and tension of flanges only, since the system is planar. Limits for the tubes

are provided as is for all the loading situations. From the determined CSCs of member parts, the overall CSC can now be selected based on the highest partial CSC.

4.1.3 Definition of load limits

Generally, the Eurocode 3 [2] requires that the design value of the occurring force on any of the structural members doesn't exceed the design value of the resistance. In this chapter, we assess the definition of the design resistance values for all the loading types on beam sections. These design resistance types are resistance to normal forces N_{Rd}, resistance to bending moments M_{Rd}, resistance to shear force V_{Rd} and resistance to buckling $M_{b,Rd}$. Some of these values also include directional properties or dependencies to cross-section classes, but all this is addressed in their respective chapters. Torsion resistance or design values are omitted completely, because torsional buckling and actions in general are outside the scope. It is to be noted, that the approaches presented are limited to those applicable to the structures within the scope of this thesis. Throughout the resistance calculations, partial safety factors will be used according to the standard's suggestions. Partial safety factors and their suggested values for resistance of cross sections are as follows ([2] p. 43):

$$\gamma_{M0} = 1{,}00; \quad \gamma_{M1} = 1{,}00; \quad \gamma_{M2} = 1{,}25 \tag{44}$$

where γ_{M0} is the safety factor for cross-section durability regardless of the CSC, γ_{M1} is the safety factor for member stability and γ_{M2} is the safety factor for resistance against tension fracture.

The axial design resistance is determined similarly for both tension and compression with the only difference being the use of effective-area (A_{eff}) when calculating compression resistance for sections of CSC 4. Generally, the design axial resistance for sections without significant holes is determined as shown in Equation (45) ([19] p. 49):

$$N_{Rd} = \frac{A_{tot} f_y}{\gamma_{M0}} \tag{45}$$

where A_{tot} is the total cross-sectional area of the section in question and f_y is the yield strength. As mentioned, total area is replaced by effective-area when evaluating compression resistance of CSC 4 sections.

The design bending moment resistance is based on either the elastic, plastic of effective section modulus of the cross-section. The resistance is defined as shown in Equation (46)

$$M_{c,Rd} = \frac{W_{pl} f_y}{\gamma_{M0}} \tag{46}$$

where W_{pl} is the plastic section modulus of the cross-section. In this form, the Equation is applicable for sections of CSC 1 and 2. For class 3 cross-sections, we must replace the plastic section modulus with the elastic section modulus W_{el} and similarly for class 4 cross-sections we use the effective section modulus W_{eff}.

The design shear resistance is defined completely separately for plastic and elastic behavior. Plastic shear resistance is calculated as shown in Equation (47) ([2] p. 50):

$$V_{pl,Rd} = \frac{A_v \left(\frac{f_y}{\sqrt{3}}\right)}{\gamma_{M0}} \tag{47}$$

where A_v is the shear-area of the cross-section. The shear area is used in an attempt of more accurately estimating the area capable of carrying shear loads. For rolled I-sections and H-sections loaded parallel to web the shear area is calculated as follows

$$A_v = A_{tot} - 2b_s t_f + (t_w + 2r_s)t_f \tag{48}$$

where b_s is the cross-section width, t_f is the flange thickness, t_w is web thickness and r_s is the radius between flange and web. This formulation is similar to the common idealization of assuming that the web-section is responsible for carrying shear loads with only difference being the additional parts of flange taken into account with the last term in Equation (48). Note that only the symmetric I-sections and H-sections are considered, since the portal frames are constructed from such profiles. The plastic design resistance can only be used when the profile is not susceptible for shear-buckling and thus the following condition is fulfilled ([21] p. 23):

$$\frac{h_w}{t_w} \leq \frac{72}{\eta}\varepsilon \tag{49}$$

where h_w is the web height and the factor η can be conservatively selected to be 1. If, however, the condition in Equation (49) is not fulfilled the design shear resistance of the section is based on the shear-buckling resistance of the web and the shear resistance of the flanges. This is practically always the case for the roof beam. The following equation for elastic shear resistance ([21] p. 23):

$$V_{el,Rd} = V_{bw,Rd} + V_{bf,Rd} = V_{bf,Rd} + \frac{\chi_w f_y h_w t_w}{\sqrt{3}\,\gamma_{M1}} \tag{50}$$

where $V_{bw,Rd}$ is web shear-buckling resistance, $V_{bf,Rd}$ is the shear-buckling resistance of the flange is the and χ_w represents the contribution of the web. If the section does not contain transversal stiffeners aside from the stiffeners at supports, we can omit the effect of flanges to the shear resistance design value in similar fashion to the plastic shear resistance design value consideration in Equation (47). Only this time instead of using the

shear-area in calculations we just set the $V_{bf,Rd}$ to zero in Equation (50). Now the only thing missing is the value of χ_w representing the contribution of the web. The contribution of the web depends on the stiffener configuration of the section in question. Within the scope of this thesis, all the members falling into CSC 4 (roof beam and floor beam) have rigid end posts and no additional stiffeners. Additionally, the web contribution is dependent of the modified slenderness of the web $\overline{\lambda}_w$, which can be determined as follows ([21] p. 25):

$$\overline{\lambda}_w = \frac{h_w}{86.4 t_w \varepsilon} \tag{51}$$

It is to be noted, that this equation is only valid for sections with transversal bracings only at supports. Now the web contribution can be determined according to the following table

Modified slenderness $\overline{\lambda}_w$	Web contribution χ_w
$\overline{\lambda}_w < 0.83$	1
$0.83 \leq \overline{\lambda}_w < 1.08$	$0.83 / \overline{\lambda}_w$
$\overline{\lambda}_w \geq 1.08$	$1.37/(0.7 + \overline{\lambda}_w)$

If the member is in compression, in addition to compressional resistance we must ensure, that the beam section does not collapse via buckling. While there are numerous buckling mechanisms that the section could undergo, such as torsional buckling and earlier assessed local web buckling, we are focusing solely on flexural buckling. This is because the 2-dimensional mathematical model selected is not suitable for analyzing structure response to torsional loading. Additionally, the theory presented is limited to sections falling on cross-section classes below four, because the parts of the portal frame susceptible for buckling are the vertical columns and the inner truss members. These members are standard sections, so their dimensions are selected in such manner, that they are of CSC below four regardless of the loading.

The cross-section's resistance for buckling depends primarily on the section's slenderness and the inherent imperfections present in the cross-section**.** Slenderness is dependent of geometric properties, and the imperfection factor is used to describe the section's susceptibility to buckle under load. This property is estimated according to the section type and material. Eurocode [2] provides buckling curves for different section types in relation to the material used and for the sections relevant for this thesis, the buckling curves are as presented in the Table 5 ([2] p. 58).

Table 5: Buckling curves and imperfection factors of selected section types with different materials

	Rolled sections (I & H)		Hollow sections	
Material	h/b > 1.2	h/b < 1.2	hot-rolled	cold-rolled
S 235	a (0.21)	b (0.34)	a (0.21)	c (0.49)
S 275	a (0.21)	b (0.34)	a (0.21)	c (0.49)
S 355	a (0.21)	b (0.34)	a (0.21)	c (0.49)
S 420	a (0.21)	b (0.34)	a (0.21)	c (0.49)
S 460	a_0 (0.13)	a (0.21)	a_0 (0.13)	c (0.49)

These curves are used for sections with flange thickness under 40 mm, which includes every standard HE- and I-beam. The imperfection factors presented within the actual buckling curve provide a quantifiable measurement for the imperfection, which is used when determining the actual resistance for buckling. As mentioned earlier, the non-dimensional slenderness of a cross-section also affects its tendency to buckle. The non-dimensional slenderness for flexural buckling is determined as shown in Equations (52) and (53) ([2] p. 59):

$$\overline{\lambda} = \sqrt{\frac{A_{tot} f_y}{N_{cr}}} \qquad for\ CSC\ 1, 2\ \&\ 3 \tag{52}$$

$$N_{cr} = \mu \pi^2 \frac{EI}{L^2} \tag{53}$$

where N_{cr} is the critical buckling load depending on the cross section properties and its supports. Generally, we consider four possible support conditions leading to four different buckled shapes and values for the coefficient μ. See Figure 13 (modified from [22]).

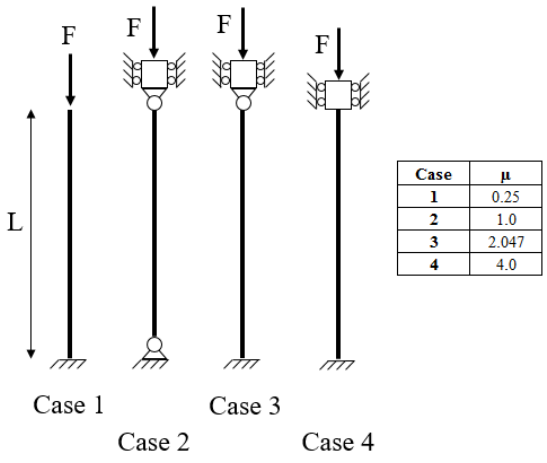

Figure 13: Different support configurations for buckling and related stiffness coefficients

From these support configurations, we use the case 2 for inner bracings due to the fact that their connections are considered pin-jointed. For the vertical columns, we use the case 3 to avoid over-estimating the rigidity of the connections when evaluating the design resistances. The calculation has been programmatically defined to accept alternate buckling cases to be used if needed.

With this information, we can now determine the reduction factor for buckling resistance graphically from charts available or by solving the equations (54) and (55) using the values of non-dimensional slenderness and imperfection factor calculated.

$$\chi = \frac{1}{\Phi + \sqrt{\Phi^2 - \overline{\lambda}^2}} \leq 1 \tag{54}$$

$$\Phi = 0.5\left[1 + \alpha\left(\overline{\lambda} - 0.2\right) + \overline{\lambda}^2\right] \tag{55}$$

Finally, we can now calculate the value of buckling resistance as shown in Equation (56).

$$N_{b,Rd} = \frac{\chi A_{tot} f_y}{\gamma_{M1}} \tag{56}$$

4.1.4 Multiaxial loading

The structural members of the system are usually under a local multiaxial loading. What this means is that a member is simultaneously under bending, shear and axial tension or compression. Linear-elastic model assumes that all these loading components are independent of each other, but the question is, how do they interact and how does one estimate their combined effect on structure's durability. This chapter assesses the Eurocode approach on considering multiaxial loading.

The basic principle for accounting multiaxial loading is considering the bending resistance to be the primary design load. What this means is that we assume that under any loading combination the structural member in question reaches its limit for bending load before reaching the design limit for any other loading type. Initially we need to determine the plastic or elastic bending load limit depending on the CSC of the member and the resistance limit for axial force and shear force as described in the Chapters 4.1.2 and 4.1.3. The Eurocode 3 provides reduction limits for the shear loads shown in Equation (57) and axial loads shown in Equations (58) ([2] p. 58-60):

$$V_{Ed} \leq 0.5 \cdot V_{pl,Rd} \tag{57}$$

$$N_{Ed} \leq \frac{0.5 h_w t_w f_y}{\gamma_{M0}} \tag{58}$$

The Eurocode also supplies an alternative limit for the axial load reduction, which is quarter of the plastic axial resistance. In order to simplify the automatic reasoning involved when using multiple limit equations to determine whether or not we need to reduce the bending resistance under axial loading we show that the limit calculated according to Equation (58) is, in fact, conservative for vertical column profiles. See Figure 14 for illustration.

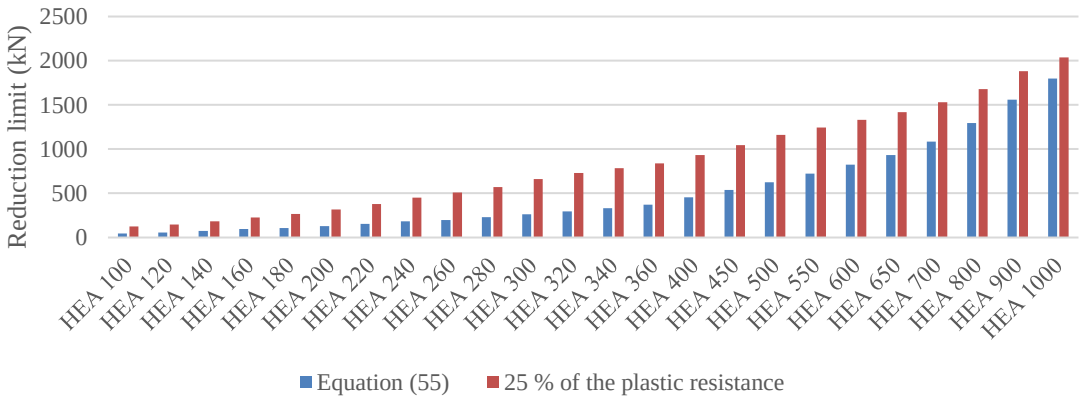

Figure 14: Reduction limits for compressive loading

Similar comparison of approaches with similar results can be carried out also for the inner truss as well as the roof beam and the floor beam. These comparisons are omitted because roof beam and floor beam are rarely under any significant axial loading. Similarly, the inner truss is considered pin-jointed and thus its durability is only analyzed against buckling and tension.

Should the loading in any of the members exceed either of the limits (57) or (58), the limit load values are reduced so that, excess shear load causes reduction in yield strength value f_y used and excess normal load causes reduction directly in bending load limit $M_{c,pl,Rd}$ or $M_{c,el,Rd}$. The reduction for the yield strength is shown in Equation (59) and for the bending load limit in Equation (60) ([2] p. 58)

$$f_{yr} = \left(1 - \left(\frac{2V_{Ed}}{V_{pl,Rd}} - 1\right)^2\right) f_y. \tag{59}$$

$$M_{N,Rd} = M_{pl,Rd}\left[1 - \left(\frac{(N_{Ed}/N_{pl,Rd}) - a}{1 - a}\right)^2\right], \qquad a = \frac{A - 2b_s t_f}{A} \leq 0.5 \tag{60}$$

The Equation (60) is only applicable for symmetric standard rolled sections with no significant fastener holes affecting the durability are present. This is a viable approach since the compression reduction is only needed for the vertical columns, which are always symmetric standard rolled sections.

4.2 Load types

This chapter covers the formulation of both the internal and external loads acting on the structure. Majority of the dimensioning guidelines are based on the Eurocodes which present approaches for design of structures of this magnitude. The standard dimensioning principles are covered only when applicable to the structure in question, which leads to a relatively case-specific representation of the standard methods. In between the Eurocode suggested guidelines, the extent at which these guidelines are used within the dimensioning tool is described.

Chapter 4.2.1 covers the effects of elevated temperatures and 4.2.2 covers assessing the structures' self-weight. Imposed loads, such as wind, snow and seismic, are covered in the chapters 4.2.3, 4.2.4 and 4.2.5. Live loading is covered in Chapter 4.2.6 and the load caused by the sway imperfections in the structure are covered in Chapter 4.2.7.

4.2.1 Temperature

The inside temperature has a significant impact on the durability of the main support frame. The main structure is made usually of structural steel S235 (EN 1.0038), which has poor capacity to withstand high temperatures. Therefore, the deviation in the member load resistance caused by high temperatures must be considered when designing the structure. Another effect of elevated temperature is the thermal expansion of the structure. Thermal expanding is *ideally* a process which causes linear increase in the length (and volume) of structural elements when they are heated. Within the scope of this thesis project, the thermal expansion is negligible due to two reasons. The ESPs with long spanning casings or high inner temperatures and thus large displacement caused by thermal expansion are supported much like bridges, with only one fixed connection to primary support structure. The rest of the connection points rest on sliders allowing the casing to expand freely and therefore thermal expansion does not cause additional stresses. See Figure 15 for illustration.

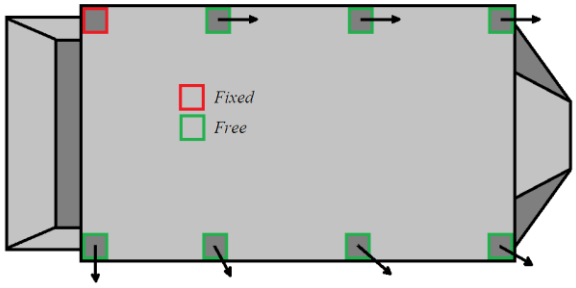

Figure 15: Casing thermal expansion joints

Additionally, it can be shown that globally isostatic structures with homogenous material, the thermal expansion of structural members is uniform and therefore does not cause forced displacement nor additional stresses to any of the members.

Temperature starts to decrease the effective yield strength of structural steel as it reaches 400 ℃ and the elastic modulus E as it reaches 100 ℃. Overview of the effects of high temperature on the effective yield strength, proportional limit and the elastic modulus is shown as a chart in Figure 16, to benefit understanding of their behavior. The table values are available in [23].

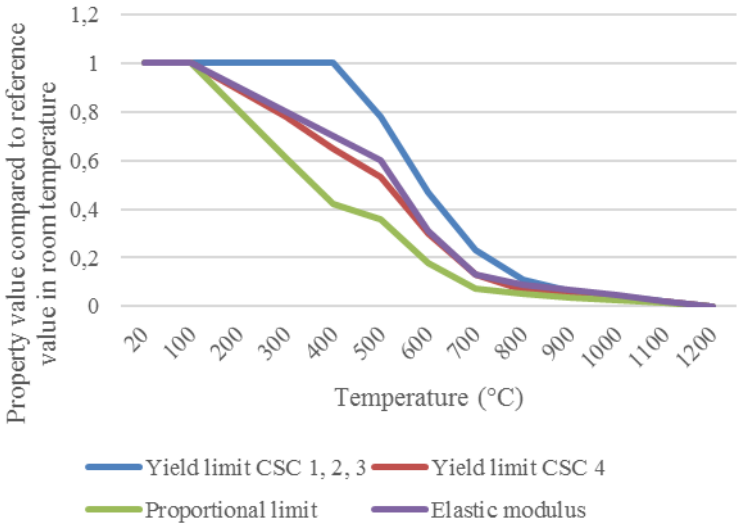

Figure 16: Effect of temperature on material properties

The figure shows the reduction of yield strength f_y, proportional limit f_p and elastic modulus E. The yield strength reduction is considered more influential with sections of CSC 4; thus, the reduction factors are specified separately. Temperature's effects on material properties are calculated using linear interpolation when the temperature is between the table values. Illustration of the different properties shown in the reduction figure are shown in the Figure 17 for general stress-strain curve of metal materials.

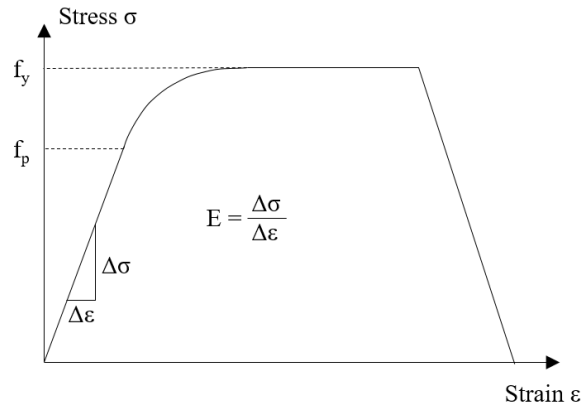

Figure 17: Stress-strain curve of a general metal material

The temperature inside the casing varies between $100\,℃ - 400\,℃$ so theoretically it should not affect the yield limit of members of CSC under 4. However, to stay on the safe side we formulate the reduction mechanism for all the properties to assure tool functionality even if the design temperature happens to increase in the future.

As illustrated in Figure 17, the linear response ends when the proportional limit is reached. Additionally, we can assume that the behavior is somewhat linear until the yield limit. When either of the limits is reduced due to the elevation in temperature, the area at which the utilized linear-elastic approach is applicable. When using the dimensioning tool, however, excessively elevated temperatures lead to tool's inability to find a suitable structure.

4.2.2 Self-weight

Self-weight forms the basic static load present on the system at all times. This chapter covers the methods used to evaluate the self-weight of the structure in an arbitrary configuration. Self-weight is often referred to as dead weight and it consists of the weight of the *structural and non-structural* elements of the system. The Eurocode 1 [18] states, that the self-weight of a structure should be determined according to the nominal dimensions and densities of all the structure parts. When conducting preliminary design where great deal of structure details is yet to be determined, the rule must be adjusted a little.

The self-weight calculation used within the dimensioning tool can be divided into two approaches. Nominal volume based calculation of those elements with known dimensions and estimation of masses of those elements with unknown dimensions or structure.

All the structural elements are calculated for their actual volume by using cross-section area data from tables and member length data from the wire model. Similarly, mass of one of the largest group of non-structural elements, collecting plates, is also calculated using actual dimensions, since they are easily available from the user-input dimension data.

The masses of the rest of the non-structural elements are evaluated based on historical data. This data was gathered by going through the 3D-models of numerous existing products and collecting the masses and surface areas of those parts. This data was then used to calculate average pressures caused by each of the non-structural elements. This included structures such as roofing, walls and insulation. Additionally, the emitting system was measured by comparing its mass-data to chamber volumes to end up with a density value to be used. This analysis of historical data resulted in a list of pressures that could ultimately be turned into masses when structure's global dimensions become available during the dimensioning tool execution.

The self-weight of the structural members is applied to each of the elements individually. The calculated weight of collecting plates and the approximate dead-weight of the structures above roof beams are applied to the FE-models of the frames according to the sizes of the fields connected to that portal. Wall masses are laid on the vertical column elements respectively and the approximate density of the emitting system is used to calculate the dead-weight of the emitting system and apply it to each of the roof beams, again, depending on the lengths of the connected fields.

4.2.3 Wind load

The contents of this chapter are based on the Eurocode [24], concerning wind loads on structures, unless stated otherwise. Even though the actual effects of wind are very complex due to the turbulent nature of high-speed winds and varying environment, the standard suggests highly detailed methods for estimating the pressure caused by the winds. This chapter covers the methods for calculating the effects of varying terrain, building shape, location and size have on the wind load acting on the structure.

The size of the wind load acting on a structure or its component is based on the fundamental basic wind velocity, which is used to calculate the set of pressures equivalent to the effect of the extreme turbulent wind. Wind speeds and pressures are based on the effect of both the constant and variable wind speeds. The value of the fundamental basic wind velocity $v_{b,0}$ is determined as the 10-minute mean wind velocity with an annual risk of being exceeded of 0.02 at a height of 10 meters above flat open terrain. The fundamental basic wind velocity is not direction dependent so it represents the mean wind in any direction at a given location. However, it should be noted, that the fundamental basic wind velocity is usually highly dependent of the location's altitude above sea level, and therefore the value should always be based on the data distributed by local authorities or the national annex (NA) of the standard.

If the wind conditions are subject to large seasonal or directional deviation, the fundamental basic wind velocity is corrected with season coefficient c_{season} and direction coefficient c_{dir}. The standard guideline is to set these coefficients to one if they are not supplied by the NA. This results in a conservative estimate of the wind velocity. Wind

velocity corrected with these coefficients is called basic wind velocity v_b. Furthermore, this basic wind velocity is corrected to account for the effect of terrain roughness and orography with correction factors $c_r(z)$ and $c_o(z)$ to receive the mean wind velocity (v_m). The equation for the mean wind velocity is determined in equation (61).

$$v_m(z) = c_r(z) \cdot c_0(z) \cdot c_{dir} \cdot c_{season} \cdot v_{b,0} \tag{61}$$

The mean wind velocity depends on the height of the observed point above ground, since the effect of surface roughness decreases the further the obstacles are. Mathematically speaking the coefficients of terrain roughness $c_r(z)$ and orography factor $c_o(z)$ are functions of the height above ground of the observed location. The default procedure for determining these factors is presented in the following paragraphs.

The value of the terrain roughness coefficient depends on the terrain category. The terrain categories are paired with values z_0 and z_{min} which represent the roughness lengths and minimum heights of obstacles in each of the categories. The standard also introduces a terrain factor k_r, which depends on the value of z_0 when compared to the same value of terrain category II. The classification of terrain types provided by the Eurocode 1-1-4 [24] are presented in Table 6.

Table 6: Terrain category classification

Terrain category	Explanation	z_0 (m)	z_{min} (m)	k_r
0	Sea or coastal area exposed to the open sea.	0,003	1	0,156
I	Lakes or flat and horizontal area with negligible vegetation and without obstacles.	0,01	1	0,170
II	Area with low vegetation such as grass and isolated obstacles (trees, buildings) with separations of at least 20 obstacle heights.	0,05	5	0,190
III	Area with regular cover of vegetation or buildings or with isolated obstacles with separations of maximum 20 obstacle heights (such as villages, suburban terrain, permanent forest).	0,3	5	0,215
IV	Area in which at least 15 % of the surface is covered with buildings and their average height exceeds 15 m.	1	10	0,234

The terrain factor is determined as shown in Equation (62)

$$\begin{aligned} c_r(z) &= k_r \cdot \ln\left(\frac{z}{z_0}\right) \quad for \quad z_{min} \le z \le z_{max} \\ c_r(z) &= c_r(z_{min}) \quad for \quad z \le z_{min} \end{aligned} \tag{62}$$

where, z_{min} depends on the terrain category and z_{max} is $200\ m$, which is considered the upper limit under which the approach in question is applicable. The Eurocode [24] suggests that the terrain category should be selected by evaluating the surrounding terrain up to 2 km in distance, and using the roughness data for selecting the corresponding category. The rest of the in-depth process of evaluating the terrain category is omitted due to the fact, that the tool is supposed to act according to the supplied terrain category, not select it.

While the terrain category assessment depends on surrounding obstacles, it should be noted that obstacles or features clearly representing hills or cliffs should be evaluated separately. These larger obstacles are referred to as orographic features. Due to the vast realm of different orography systems possible, the accounting for orography is omitted from the design tool and the effect of these features are not considered further. Accounting for orography is more of a detail-design phase task and thus we choose not to include the automatic orographic factor calculation to the dimensioning tool. However, if the orographic factor is available, the user is able to include it in the calculations.

As mentioned before, the wind pressure used for the dimensioning contains components from both the constant wind pressure and the fluctuating turbulent wind pressure. The pressure component caused by the constant wind pressure is called basic velocity pressure (q_b). It is a function of air density and basic wind velocity. The equation is presented in Equation (63).

$$q_b = \frac{1}{2} \cdot \rho \cdot v_b^2 \tag{63}$$

The degree of turbulent wind pressure component is presented as a function of altitude with a turbulence intensity profile $I_v(z)$.

$$\begin{aligned} I_v(z) &= \frac{k_I}{c_o(z) \cdot \ln(\frac{z}{z_0})} \quad for \quad z_{min} \leq z \leq z_{max} \\ I_v(z) &= I_v(z_{min}) \quad for \quad z \leq z_{min} \end{aligned} \tag{64}$$

where k_I is the turbulence factor which has a recommended value of 1 unless the NA states otherwise. From the Equation (64) it is seen, that the orographic features surrounding the structure (which result in a larger orography factor) in-fact decrease the turbulence intensity of the wind. This phenomenon is related to the fact that inclining ground increases the mean wind velocity near the crest of the hill and at the same time turbulence's deviation remains the same. With the turbulence intensity and basic velocity pressure we can now calculate the peak velocity pressure which is the primary loading value used when calculating the wind load:

$$q_p(z) = [1 + 7 \cdot I_v(z)] \cdot \frac{1}{2} \cdot \rho_w \cdot v_m^2(z). \quad (65)$$

To illustrate the effect of different terrain categories and structure heights to the wind pressure acting on the structure, the coefficients accounting for orography, terrain and wind turbulence can be gathered under one variable, the exposure coefficient $c_e(z)$, which when plotted provides a better perspective on the effect of structure height. By combining the definition of mean wind in equation (63) with equation (65) and (61) we get

$$q_p(z) = [1 + 7 \cdot I_v(z)] \cdot c_o^2(z) \cdot c_r^2(z) \cdot q_b. \quad (66)$$

$$q_p(z) = c_e(z) \cdot q_b. \quad (67)$$

When the value of the exposure coefficient is plotted with different terrain categories and heights the results are as illustrated in Figure 18.

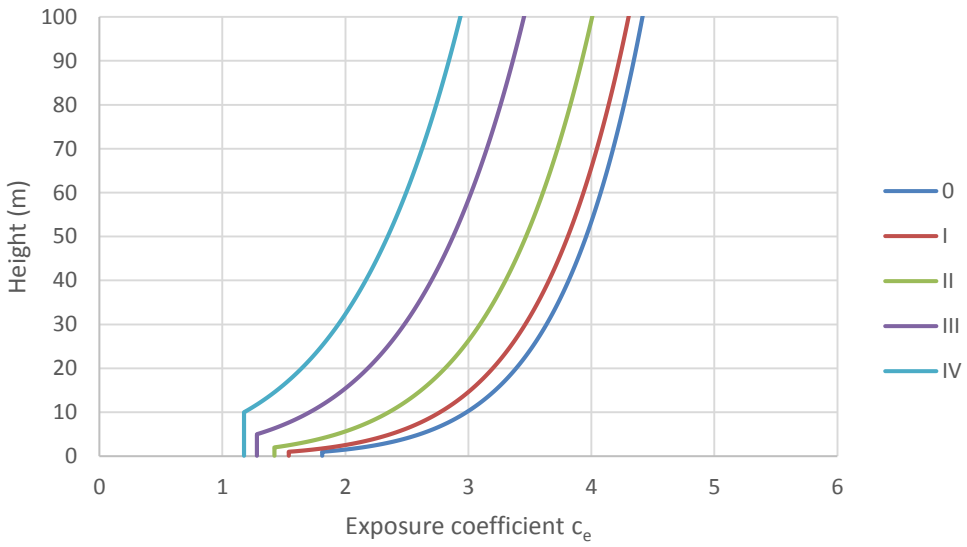

Figure 18: Exposure coefficient as a function of height on different terrain categories.

In Figure 18 the nature of the peak wind pressure calculation is seen clearly. Depending on terrain category, when certain altitude depending on surrounding obstacles is reached, the wind pressure peaks start to increase in magnitude. This is due to increase in turbulence and decrease in surface drag caused by the terrain obstacles. The exposure coefficient values are calculated with orography factor of 1, since the effect of orographic features usually present inconsistent changes to the wind pressures thus a graph considering those changes would not yield much value.

Rather than using variable wind pressure according to the height of different points on the surface and thus ending up with linearly increasing wind load, the standard suggests

that the wind pressure acting on the external surfaces should be determined according to a reference height (z_e). This pressure is corrected with pressure coefficient c_{pe} or c_{pi}, structural factor $c_s c_d$ and the force coefficient c_f. The pressure can then be used to evaluate the wind force F_w acting on the structure or its component on external (68) or internal (69) surfaces as follows:

$$F_{w,e} = c_s c_d \cdot c_{pe} \cdot q_p(z_e) \cdot A_{ref} \tag{68}$$

$$F_{w,i} = c_{pi} \cdot q_p(z_e) \cdot A_{ref} \tag{69}$$

Along with the normal wind force, the passing airflow causes frictional forces parallel to the surface. These forces are however typically quite meaningless for a rectangular wide-walled structure as the ESP. This is due to the fact that the large windward wall results in relatively large wind load resultants. Additionally, the internal wind loads are only meaningful with structures with openings, which is not the case during the usual operation of an ESP. The total wind force is calculated as a vector sum of all of the components $F_{w,e}$, $F_{w,i}$ and F_{fr}.The structural factor may be set to 1 for structures with structural walls that are less than 100 meters high and whose height is less than 4 times the length of the windward wall. This applies to all of the ESPs, so the structural factor is not included in the calculation.

When selecting the reference height z_e mentioned earlier, the standard suggests the following approach. The height-to-width-ratio of the structure in question dictates the selection of the reference height, unless the NA provides an alternative method. The Eurocode determines the reference heights in sections. This is done separately with structures of different height to width ratios, but the ESP structures generally fall into the last height-category which means that their height is over two times their overall width. The approaches of determining the reference height for this category of structures and the approach the dimensioning tool uses are presented in Figure 19.

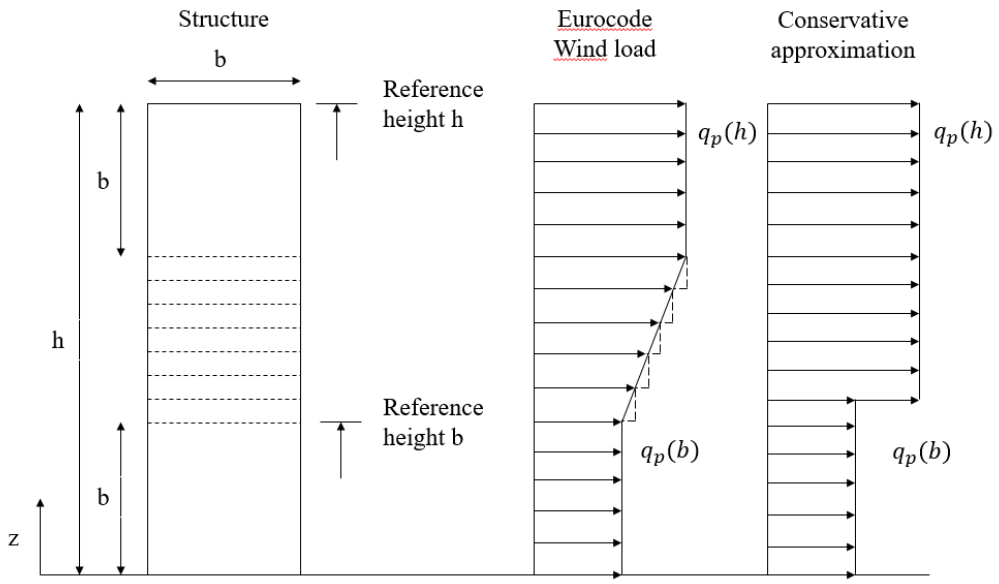

Figure 19: Reference height for structures with $h > 2b$

When the Eurocode approach is combined with the fact that the design tool is aimed for the preliminary design phase, we can omit the linear increase in the middle section between and consider it for the higher reference height. This approximation can be justified because it leads to much simpler programming because the same approach can be used for all the structure height regardless of the fulfillment of the assumption we made on the previous page of structure height being over two times casing width. Evidently the resulting wind load resultant is also larger and therefore on the safe side.

The external pressure coefficients used in Equation (68) are based on the aerodynamic properties of the structure or structure part in question. The coefficient is defined depending on the wind-exposed area of the component. The Eurocode provides the values of these coefficients for different structural parts with areas smaller or equal to $1\ m^2$ ($c_{pe,1}$) and larger or equal to $10\ m^2$ ($c_{pe,10}$). Since the tool focuses on global loading the exposure coefficients can be considered for the areas larger than $10\ m^2$. The standard provides values for the $c_{pe,10}$ for multiple different types of structures. For the purpose of this thesis, determining the wind load of vertical walls is the most important, thus, the pressure coefficients for vertical walls on different zones of the outer perimeter are shown in Table 7 and the different zones are illustrated in Figure 20.

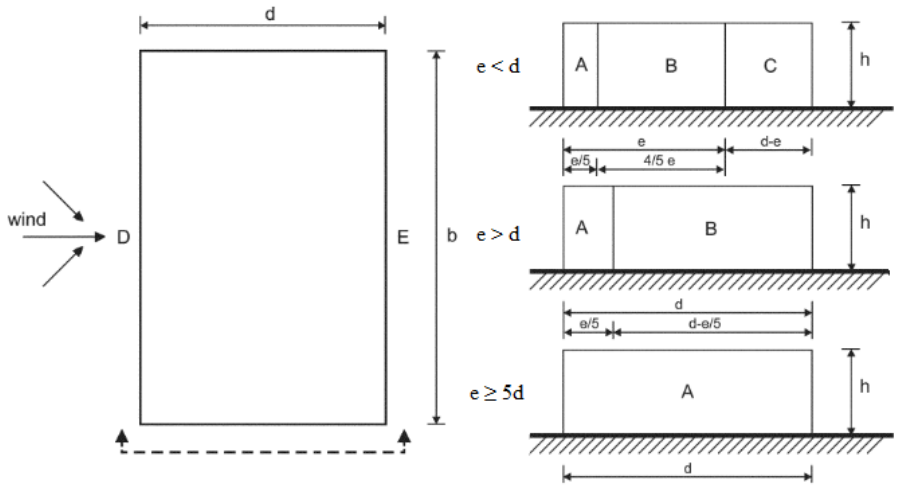

Figure 20: Pressure zones on vertical walls. Picture modified from [24]

For the purpose of this thesis, the most influential pressure zones are the ones with normal parallel to the wind direction.

Table 7: External pressure coefficients for vertical walls of rectangular structures

Zone	A	B	C	D	E
h/d	$c_{pe,10}$	$c_{pe,10}$	$c_{pe,10}$	$c_{pe,10}$	$c_{pe,10}$
5	-1,2	-0,8	-0,5	0,8	-0,7
1	-1,2	-0,8	-0,5	0,8	-0,5
≤ 0.25	-1,2	-0,8	-0,5	0,7	-0,3

As the table indicates, the wind velocity causes positive pressure on the windward wall and varying negative pressure on other walls of the structure. The negative pressure is caused by suction generated when the flowing air separates from the wall surface and creates pockets with negative pressure. If the roof is pitched, the height value used for determining the ratio is the peak height.

Within the scope of the dimensioning tool, we are interested only in the extreme effects wind load has on the structure which occur on the largest side surface of the casing. The wind load resultant is calculated according to the wall area of each of the fields so that each portal is opposed to half of the wind pressure acting on each of the corresponding fields. The wind load acting on the possible penthouse structure is divided in similar fashion while assuming, that the penthouse columns are collinear with the casing columns. Ultimately, the end-portals are additionally opposed to the wind pressure acting on the inlet and outlet nozzles.

4.2.4 Snow load

The contents of this chapter are based on the Eurocode 1-1-3 [19] covering the formulation of snow loading. Similarly to the approach used with wind load, we focus on a simplified model of snow loading. This includes omitting the case-specific snow drifting caused by neighboring structures and custom roof profiles. As the surrounding obstacles and roof structures increase in complexity, the changing geometry starts to generate aerodynamic shades. These shades allow snow to drift and therefore may increase local snow loads drastically. To maintain the ability to include possible drifting we incorporate a so-called exceptional snow load factor.

Snow load is seen as a slowly fluctuating vertical force acting on horizontal planar surfaces, in this case, the roof of the structure. The key factor influencing the size of the snow load is the site location. In order to predict the amount of snow present at the roof, the factors to be taken into account are the shape of the roof, its thermal properties and surface roughness along with the wind conditions on the area. The roof shape and its surface roughness affect the snow accumulation as well as drifting. The wind and heat properties affect the snow dispersion. The effect of the snow melting on the roof is neglected because the ESPs built on locations with snow present are always equipped with penthouse and thus the snow-laden roof is never directly above the hot casing.

The roof types used are flat, mono-pitched and duo-pitched. The Eurocode's approach on snow load modelling is covered for the parts that are applicable for these roof types within the assumptions we made about drifting and effect of neighboring structures. The basic order of the load modelling process is following:

- Determining the characteristic value of snow load at given location (s_k). This is done using data provided by local authorities or by conducting an actual statistical analysis on site.
- Determining the snow load shape coefficient (μ_i) in accordance with roof shape. This coefficient accounts for the increase or decrease in snow load due to drifting. The shape coefficient on different roof slope angles is illustrated in Figure 21 with both the extreme loading and normal loading cases.
- Determining the effect the structure's surroundings and wind conditions have on the drifting snow. These effects are taken into account with exposure coefficient (c_{se}). For used values see Table 8.
- Determining the design value for exceptional snow load via exceptional snow load coefficient (c_{esl}), which has a recommended value of 2 unless the NA provides an additional value.

The snow load analysis should consider both normal and exceptional conditions regardless of location. The exposure coefficient used to take wind conditions to account is determined for different wind conditions as shown in Table 8.

Table 8: Exposure coefficient

Topography	c_{se}
Windswept	0,8
Normal	1
Sheltered	1,2

The effect of roof angle to snow accumulation is taken into account with the shape coefficient which is determined separately for both the normal conditions and accidental snow accumulation.

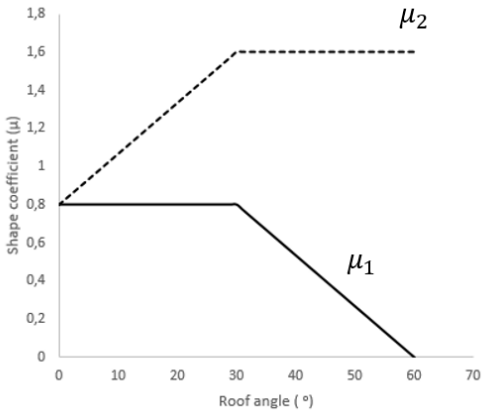

Figure 21: Shape coefficient for normal snow load μ_1 and extreme snow load μ_2

This chart is applicable for all roofs with flat sections, even with single or multiple pitches. As we concluded in the beginning of this chapter, all the special situations concerning the snow accumulation on roof are omitted. Along with neighboring structures, snow drifting could occur for example due to railings on roof or unorthodox surface geometry. These situations will need to be considered separately.

The dimensioning tool determines the snow load on roof according to the procedure presented earlier. The area-specific snow load values on ground are not automatically determined but the user is provided with extensive contour maps of both European and American regions containing the typical snow load values for different regions. From there the calculation is only matter of selecting the roof angle and wind conditions and changing the accidental snow load coefficient if need be. Similarly to other imposed loads, the snow loading is considered to be proportional to the lengths of fields neighboring the portal in question.

4.2.5 Seismic load

Seismic actions may prove to be very critical especially when designing structures on areas close to the edges of tectonic plates. Seismic loads occur as strong vibrations due to

release of large amount of energy when tension on earth's upper crust is suddenly released. The dislocation of tectonic plates causes acceleration to the foundation of the structure. While the direction of the acceleration of the foundation may be both horizontal and vertical, the horizontal acceleration has generally more influence to the design aspects. [25]

The severity of an earthquake is quantified with a logarithmic magnitude scale where an increase of 1 in magnitude represents ten times increase in dislocation of the foundation. In the design point-of-view, the relevant quantity concerning seismic activity is so-called peak ground acceleration (PGA). PGA value is location-dependent and different regions of seismic activity are presented in Figure 22 where the areas with high seismic activity are marked with red.

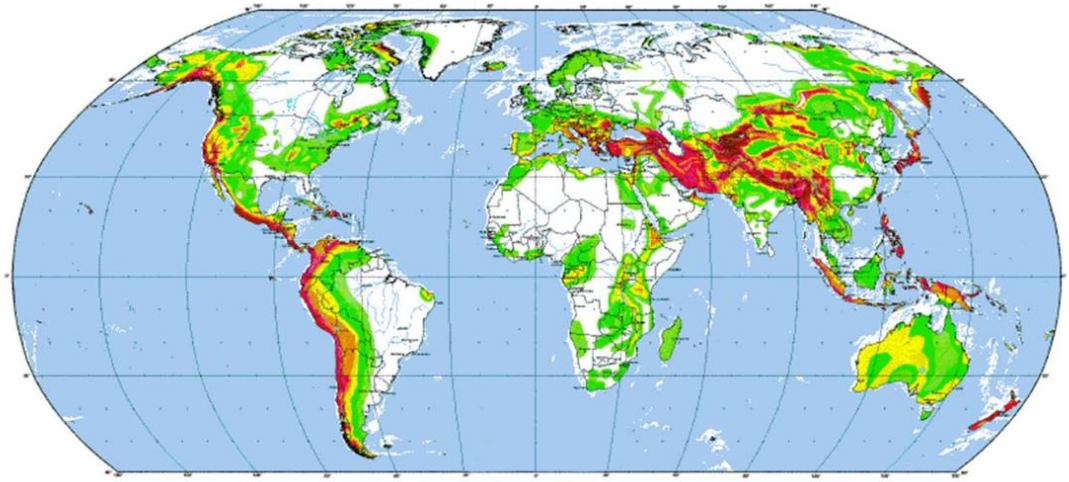

Figure 22: Illustration of global seismic hazard [25]

Along with the PGA value the seismic load depends on the following aspects: [25]

- Ground type
- Structure importance
- Distribution of mass
- Stiffness properties

These aspects affect directly to the dynamic properties of the structure in seismic situations. Ground types are defined in [26] according to a classification with 7 classes. The primary classes go from A to E with A being rock and E being soft soil and the additional two classes are marked for special evaluation. The importance classification is like the one mentioned when describing the limit state design process in Chapter 4.1.1 and it's considered via direct multiplication with the PGA value thus increasing or decreasing it [18]. For industrial structures as the ESP, we use importance multiplier of 1. Mass distribution has direct effect on the dynamic response of the structure via the acceleration on its foundation. The so-called seismic mass is calculated from dead load and parts of live

loading in order to anticipate the effect of inertia when the structure is subject to acceleration. The greater the seismic mass is, the larger is the structures inertia and thus the shear force on the foundation anchors. Seismic mass consists of the total dead load of the structure in question, 25 % of the live loading, 20 % of the snow load if its intensity exceeds 1,44 kN/m^2 and the total weight of all the structures residing on top or in direct contact with the structure [27].

The selected approach of the seismic analysis is the so-called lateral force analysis (LFA) for various reasons. Firstly, the LFA is a simple method based on static analysis and is therefore suitable for the mathematical model the tool uses. Additionally, carrying out intricate analysis for preliminary phase with relatively uncertain geometrical data to begin with would seem exaggerated. The required accuracy for seismic analysis should always be based on the criticality of the structure and the accuracy of the mathematical model. Furthermore, as we are developing a tool used for the design process of only a section of a structure, we would need additional mathematical model to represent the whole support structure to effectively estimate the global effects an earthquake would have.

The basic concept of the LFA method is to replace the dynamic load and response with equivalent static force system with the same ultimate deformation shape. LFA is based on an assumption of the lowest mode of natural vibration being the dominant one. The time period T_1 of this so-called first vibration mode is calculated via either modal analysis or some kind of estimation based on the structure type. Ultimately, this time period is used in unison with design response spectrum (Figure 23) to work out the acceleration acting on the seismic mass of the structure. Resulting seismic load is then applied in the structural analysis. [28]

The elastic design response spectrum for ultimate limit state is defined in Eurocode 8 [26] per three period times (T_B, T_C and T_D) and soil factor (S). The resulting idealized spectrum for horizontal acceleration is shown in Figure 23 along with the equations for different sections of the spectrum. The equations are following

$$S_d(T) = \begin{cases} a_g \cdot S \cdot \left[\frac{2}{3} + \frac{T}{T_B} \cdot \left(\frac{2.5}{q} - \frac{2}{3}\right)\right] & for\ 0\ \leq T \leq T_B \\ a_g \cdot S \cdot \frac{2.5}{q} & for\ T_B \leq T \leq T_C \\ a_g \cdot S \cdot \frac{2.5}{q} \cdot \left[\frac{T_C}{T}\right] & for\ T_C \leq T \leq T_D \\ a_g \cdot S \cdot \frac{2.5}{q} \cdot \left[\frac{T_C \cdot T_D}{T^2}\right] & for\ T_D \leq T \leq 4\ seconds \end{cases} \quad (70)$$

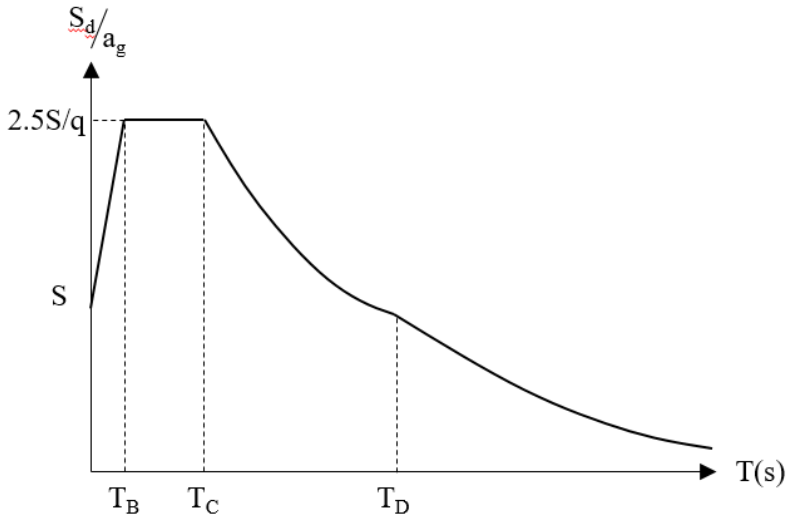

Figure 23: Elastic response spectrum, general shape

The purpose of the design response spectrum is to mimic the actual response spectrum with this idealization formulated according to the ground type under the structure. In the equations shown in (70) T_n is the vibration period of the nth vibration mode, a_g is the ground-type specific PGA value for ground type A and q is the structure's behavior factor. The Eurocode [26] suggests two types of elastic response spectra to be used when analyzing the seismic behavior in ultimate limit state of a structure and the corresponding period values and soil factors are presented in Table 9.

Table 9: Soil factors and vibration periods to be used for type 1 and type 2 horizontal elastic response spectra [26]

Ground type	S	$T_B(s)$	$T_C(s)$	$T_D(s)$	S	$T_B(s)$	$T_C(s)$	$T_D(s)$
A	1,00	0,15	0,40	2,00	1,00	0,05	0,25	1,20
B	1,20	0,15	0,50	2,00	1,35	0,05	0,25	1,20
C	1,15	0,20	0,60	2,00	1,50	0,10	0,25	1,20
D	1,35	0,20	0,80	2,00	1,80	0,10	0,30	1,20
E	1,40	0,15	0,50	2,00	1,60	0,05	0,25	1,20
Spectra type	1				2			

Similar response spectrum is defined for the vertical seismic actions by replacing the 2,5 multiplier appearing in the equations presented in (71) with multiplier of 3 and the horizontal PGA value (a_g) with the vertical PGA value a_{gv}. The behavior factor is incorporated in to the elastic response calculation to predict the structure's ability to dissipate energy. While the definition of the behavior factor is largely dependent of the structure ductility as well as support configuration, standard uses the behavior factor as a way to reduce the response spectrum to meet the requirements of elastic analysis and therefore behavior factor should be selected between 1 and 2.

Now that both the design elastic response spectra have been formulated for type 1 and type 2, the lowest vibration period-time is used to find the appropriate acceleration acting on the structure. Due to the fact that the analysis of the dynamic properties of the ESP casing falls outside the thesis scope we must settle for reference values from old structural analysis calculations concerning the ESP. Generally, a time-period of 1 second is the most commonly used.

On the application side, the tool utilizes a locally common method of setting the behavior factor to 1.5 but leaves the freedom of selecting alternative input to the user. Similarly, the dominating time-period is set to 1 second but the value is also changeable by the user. The tool applies the vertical and horizontal seismic loads to the roof beams according to the dead-weight above them combined with the mass of collecting system and emitting system and parts of live loading as explained earlier. The seismic load of the vertical columns is applied according to the weight of the wall structures and column self-weight. It should be noted that this type of seismic analysis is not sufficient for detailed seismic calculation, but gives a rudimentary idea of the seismic loads acting on the structure.

4.2.6 Live load

The terms ‘live load’ or ‘imposed load’ are often used to refer to a non-static load acting on a structure without further limitations placed to its origin *or* the load caused by the presence of people. In this thesis, live loading is used to refer to all the non-static loads except those addressed in the earlier chapters, ergo snow, wind and seismicity. The distinction between other imposed loading types is necessary, since the standard requires the additional live loading to be considered separately. The formulation of live loads is based on the Eurocode 1 [18].

In a way, live loads consist of what’s left of dynamic loading, in this case the ash congregation and moving people and equipment. The weight of congregated ash is one of the most influential loading factors of the whole system. When compared, for example, to the weight of the collecting plates, the right kind of ash could account for loads over 25 % of the magnitude of the dead weight of the plates (5 mm ash film on 1.5 mm collecting plate with as density of 300 kg/m^3). Due to the complex and unpredictable nature of the ash congregation and live loading in general the load magnitudes are assessed with approximate and conservative evaluation methods. What this means is that we expect the structure to undergo the worst loading cases during its service time. Examples of such unpredictable events could be the ash arching inside the inner structures, ash congregation on unpredictable places like electrodes or unexpected presence of heavy equipment on the structure roof.

The calculation behind the ash mass on plates evidently relies on the assumption that the congregation occurs in a uniform manner to all the plates, which is most likely not the

situation, but the approximation is conservative. Additionally, the ash could be accumulating to the bottom hopper where it would be outside of the scope of this thesis, but with a flat bottom structure could still have an effect on the floor beam and thus inner truss bracing. All of these cases are checked during the calculation procedure of the dimensioning tool. The densities, such as the ash density and weight of people are based on characteristic values.

The actual calculation concerning the magnitude of live loading is based on user-defined values of ash film thickness and ash density. The people and equipment on roof are expected to occupy all the accessible parts of the roof area. The default value for accessibility percentage of the roof is 80 % based on historical data. The distributed load used for the roof areas caused by people is based on area type classification provided in Eurocode 1 ([18] p. 31). The roof space can be classified as an area where people may congregate and the characteristic value should be between 2 kN/m^2 and 3 kN/m^2.

4.2.7 Imperfection load

Imperfections in the geometry of the structure are considered in linear-elastic analysis for the global imperfections only. Linear-elastic analysis relies on an assumption of the structure maintaining its original geometry under loading, so the method of accounting for so-called sway imperfections is to use an additional vertical load caused by the swaying of the frame. The approach presented in Eurocode 3-1-1 [2] p. 33 uses approximate methods to link the total vertical force to the horizontal load caused by imperfection of geometry. For global initial sway imperfection loads, we use Equation (71)

$$H_i = \phi N_{Ed} \tag{71}$$

where H_i is the horizontal load caused by vertical imperfections and ϕ is the global initial sway imperfection factor. The factor is defined as follows:

$$\begin{aligned} \phi &= \frac{1}{200}\alpha_h \sqrt{0{,}5\left(1+\frac{1}{m_c}\right)} \\ \alpha_h &= \frac{2}{\sqrt{h_s}}\ but\ \frac{2}{3} \le \alpha_h \le 1{,}0 \end{aligned} \tag{72}$$

where α_h is the reduction factor for height, h_s is the structure height in meters and m_c is the number of columns in a row. It can be seen from the definition of the reduction factor for height, that for structures that are higher than 9 meters tall, the lower limit presented is effective and thus we can simplify the Equation (72) for two-column portal such as presented in Figure 4 as follows:

$$\phi = \frac{1}{200}\frac{2}{3}\sqrt{0{,}5\left(1+\frac{1}{2}\right)} = \frac{\sqrt{3}}{600} \approx 0{,}0029.. \quad (73)$$

The height of and ESP is practically never under 9 meters, so for added simplicity we can use the sway imperfection factor shown in Equation (73) in all the cases.

5. DIMENSIONING TOOL

Along with a general survey on configurators, this chapter covers the functionality of the dimensioning tool. Along with the required input and generated output, the solver topology and the accuracy of the calculations are addressed.

5.1 Configurators in general

The design tool created as a part of this master's thesis represents a type of product design configurator. Configurator is a software-based expert system, a piece of artificial intelligence capable of some level of decision making concerning a product or product family. The exact functionality and the depth of design process varies from intricate detail-oriented processes to more approximate high-level design processes such as in the scope of this thesis. Configurators are mainly used in mass customization and they provide improvements in the design process in the fields of time, quality and preservation of knowledge. [29]

Configurator oriented design shifts the design process' goal from designing a single product to designing a generic product architecture. What this means is that we need to establish a realm of possibilities of design selections and their effects on product properties. Then we need to set range of allowed selections inside this realm of possibilities based on rules concerning the product properties. This range could be, for example, the fixed set of beam profiles selectable for vertical columns. We need to generate a standard interface for component interaction as well as the combined effect of component selections to the product properties. This is to be done so that certain changes in design selections inflict corresponding changes in product properties and when these product properties are compared to the desired ones we may acquire an optimal solution (See Figure 24). [30]

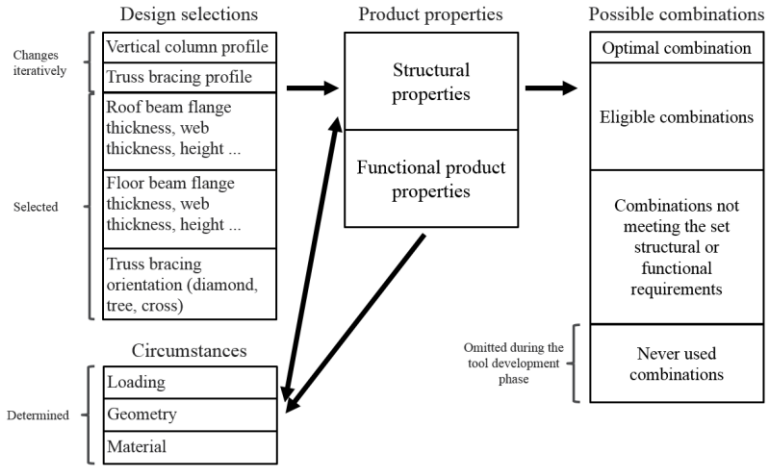

Figure 24: Functionality of a configurator

As shown in Figure 24, a common goal for all configurators is to generate an optimal solution for a design situation under arbitrary circumstances using predetermined fixed set of design elements of which the complete solution is formulated. What differs between configurators is the definition of the word optimal. Optimal solution is usually one that is the most accurate and requires the lowest amount of resources. However, these two properties typically are directly dependent of each other so that when accuracy increases, so does the solve time (amount of resources). This results in a situation where one must evaluate the significance of each property and compromise.

In a way, the process of designing a configurator leads us to a situation where we have already designed number of different variations of the product without ever even thinking about these variations.

5.2 Tool functionality

The basic functions of the developed configurator tool can be divided into two main objectives; determining the loading and determining the structure's response to the loading as illustrated in Figure 25

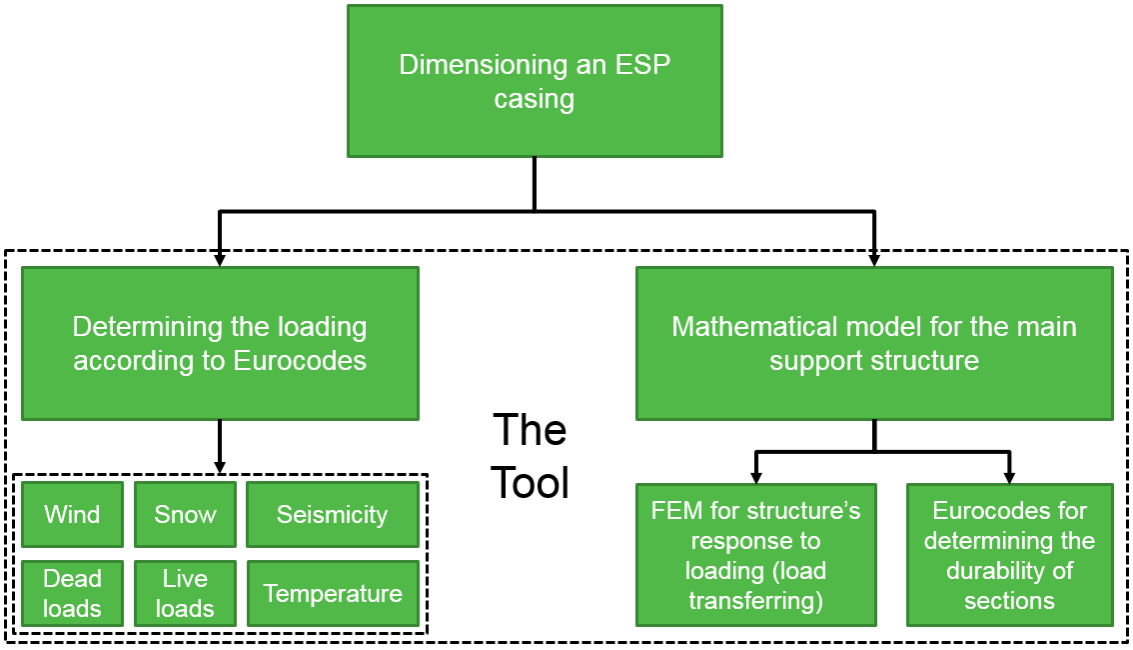

Figure 25: The functionality of this configurator

The path taken to achieve these two objectives includes smaller secondary objectives covered individually in the next chapters. In general, the tool is developed to be as user friendly as possible. The user-interface utilizes a single user-form where majority of the input is supplied. The amount of required input is kept at the absolute minimum and data-validation is used where possible to prevent odd behavior due to misinformed input. All

the cells containing sheet equations able to affect the calculation procedure are on hidden worksheets not visible to the user.

5.2.1 Geometry generation

The nominal dimensions form the backbone of the casing geometry and they are provided with a standardized ESP-code containing the main functional details of an ESP. The input fields are restricted by using drop-downs to make the tool easier to use and to avoid wrong input. The product code input field is shown in Figure 26.

Figure 26: Product code fields

The input values from left to right are number of fields, nominal field length, collecting plate type class, collecting plate spacing, nominal field width and nominal height. These values are so-called functional dimensions selected based on the required product properties. What this means is that the casing width, for example, represents the distance across the casing from the inner flange of the first vertical column to the inner flange of the second. This results in the need of correcting the distances to represent the centerlines of the sections for the wire mode. The correction is based on current profile selections for each structural member. The user can change the currently selected profiles from the settings menu's 'Profiles' tab, which is shown in Figure 27. This selection concerning vertical columns and inner bracings naturally only has an effect when using the 'Check structure –mode'.

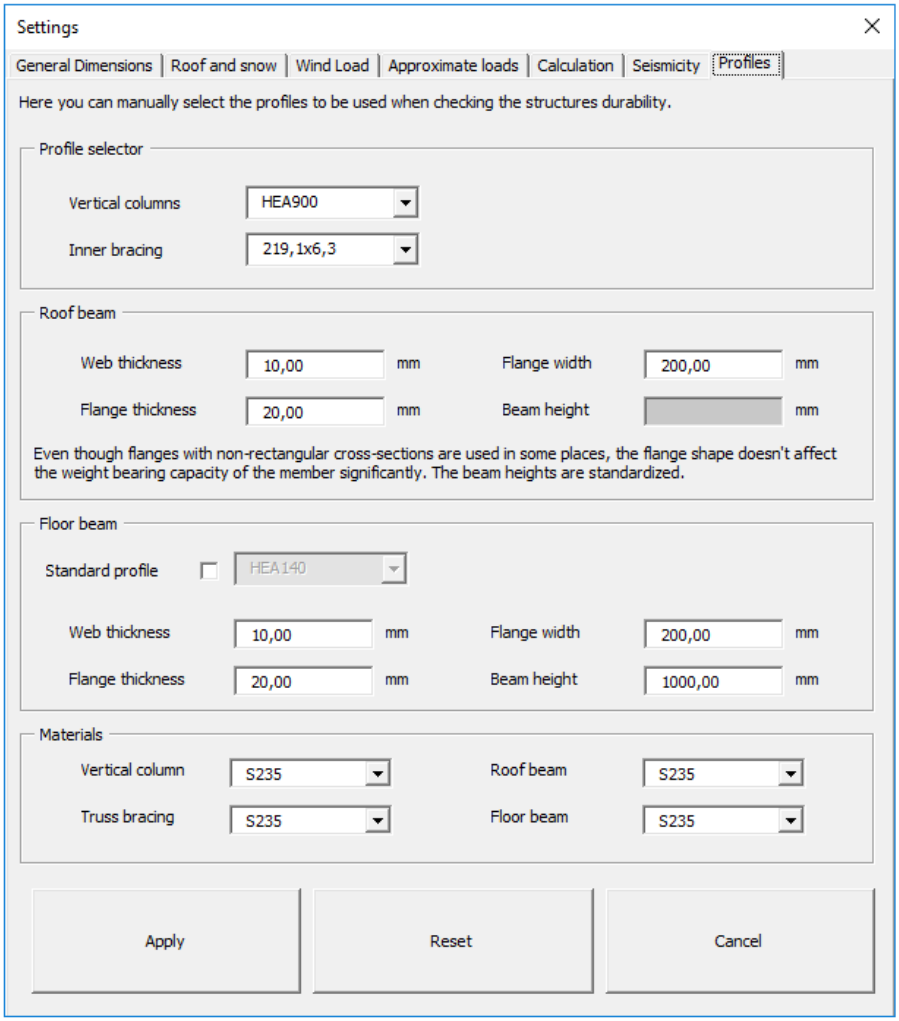

Figure 27: Profile preset selection

The user has an opportunity to alter the welded sections used for roof beams and floor beams. Additionally, the tool is required to accept variable field lengths and collecting plate spacing. This information does not fit to the format of the ESP-code so the individual field dimensions are entered through the settings menu. The form is shown in Figure 28.

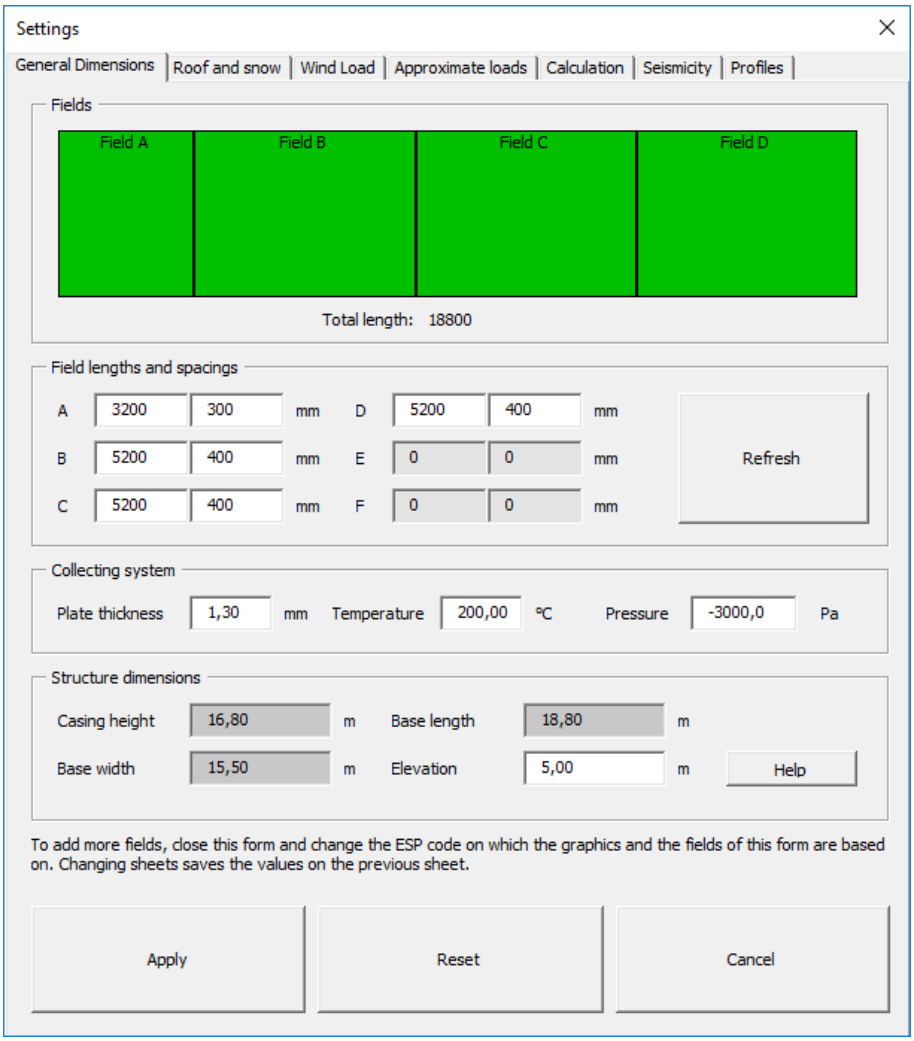

Figure 28: Additional geometry data

Here the spacing and field lengths can be set separately for all the fields and the form displays visualization of the casing as well as the structure dimensions based on the profile selections and nominal dimensions. The elevation height is used with wind load reference height calculation and contains both the primary support structure height and the height of any structures under the ESP.

Finally, the user must select the configuration of inner bracings to be used within the design. User is supplied with numerous different setups of bracing placement, so that the portals not neighboring the nozzles (mid-portals) have 6 different configuration options and the portals neighboring the nozzles (end-portals) are only horizontally braced to avoid interfering with the equipment situated there. The selection option panel is shown in Figure 29.

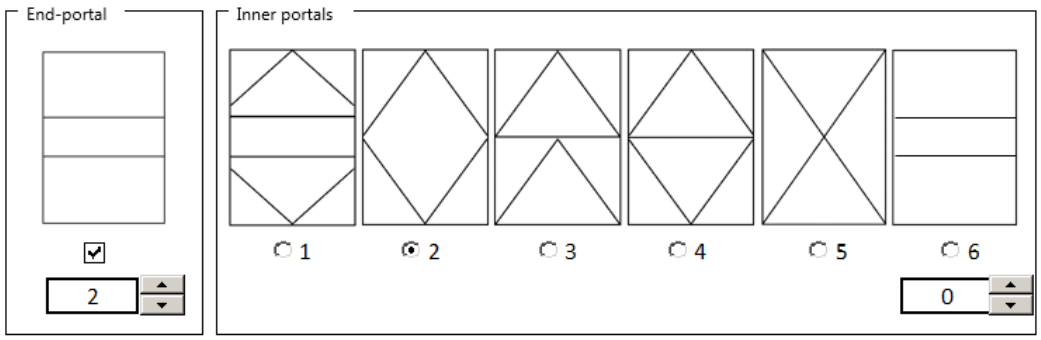

Figure 29: Support configuration selector

The user can set the number of horizontal end-portal bracings from none to four and the wire model will change accordingly. Similar range of horizontal bracings is also available for the mid-portals when the configuration number six is selected.

5.2.2 Cross-section properties

The cross-section properties are divided to three classes according to their source: static properties, system-dependent durability properties and environment-dependent durability properties.

Static properties represent the dimensions, cross-sectional areas, second moments of area, section moduli and buckling curves that are considered constant regardless of loading or time. The static properties are stored to the profile tables from where the data is retrieved when needed. The calculation operations referring to the cross-section properties are formulated so, that changing the profile sets does not affect the calculation. In other words, the profile data is completely independent and this makes it easy to change from standard profile set to another if needed.

System-dependent durability properties consist of the design resistance values calculated in accordance to Chapter 4.1.3. These properties are descendants to the static properties as they are only dependent of the geometry of the cross-section and temperature-corrected strength values. Therefore, these properties can be calculated before the tool has access to external loading data. The tool is programmed to evaluate both the plastic and elastic resistances to all the sections. When running the solver sequence, the tool then selects the proper resistance value according to the cross-section class of the member. The temperature-dependent strength values are calculated according to the user-defined member material selection and casing temperature based on linear interpolation on the standard provided temperature reduction data.

Ultimately, environment-dependent durability properties consist of the cross-section class and reduced resistance limits. The CSC depends on the loading state of the member and can therefore be only calculated when the loading state has been solved. The reduction in

the yield strength depends on the shear force acting on the element and similarly the reduction in bending resistance is connected to the axial loading state. The reduction methodology is addressed in detail in the Chapter 4.1.4. These values are evaluated respectively for each of the elements to avoid the problem of proving explicitly that a certain element is the most critical. The solving sequence involving also the element durability evaluation is considered separately in Chapter 5.2.5.

5.2.3 Loading

The external loading calculation is implemented in such manner that the required user input is at the absolute minimum but in the same the input could still be supplied should the user want to. The details on the actual loading value calculation are addressed in detail in the Chapter 4.2. In this chapter, we focus on the application side of the loading calculation and go through the loading input tabs from the settings menu of the dimensioning tool. The first input tab contains the roof structure related inputs and the snow load calculation. See Figure 30.

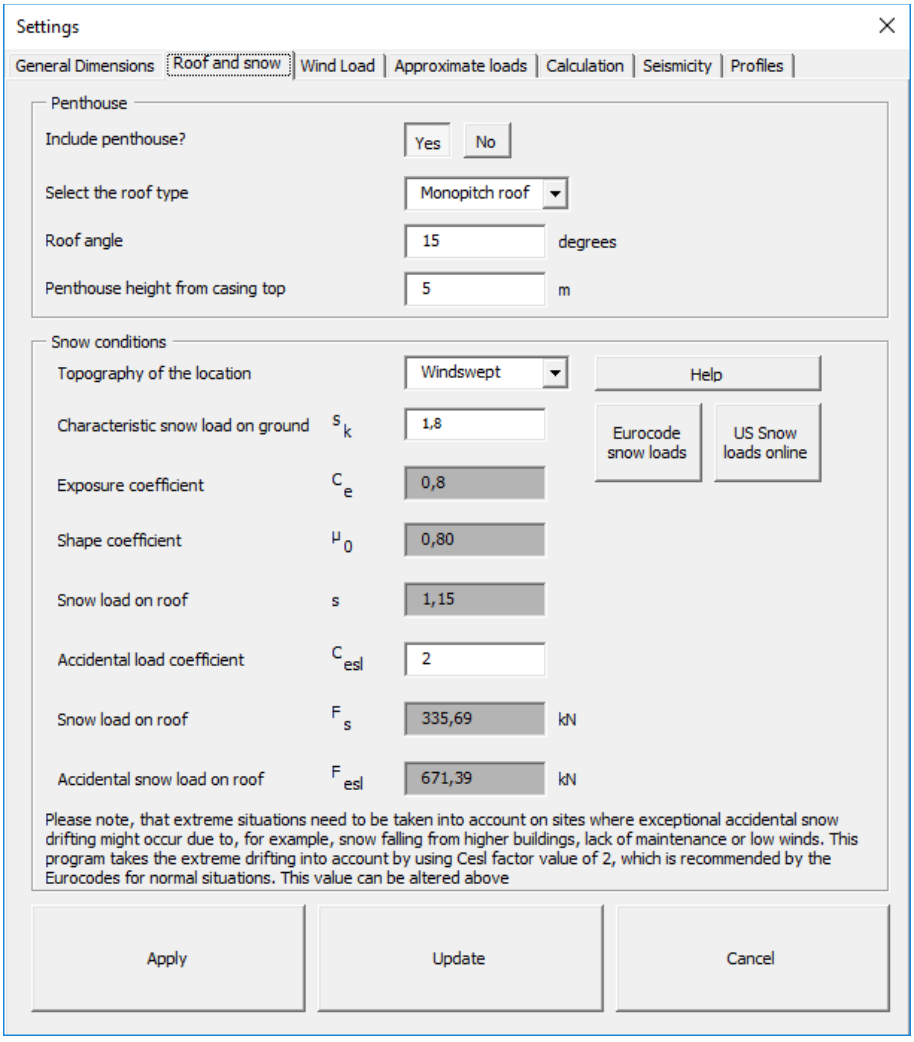

Figure 30: Roof geometry and snow load

If the ESP has a penthouse, the effective surface area for imposed loading changes drastically. In addition, including a penthouse to the structure shifts the possible snow load from the casing roof beams to the penthouse roof. This is all done automatically based on user input.

The casing roof is always flat, but the penthouse roof could be inclined and thus an option of setting the roof angle is included within the input parameters. As described in the snow load chapter 4.2.4, the snow load acting on ground level is modified according to the roof angle, and the wind conditions of the system.

The penthouse calculation relies on an approximation of its structure, since actual structure details are not available during the preliminary design. The penthouse structure is divided into frame portals in a similar fashion to the main portal frames and opposed to the same wind load as the rest of the structure added with the possible snow load on the roof and the penthouse roof structure dead weight. The FEM-solver outputs the base loads individually for each of the penthouse frames (see Chapter 5.2.5). The resulting base loads are later added as point loads to the primary frame portals. The individual analysis of each of the penthouse sections enables us to account for the possibly changing field lengths and thus changing imposed load resultants on different penthouse portals.

The wind load calculation is similarly as automated as possible. The reference heights are suggested by the program itself based on the wire model generated according to earlier input. All the coefficient values are proposed but left changeable for situations where the values proposed do not apply. When the user provides the terrain category of the target build site as well as local fundamental basic wind velocity, the tool calculates the basic wind pressure as well as peak wind pressures for each of the reference heights, if there are multiple. Tool also displays the wind load resultants acting on the whole structure. The resultant values are not used in the calculation but they are provided for quick calculation control and the possibility to export these load values elsewhere. The wind loading form is shown in Figure 31.

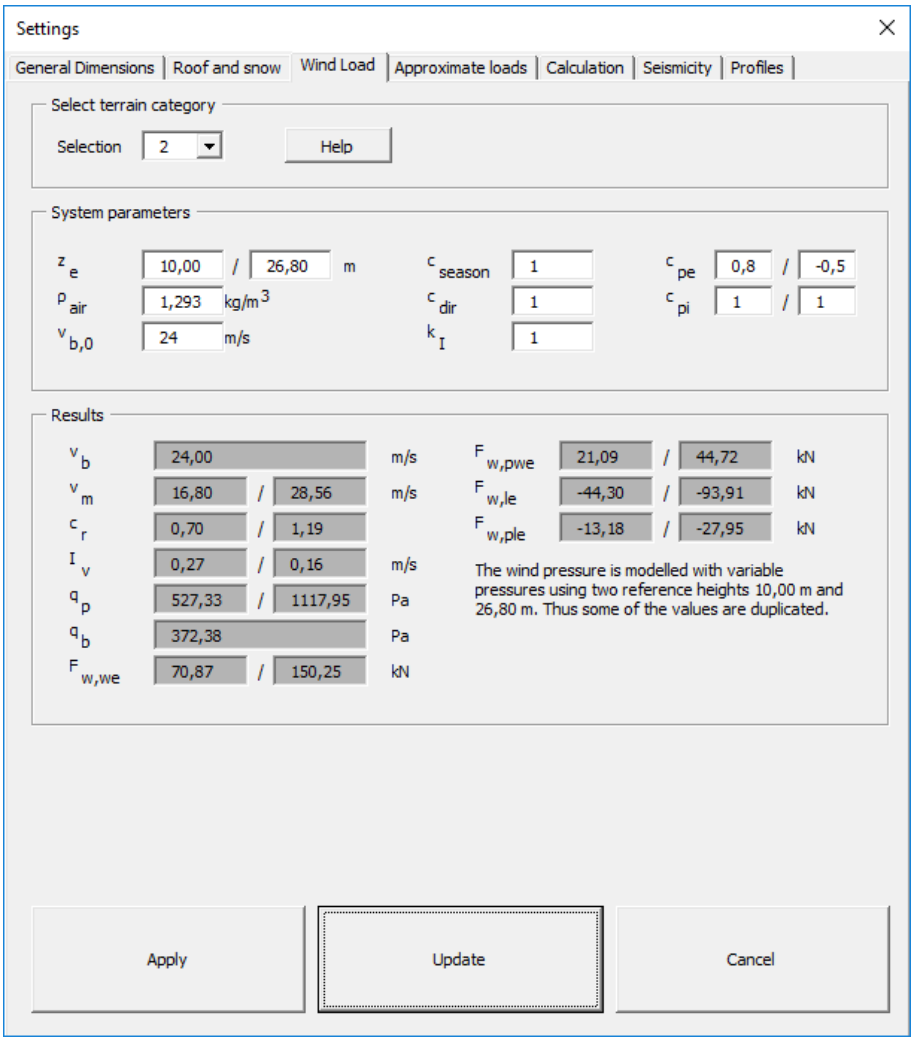

Figure 31: Wind load input

As seen from the figure above, the user has the possibility to alter the seasonal and directional factors as well as the pressure coefficients where needed, but the recommended values of one are set as a default. External pressure coefficients for both the windward and leeward wind direction are selected based on the structure's shape.

The next input tab concerns the approximations of the dead-loads caused by the secondary structural members and non-structural elements. This tab contains all the mass data related to different parts of the structure with no exact geometry available during the preliminary phase. See Figure 32.

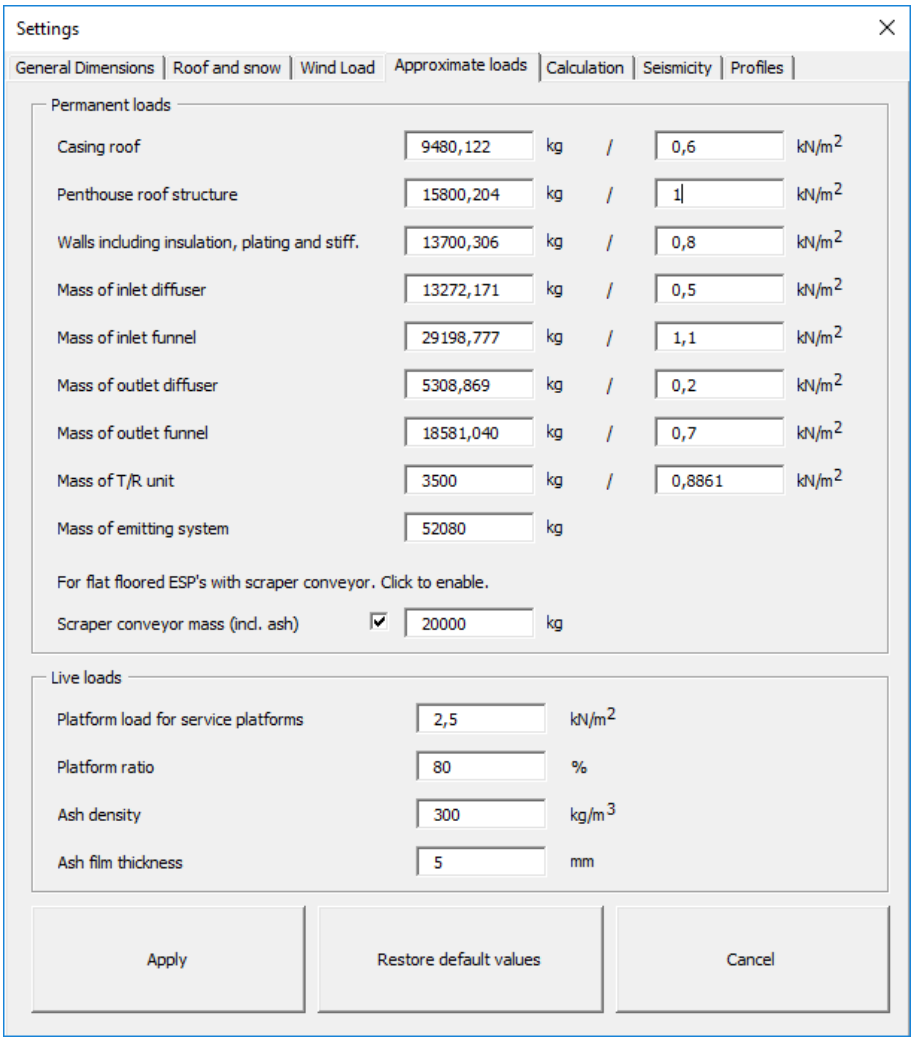

Figure 32: Approximate load input

The user is able to input the total dead weights in masses directly or as pressures for convenience. The pressure inputs are enabled to promote usability, since the data about approximate structure masses is commonly available as pressures. When either of the values is changed for any of the elements, the other one is automatically calculated based on the geometry of the part. The tool is able to suggest some rudimentary pressures based on historical mass data as explained in the Chapter 4.2.2. The pressures are calculated by comparing the actual masses of, for example, casing roof structures and comparing them to the casing roof areas. The used pressures were acquired by calculating the average pressures of each of the ESP parts from multiple existing ESPs. While this data is not necessarily of the most accurate nature, it might be the best we have for the time being.

Along with the dead loads, the tab pictured in the Figure 32 also contains the live load (people and equipment) estimation as well as the input fields for ash congregation. The live load pressure is based directly on standard suggested values and the platform ratio is used to estimate the area accessible for people to enter on the roof. The 80 % platform ratio is also suggested by the tool when default values are restored and it is based on similar historical analysis as the average weights. The ash density and ash film thickness

is used with the collecting plate dimensions to generate an estimation of the ash mass on congregated on the collecting plates.

The final loading related input tab is the seismicity tab. The calculation is solely based on the ground type, PGA and time-period inputs. As mentioned, the used can supply different values to the suggested importance factor and behavior factor. The forces acting on different parts are based on the seismic mass calculated separately. See Figure 33.

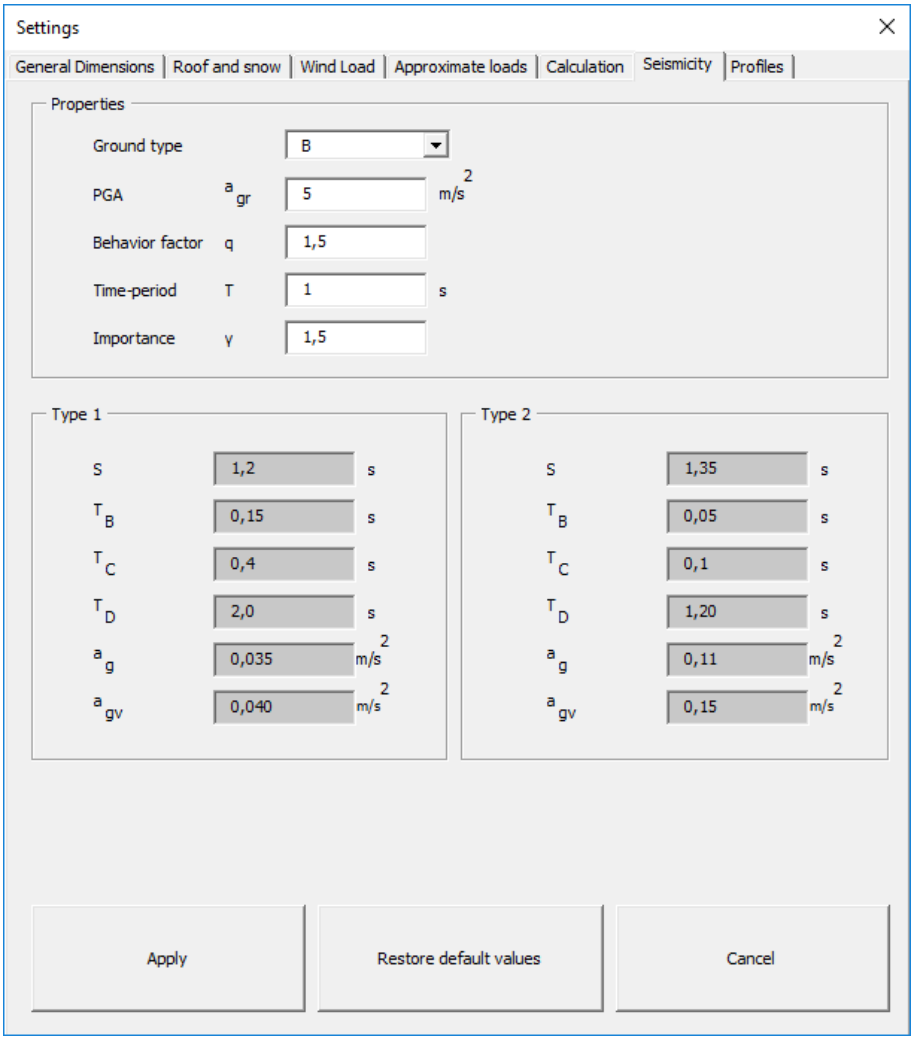

Figure 33: Seismic loading input

The spectrum values are supplied for reference. When the user presses apply or leaves the tab, both of the spectra are generated automatically and the imposed acceleration as well as the force resultant is calculated behind the scenes.

5.2.4 Calculation options

To make the tool as versatile as possible but simultaneously adequately foolproof, only some of the calculation options are left for the user to alter. As mentioned before, all the

calculation is hidden from the user and the dimensioning tool acts as a black box taking input and displaying output. The calculation options tab is shown in Figure 34.

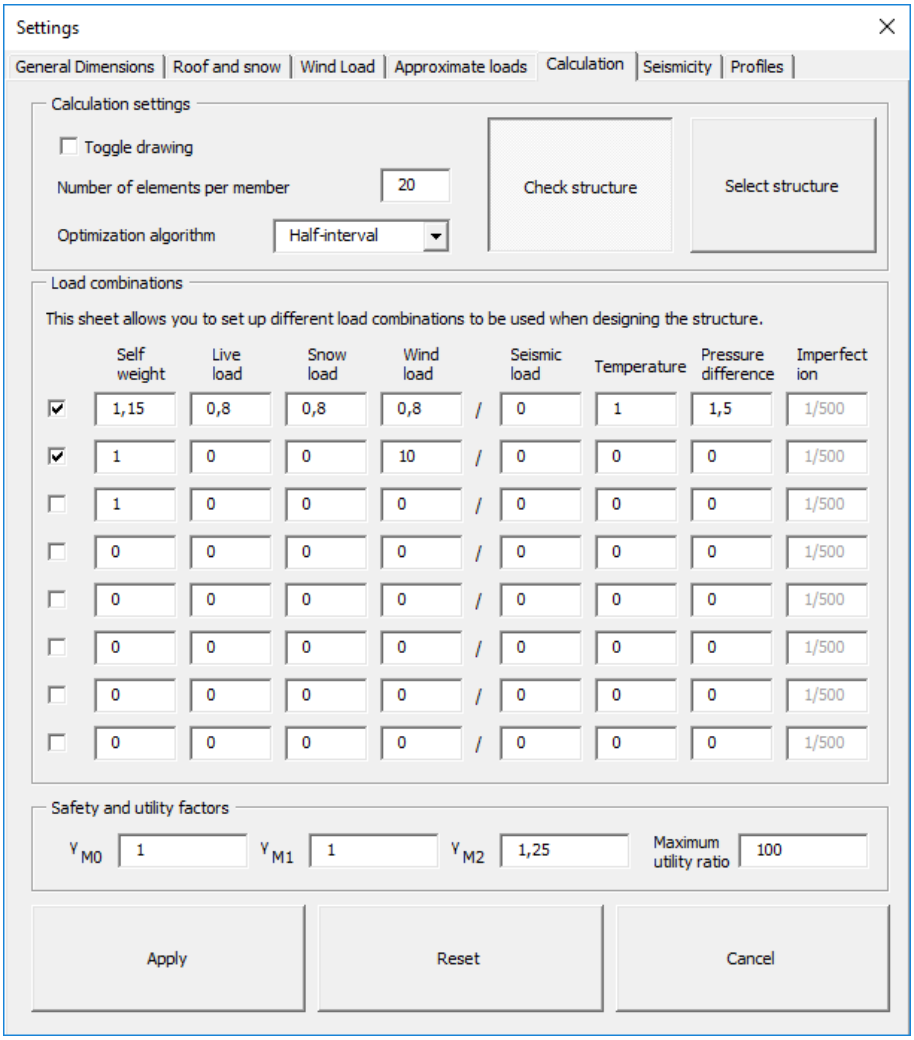

Figure 34: Calculation options

The options left for the user to alter are the calculation mode, drawing mode toggle, optimization algorithm and the number of elements used per member with the FEM-model. The calculation mode determines whether the tool checks the utility ratios for user-provided profiles or selects the profiles to fulfill the user-determined limit for maximum utility ratio. The optimization algorithms include both the naïve iteration and half-interval search presented in the Chapter 5.3. If the drawing mode is turned on, the tool plots the deformed shape of one of the portals and colors it in accordance to internal loading but this only works with low number of elements due to Excel's limitations. It should be noted that the drawing mode slows the tool down significantly.

Aside from the options directly related to calculation approach used, this tab also contains the loading combinations user wants to analyze. Eight different combinations of the loading components can be analyzed at a time. Each of the loading types is given an individual multiplier. Under the loading state properties, the user can also supply the partial safety

factors for resistance limits and the maximum utility ratio used with the ‘Select structure -mode’.

5.2.5 FEM-Solver

The mathematical approach used by the FEM-solver is described in detail in the respective theoretical chapter (see chapters 3.1.2 and 3.2). The most important requirements for the solver were standalone implementation and completely hidden execution. What this means is that the general implementation is formulated so, that the solver itself can be utilized easily elsewhere. When the solver runs, the user does not have to understand how it works.

The general workflow of the solver and its components is shown in Figure 35.

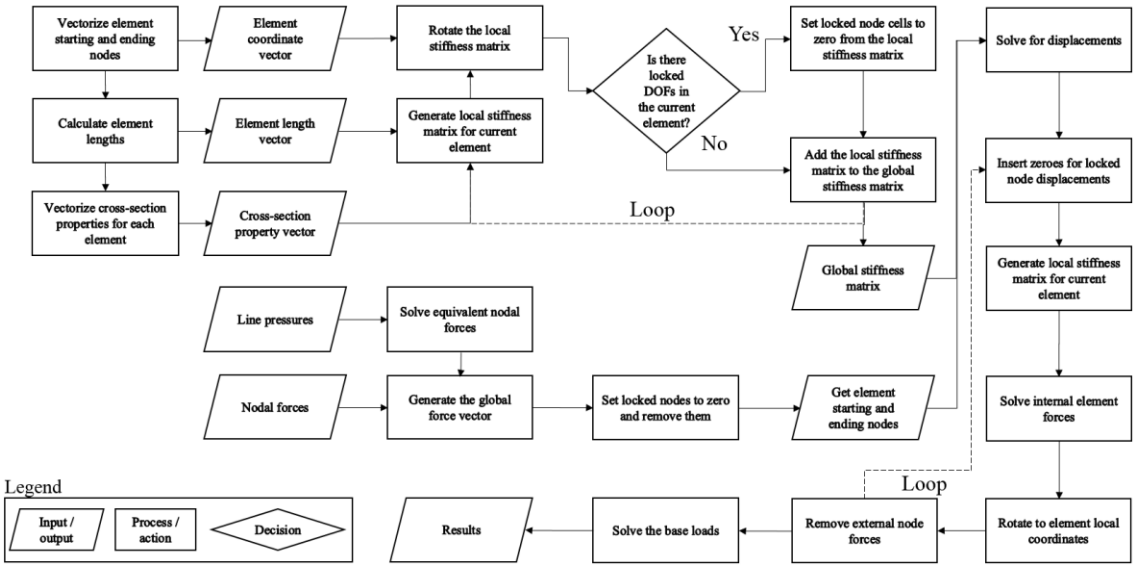

Figure 35: FEM-solver workflow

The general workflow of the FEM-solver is following: Loop through elements to create the global stiffness matrix, generate the global force vector, solve the global displacements, solve the internal loads and additionally solve the base loads.

As mentioned, this phase of the calculation is autonomous and the user has only a little control of what happens inside the FEM-solver. The only effect achievable from the user-interface is the number of elements used for each of the members. This option, however, has a possibility to significantly alter the results and cause error if inadequate number of elements is used. The problem with small element counts is the fact that the loading is analyzed only effectively on the nodes. If the maximum deflection was to occur between nodes, it would not show in the finite element model not containing a node there. While there are numerous mathematical methods available to aid in this problem, it is easier to solve by simply increasing the number of elements.

To gain understanding on the number of elements per member needed for accurate representation of the frame structure the results were compared with different element counts. Initially a randomly selected frame structure was analyzed with 100 elements per member resulting in a reference set of maximum utility ratios. Then the number of elements was gradually decreased and the results logged. When the results are compared to the reference values, the following graph of result variation can be plotted. See Figure 36.

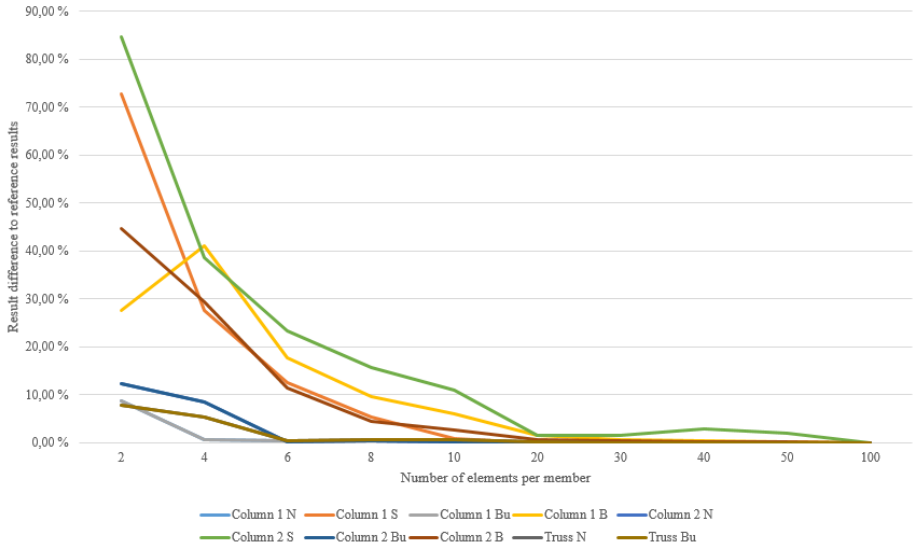

Figure 36: Effect of number of elements per member to the result accuracy

As the figure shows, the results start to converge when the element number reaches 20 elements per member and there is no significant improvement after that point. The average difference between maximum force reactions with 20 elements per member and 100 elements per member is only 0.42 %. The peculiar increase in second column shear load utility ratio is most likely caused by exceedance of a reduction limit and therefore decrease in design resistance value.

5.2.6 Solver algorithm

The solving algorithm has two distinctive parts:

- Automatically updating real-time calculation
- Manual on-demand calculation sequence

Automatically updating real-time calculation refers to the geometries, masses, pressures, temperatures constantly changing based on user input. The dependencies of these attributes are constantly in place, for example, when the user increases the number of fields, the collecting plate mass is corrected for the newly added field. This in turn increases the available plate area for ash congregation and causes an automatic increase in the live load caused by the ash. The methodology used within these automatic calculations are considered in their respective Chapters 5.2.1, 5.2.2 and 5.2.3

The on-demand calculation sequence contains the operations taking place when the user presses calculate. The main components of this calculation sequence are setting up the finite element model respectively for each of the portals, running the solver with the user-defined options, processing, and displaying the results. In this chapter, we focus on the overall solving algorithm disregarding any functional details addressed in the earlier chapters. The solver workflow is provided on a general level as a flowchart in Figure 37.

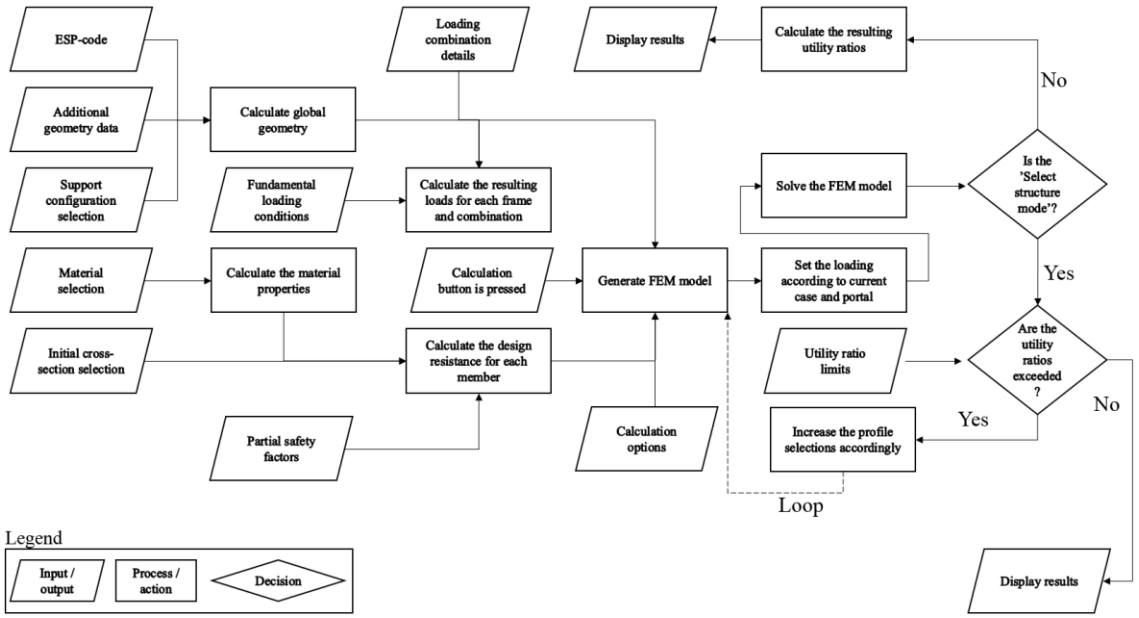

Figure 37: The general solver workflow

The part where utility ratios are calculated incorporates acquiring the CSC of each of the finite elements and then comparing the corresponding plastic or elastic resistance values to the actual loads. Only the maximum utility ratios occurring throughout the frames and loading combinations are compared to the user-defined utility ratio limit. If the limit is exceeded within any of the elements, the corresponding structural element profile is increased, which causes automatic re-evaluation of all the linked properties of the mathematical model. The whole FEM-model is then re-generated and the system loops through this sequence until the utility ratio no longer exceeds the limit. The automatic logging of calculation data results in a situation where the tool knows the maximum utility ratios for each of the members against all the loading types. The stored data also includes information at which loading case, which portal and which element this maximum utility occurred.

5.2.7 Results

While the amount of actual calculation data results in an accurate interpretation of the structure's response to loading and the severity of said loading, displaying everything is beyond unnecessary. The displayed results are limited to the bare minimum to promote usability of the product by not hiding the relevant information among the irrelevant.

All the results are displayed on the main page of the dimensioning tool, starting with the loading information transferred directly from the calculation details. The displayed loading information is shown in Figure 38.

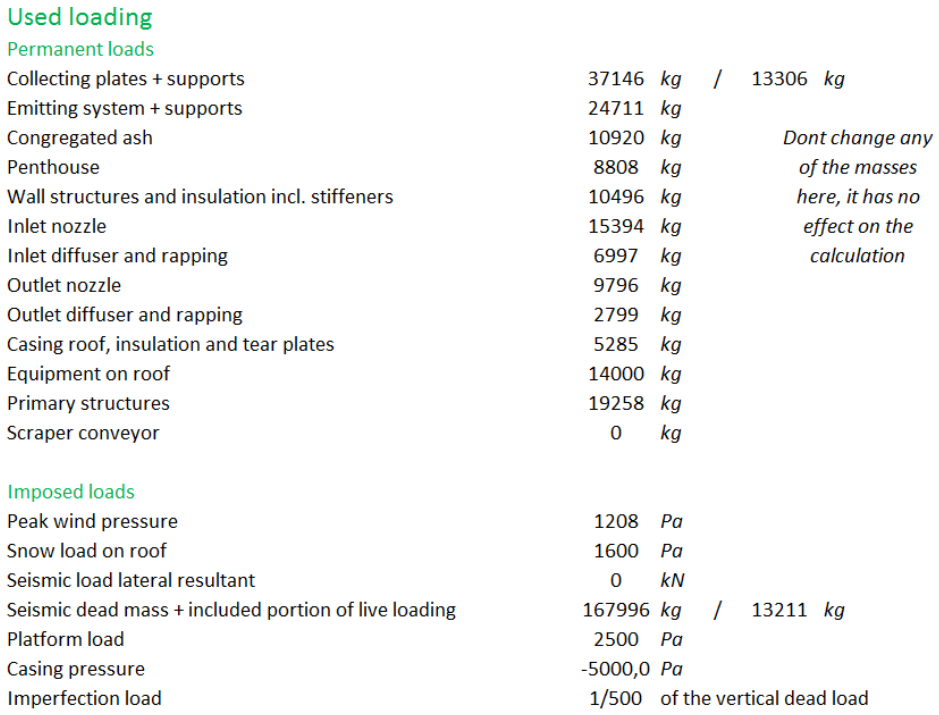

Used loading

Permanent loads

Collecting plates + supports	37146	*kg*	/ 13306	*kg*
Emitting system + supports	24711	*kg*		
Congregated ash	10920	*kg*		
Penthouse	8808	*kg*		
Wall structures and insulation incl. stiffeners	10496	*kg*		
Inlet nozzle	15394	*kg*		
Inlet diffuser and rapping	6997	*kg*		
Outlet nozzle	9796	*kg*		
Outlet diffuser and rapping	2799	*kg*		
Casing roof, insulation and tear plates	5285	*kg*		
Equipment on roof	14000	*kg*		
Primary structures	19258	*kg*		
Scraper conveyor	0	*kg*		

Dont change any of the masses here, it has no effect on the calculation

Imposed loads

Peak wind pressure	1208	*Pa*		
Snow load on roof	1600	*Pa*		
Seismic load lateral resultant	0	*kN*		
Seismic dead mass + included portion of live loading	167996	*kg*	/ 13211	*kg*
Platform load	2500	*Pa*		
Casing pressure	-5000,0	*Pa*		
Imperfection load	1/500	of the vertical dead load		

Figure 38: Displaying the loading information

All the loads here are self-explanatory. They are shown for easier backtracking of the dimensioning process and error checking. As mentioned earlier, the data accessible for user is for display only and miss-clicking on the front page does not mess up the calculation. In the next section, the primary profiles selected by the solver algorithm or by user are displayed with their maximum utility ratios (see Figure 39)

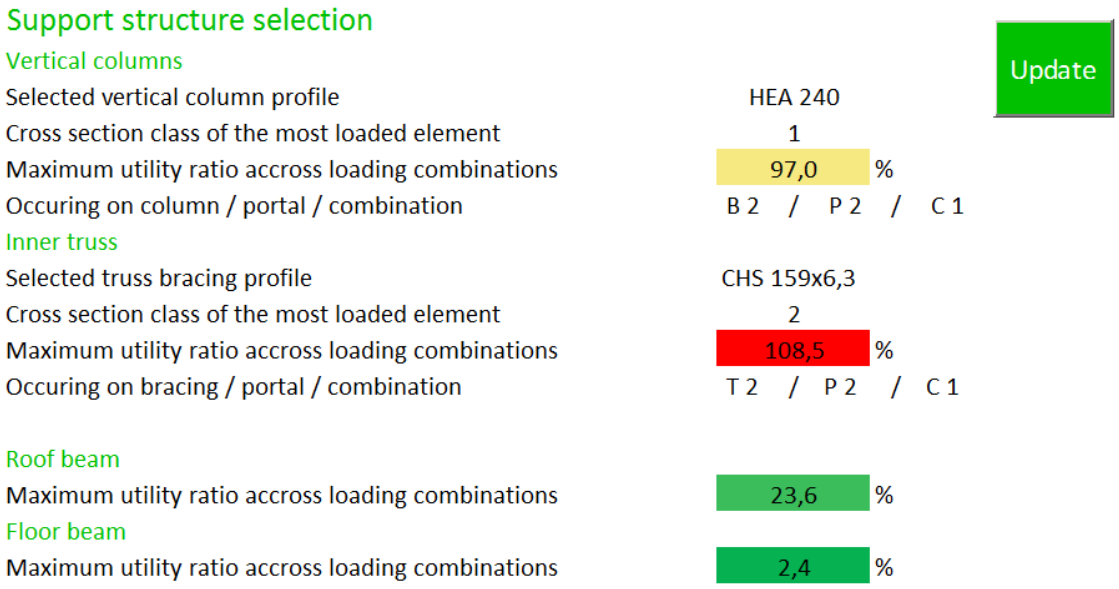

Figure 39: Displayed results

As seen from the previous figure, the CSCs of the most loaded elements are also included in the displayed results. In addition, the user is provided with the location of the most critical member within the casing structure. For example, in the previous figure, the vertical columns are loaded in the most critical manner on the second portal's latter vertical column, when load combination number one is considered. The latter column in this case means the column on the leeward wind side. Similarly, the most loaded inner truss member among all the frames is situated on the second portal's second bracing when combination number one is considered. Since the number of inner truss bracings changes depending on the user-defined truss configuration, the user is provided with configuration-dependent legend describing the numbering. The utility ratios are colored according to the user-defined limits so, that they turn red if the limit is exceeded.

Ultimately, the base loads acting on the connections of each of the portals are shown for all the loading combinations.

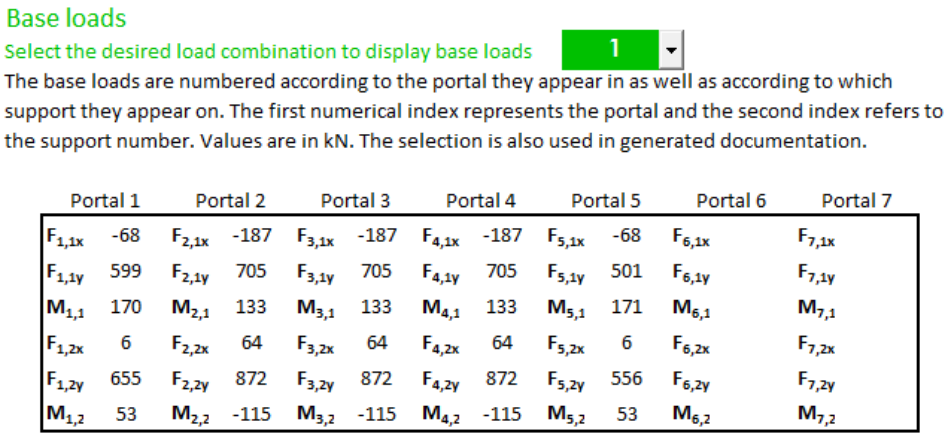

Figure 40: Displayed base loads

In the table displaying base loads all the portals are displayed in respective columns and the base load components for the selected loading case are shown next to their identifier. While some kind of visual representation of these results would be much more effective, they would slow down the tool in its normal operation.

5.3 Algorithms

As described earlier, the configurator tool includes two ‘modes’ of structural analysis. One being the so-called ‘Check structure’ -mode, which allows the user to determine the used profiles, and the loading after which the tool calculates the utility ratios for different members. Another mode is the ‘Select structure mode’, which picks the profiles according to user-defined limits of utility ratio. Utility ratio is the ratio at which the structural member is loaded when compared to its design resistance, utility ratio is considered in detail in Chapter 4.1.3. Even though the dimensioning task only includes two main variables, which are the vertical column profile and the inner bracing profile, there are still thousands of combinations to pick from. The geometries of the roof beam and floor beam are considered standardized due to the fact that they are welded sections, but the user has an opportunity to change their dimensions for either of the modes.

To effectively select the profiles for the structure so that all the utility ratios are under the specified limits there is a variety of different optimization approaches of varying level of complexity available. Due to the relatively simple nature of the dimensioning task and small number of variables, we can limit our optimization algorithms to simple methods. Before selecting the actual algorithm, however, we need to fully understand the dependency between the column profile selection and truss profile selection in terms of durability. In other words, “How should the search for optimal solution continue if we find out, for example, that the vertical column exceeds the maximum utility ratio?”

In order to understand the behavior of the system, a graphical sensitivity analysis was carried out. This analysis involved programmatically setting the dimensioning tool to loop through all the possible variable combinations and logging the resulting maximum utility ratio. When the utility ratio values are limited to those under one (100 % utility), we can create surface plot of the utility ratio as a function of vertical column profile and truss bracing profile. The results are shown in Figure 41 and Figure 42

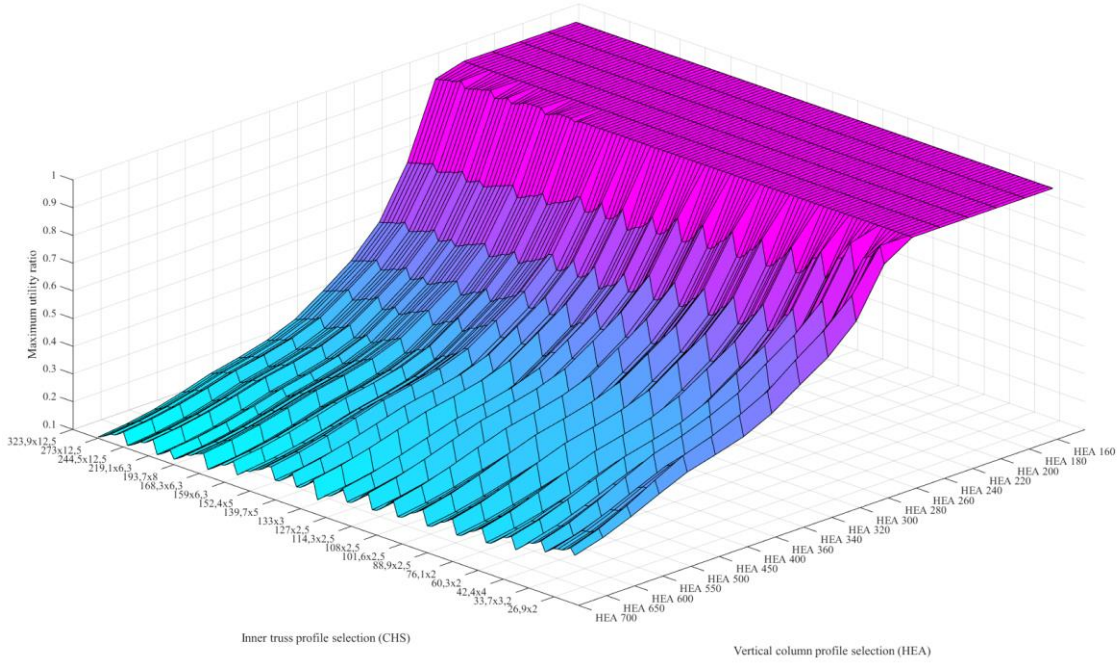

Figure 41: The development of the maximum utility ratio of the vertical columns

From the surface plot we can clearly see, that when the utility ratio of the vertical column is nearing the limit set to 100 %, the final step leading to sufficient utility ratio must always be increment in vertical column profile size. This is due to the fact, that the ridge of the surface is parallel to the axis containing the inner truss profile selection. This is a relieving remark, since it makes the decision-making logic to be incorporated straightforward; if the utility ratio of vertical column is exceeded, the solution is to increase the vertical column size and never anything else.

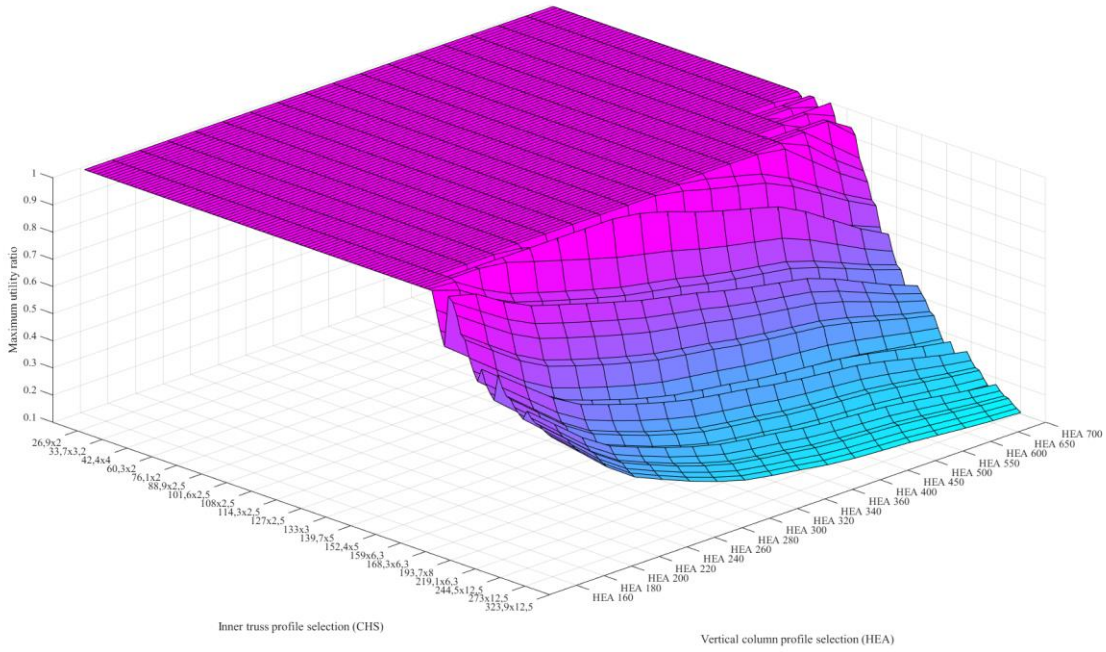

Figure 42: The development of the maximum utility ratios of the inner truss members

Similarly, to the vertical column profile, the inner truss utility ratio surface plot shows signs of being mainly dependent of inner truss profile selection. The independency is not as clear as it is with vertical columns, meaning that sometimes inadequate durability within truss bracing profile can be fixed by increasing the size of the vertical column. This occasional effect can, however, be neglected since inner truss members usually comprise of much less material than the vertical columns, meaning that it is cheaper to increase inner truss size. Therefore, we can treat the design variables independently and the optimization can be based directly to increasing the size of whichever profile exceeds the utility ratio limit. The waviness of the surface is the result of changes in the position and type of the most influential loading type e.g. when the vertical column is increased in size, sometimes the critical point of the inner truss shifts to another truss bracing. Another reason for such waviness is the fact that the order the profiles are listed and indexed in is not necessarily running from least durable to most durable.

Now that we know how to treat situations with exceeding utility ratios, we must select an approach to changing the variables. The most basic approach for the optimization task would be so-called naïve iteration. Naïve iteration is based only on the exceedance of the maximum utility ratio. If the maximum utility ratio is exceeded the corresponding profile is increased by one. This approach is obviously inefficient, since it does not account the level of exceedance or the rate at which we are approaching the control limits. What this means, is that even if it detects that the loading value on some structural member is exceeded for example thousand percent compared to the design value, it would still only increase the profile selection by one. The behavior and inefficiency of this method is illustrated in Figure 43, where the optimization process using naïve iteration carried out by the dimensioning tool is logged and visualized.

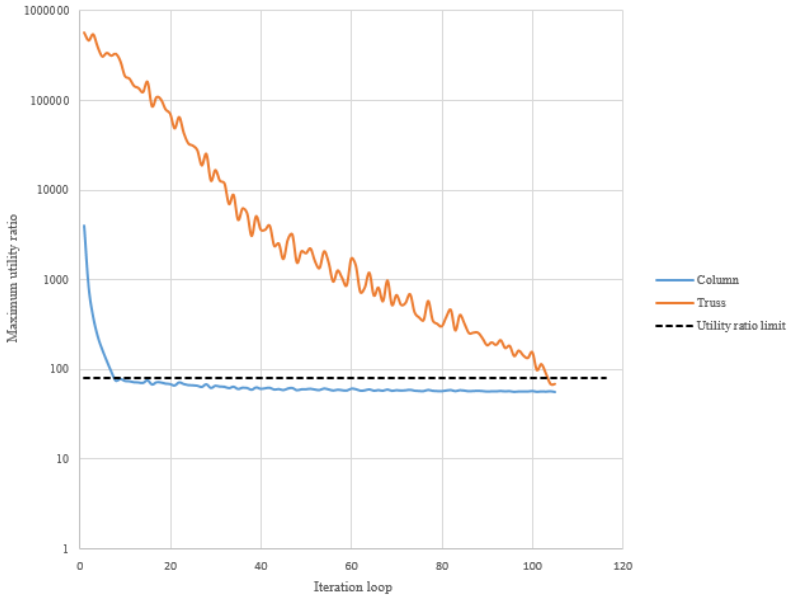

Figure 43: Development of maximum utility ratio of vertical column and truss bracing through optimization procedure with naive iteration

Another problem with naïve iteration is seen from the results of the Figure 43. The adequate column profile is found on loop number 9 and adequate truss profile on loop number 106. This results in the tool selecting a vertical column profile that is too robust. Aside from leading to inappropriate results, the naïve iteration is also slow, thus it was only used during the tool development process for its simplicity.

To enhance the optimization, we utilize a search algorithm called half-interval search. This algorithm is based on narrowing down the realm of possible solutions by splitting the solution space from the middle and then focusing on only the viable half. When the split is repeated enough times, we end up with a single value that is close to the target value. How close, is dependent of the user defined error criterion. For this approach to work, the variables, or in this case the available profile selection options have to be sorted from least durable to the most durable. For vertical column profiles, this is achieved by using the default order from HEA100 to HEA1000 but for truss bracing profiles we must sort the profiles according to buckling resistance.

With the half-interval search, the optimization procedure is drastically faster and simultaneously it becomes much easier to control the development of the utility ratios within each iteration loop and therefore avoid over-dimensioning the profiles. This is shown in Figure 44.

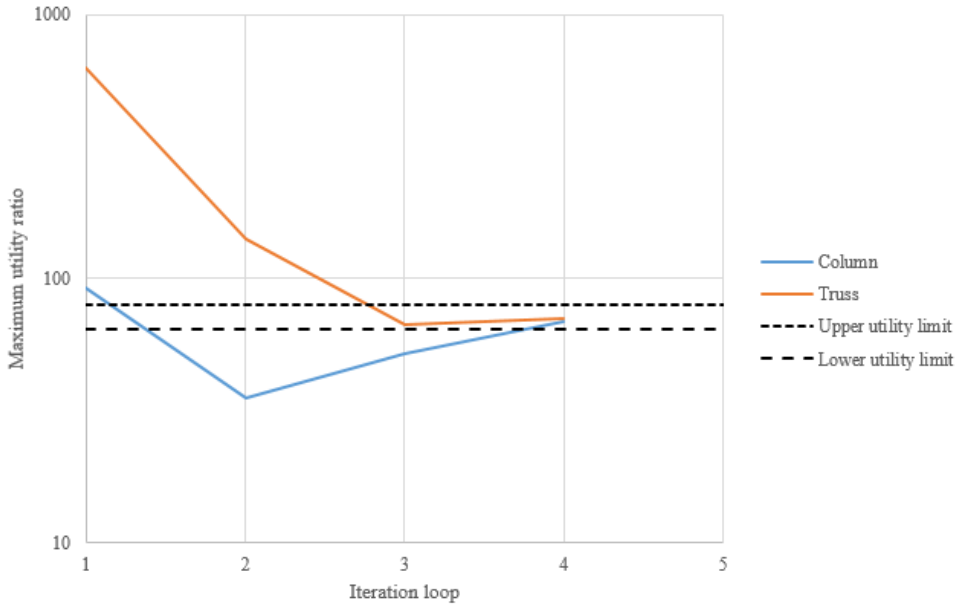

Figure 44: Development of maximum utility ratio of vertical column and truss bracing through optimization procedure with half-interval search

As seen from the figure above, the half-interval search reaches the optimal solution on fourth iteration and it is thus over 25 times faster than the naïve iteration in this example case. The efficiency depends largely on the limits we set for the utility ratio. The basic approach used by the dimensioning tool is to avoid any exceedance in the maximum utility ratio but when it comes to utility ratio being lower than the target utility ratio, we must

declare a tolerance for how much under the limit the utility ratio can be. A heuristic analysis shows that by allowing 20 % deviation under the utility ratio limit the tool finds a solution every time. Too small tolerance value results in an infinite loop.

5.4 Validation and verification

This chapter addresses the accuracy, validity and efficiency of the design tool created as a part of this thesis project. The accuracy is discussed from two different viewpoints; first, we compare the results provided by the FEM-solver to results provided by similar commercial software in Chapter 5.4.1 for verification. For validation, we compare the structures selected by the dimensioning tool to structures selected for past projects in Chapter 5.4.2 for validation. Since data about the dimensioning approaches used for existing structures is rather scarcely available this comparison is somewhat naïve. On the other hand, it is also an effective way of comparing the decisions made by the dimensioning tool to the reasoning of an actual design engineer. Ultimately, we assess the solve times for different problem types in Chapter 5.4.3.

The commercial products used for benchmarking are ANSYS Workbench 17, which is commonly adopted tool for structural analysis. ANSYS is considered one of the most advanced tools for structural analysis and its long history in the field of engineering makes it a viable reference point for analyzing the accuracy of the dimensioning tool. For thorough benchmarking results, we additionally use Ftool 3.00, which is a simple, yet powerful structural analysis tool for planar structures which uses a similar finite element model for solving structure response as the dimensioning tool.

5.4.1 Finite element model accuracy

In order to obtain thorough comparison of calculation accuracy we select two different inner bracing configurations so that the first one is typically used for narrow casings and the second one is more common with wide casings. This is done to detect any inconsistency in the error between them. Additionally, we apply loading to the model so, that light, moderate and high loading is considered and compared to commercial products. These loading states are achieved by first defining the loading state to represent a randomly selected design situation and then using the ‘select structure’ mode and setting the target utility ratio to 20 % for light loading, 60 % for moderate loading and 100 % for heavy loading. This results in six different combinations of vertical column profiles and truss bracing profiles.

The two different inner bracing configurations are presented in Figure 45. Historically, these two configurations appear to be the most commonly used, the one labelled with (a) for narrow casings and the one labelled (b) for wide casings.

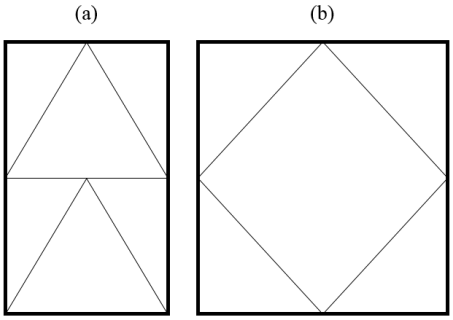

Figure 45: Truss bracing configurations used for FEM-model benchmarking

The attempt is to recreate actual loading situations so, that the external loading remains the same but changing geometry affects the resulting internal forces. For the first configuration, we use standard HEA beam for floor beam as it is only opposed to gravity due to fixed base, and for the latter the profile is changed to custom welded section, since much more resistance is required to bear the loads transferred by the bracings. Details about the loading used in the benchmarking case are trivial, since its inducers are not changing with the profile selections. As explained earlier, we achieve the different loading 'levels' by using different profiles for structural members. The loading and structure details used for benchmarking are provided in Appendix C.

When the 'select structure' -mode is run in order to select the profiles used for benchmarking, the following profiles get selected by the dimensioning tool:

Table 10: Structure configurations for FEM-benchmarking

Configuration	Loading	Utility ratio limit (%)	Maximum utility ratio (%)	Vertical column	Truss bracing
(a)	**Light**	20	17,9 / 12,8	HEA 550	CHS 244,5x8
	Moderate	60	52,6 / 54,3	HEA 300	CHS 168,3x10
	High	100	99,3 / 90,8	HEA 240	CHS 159x6
(b)	**Light**	20	19,4 / 19,4	HEA 900	CHS 323,9x8
	Moderate	60	55,8 / 54,8	HEA 340	CHS 219,1x12
	High	100	93,9 / 94,3	HEA 280	CHS 193,7x10

These structures were evaluated using the 'Check structure' -mode and the results of the finite element analysis were compared to the commercial software equivalents. To reduce the massive amount of comparison data available, we limit the comparison to the maximum load values on each structural member and the resulting base loads on the supports. The maximum loading is obviously the most critical calculation detail to get right.

When the structures (a) and (b) are opposed to same external loading with the dimensioning tool, Ftool and ANSYS and the results are compared, the following chart can be composed. The Figure 46 represents the percentage at which the individual maximum internal

load values for each member given by the dimensioning tool vary from the same values given by the commercial alternatives.

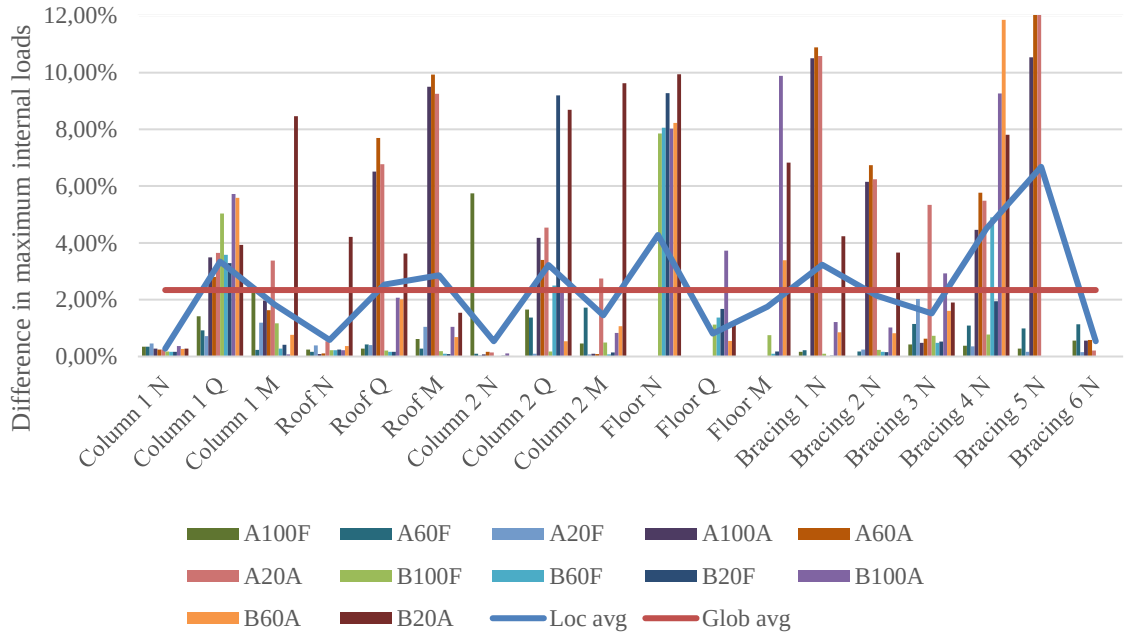

Figure 46: Variation in results given by the dimensioning tool and similar commercial software

The comparison is done with the absolute values of the resulting forces, so all the percentages are positive. On the horizontal axis the different load types for each of the frame structure members are listed so that the windward column is appended with one and the bracing numbering starts from upper-left corner and runs clockwise. The histogram bars on the horizontal axis represent the *difference* in the maximum values of that particular load when it is calculated with the dimensioning tool and with the commercial alternatives. The bars are colored so, that those labelled with the prefix A represent the configuration (a) and bars labelled with the prefix B represent the configuration (b). The number after the initial prefix mark the loading 'level' of loading with the number being the maximum utility ratio of that level. Ultimately the suffix marks the comparison opponent used F for Ftool and A for ANSYS. The two lines represent the local average error and global average error.

The deviation in the results between different software is moderate. Global average error in maximum loading values between the dimensioning tool and both of the reference structures is only 2.34 %. When looking at the bars exceeding the local average in value, one notices that the highest variations between results are related to the results calculated with ANSYS. The difference between the dimensioning tool and ANSYS results is 3.53 % on average when it is only 0.99 % between the dimensioning tool and Ftool.

The reason for the larger result difference with ANSYS is that it calculates the cross-section properties based on the section geometry without leaving ability to change them.

The dimensioning tool uses properties based on literature taking the whole section, for example the radius between the web and the flange, into account. This matter doesn't affect the Ftool results since its results are calculated based on user-provided cross-section properties. Additionally, ANSYS might use different formulation for the beam element, such as Timoshenko beam element, which is slightly more accurate for high beams than the Euler-Bernoulli beam element the dimensioning tool incorporates. Most of the deviation between Ftool and the dimensioning tool results is caused by the fact that the Ftool only accepts location coordinates on 10 mm intervals whereas the dimensioning tool uses floating-point coordinates.

It is evident, that a chart displaying such a large amount of data makes it hard to get a clear view of the accuracy related to individual results. These results are also heavily affected by static error. What this means, is that if there exists a member with numerically small load, for example 2 kN, then a static error of 1 kN causes 50 % deviation. To get a better understanding of the actual *effects* of the deviation, we incorporate a comparison of the actual numerical value of the error to the design resistance of the used section profile. In other words, we find out what is the risk that an error related to the finite element method causes wrong estimation of durability. The results of this comparison are displayed in Figure 47.

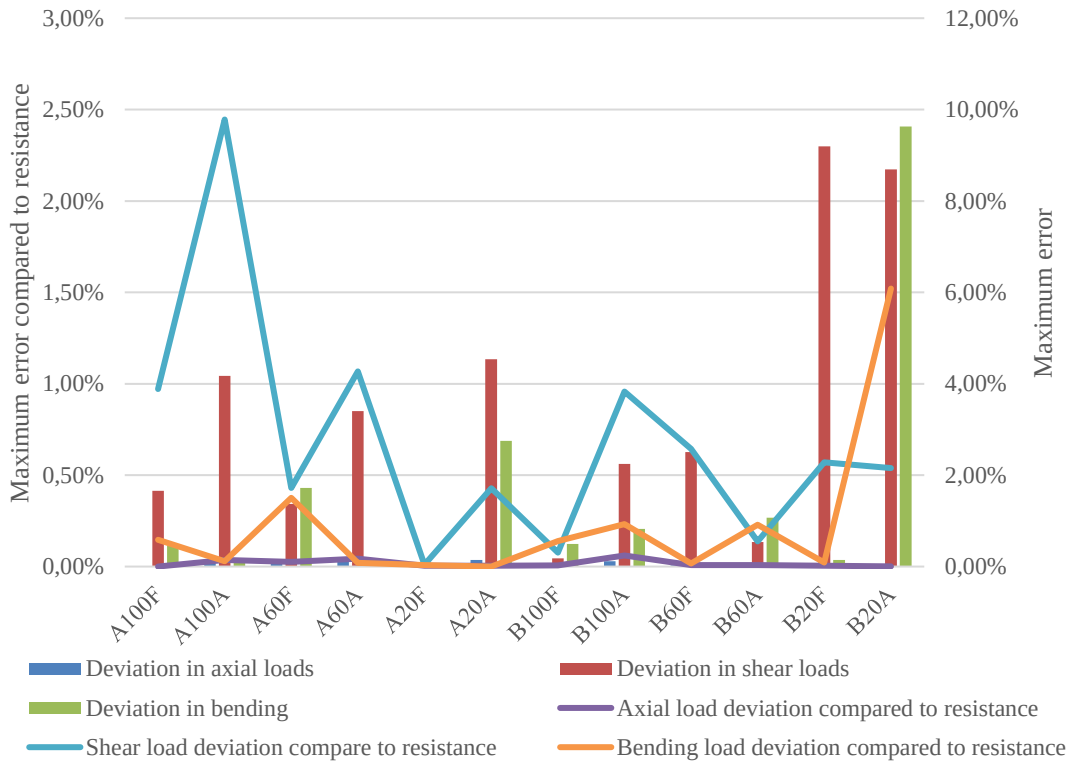

Figure 47: Comparison of the latter vertical column internal load values across software

The histogram bars contain the same error values displayed in the Figure 46 containing the error percentages for all the members. Contrary to the earlier visualization, the horizontal axis now contains the different test cases labelled similarly to earlier. The lines represent the ratio of the numerical error value to the maximum load resistance of the beam section used for that case has for that load type. The line values are displayed on the primary vertical axis on the left and the bar values are represented on the secondary vertical axis on the right. For an example of interpretation, we select the two cases containing the extreme values: A100A and B20A.

The A100A case uses a HEA 240 beam profile for the latter vertical column. The highest error is related to the maximum internal shear load value, which is 4 % higher according to the dimensioning tool than according to ANSYS. When we compare this error to the profile's plastic resistance for shear load, which is 261 kN while the numerical value of the error is only 4.28 kN we get 2.5 % error compared to the resistance value. For B20A the used vertical beam profile is HEA 900. The highest error is now related to the maximum internal bending load value, which is 9.6 % lower according to ANSYS than according to the dimensioning tool. When we now compare the numerical value of the error in internal bending moments, 33 kNm, to the bending resistance of the profile used, 2216 kNm, we get a relative error of only 1.5 %. What this proves, is that many of the larger absolute error values prove to be uninfluential when compared to the actual load limits, especially with larger profiles.

When this remark is combined with the apparent fact that the cases with lower utility ratios and thus generally larger profiles seem to contain relatively larger absolute error (see Figure 46), we can deduce, that generally the error related to the FEM-solver is insignificant when it comes to the dimensioning calculations carried out by the tool. Similar analysis comparing maximum error to the resistance value of profiles used for the rest of the internal loads presented in Appendix D.

In addition to the maximum member loading resultants, the base loads were compared across platforms as well. The deviation is presented similarly to the previous chart in Figure 48.

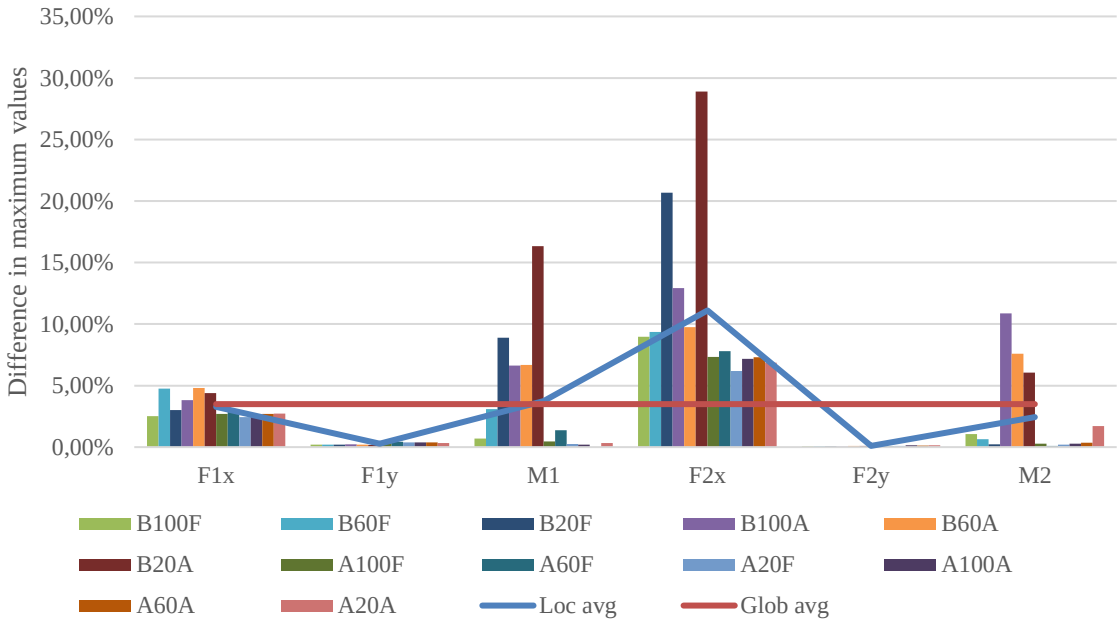

Figure 48: Variation in calculated base load components with the dimensioning tool and commercial software

The base load variation is, similarly to earlier, higher with ANSYS (4.26 % vs. 2.73 % with Ftool) and most likely due to same reasons as earlier. The base load variation is also moderate, as the average absolute error is 3.49 % across platforms. On average, the base load values seem to be on the conservative side with the dimensioning tool so, that Ftool values are approximately 0.3 % smaller and ANSYS values approximately 0.7 % smaller. The same does not occur with the averages of the maximum member loads, but generally, these averages are within 0.1 % radius of each other.

5.4.2 Result consistency

In this chapter, the differences in design selections made by the dimensioning tool and actual structural engineers are compared. As mentioned earlier, this approach is somewhat naïve due to the limited availability of the design rationale behind the selections, but then again offers a good insight on the relation between the two. For this comparison, we used global utility ratio limit of 80 % and utilized the tool-defined approximate dead loads to gain additional understanding of their accuracy. It is to be noted, that this comparison is heavily affected by the fact, that some of the loading data used when designing the reference products was unavailable. This unavailability of information, however, enables one to effectively estimate the results the tool gives even when loading information is preliminary.

For the purpose of this comparison, four already existing products were selected in an attempt to represent the most common ESP types and casing geometries. The geometry data was given to the tool according to the existing dimensions and loading values were

based on regional data and estimates as well as the tool-provided rudimentary mass values. Both of the design variables were selected with the dimensioning tool and then compared to the existing ones. The results are shown in Table 11.

Table 11: Result comparison with historical data

	Support	Reference	Own	Utility with reference
5-field narrow ESP	Column	HEA 300	HEA 280	57,6
	Bracing	CHS 168,3x6	CHS 168,3 x 10	87,6
5-field wide ESP	Column	HEA 320	HEA 400	82,3
	Bracing	271,41x5	CHS 244,5x8	70,9
2-field narrow ESP	Column	HEA 260	HEA 280	88
	Bracing	CHS 168,4 x 5	CHS 133x4	34,9
4-field wide ESP	Column	HEA 400	HEA 450	81,1
	Bracing	CHS 273 x 10	CHS 276 x 6	52,1

The table includes the reference profiles used in the existing products and the profiles the dimensioning tool selected. In the last column are listed the utility ratios resulting when the 'Check structure –mode' was run with the reference profiles. This helps one understand the level of difference between the dimensioning tool and a design engineer.

As seen from the result table, none of the selections are exactly same, but they are close. The differences could stem from numerous factors such as differences in mass evaluation, as the tool uses averaged historical data to acquire the used masses. Similar error is caused by the differences in used imposed loading. The used values are based on location data only, as there could be some undocumented factors causing increase or decrease in the loading data used when designing the existing ESP. Additionally, there could be differences in used allowable utility ratios between different projects. Some of the casings may have been designed by using 100 % utility as the limit, while in this test we set the limit to 80 %.

One of the error-inducers with the most room for improvement is the error-limit of the half-interval search. The error-limit determines when the utility ratio is close enough to the desired value, in this case 80 %. The error-limit is defined as a constant percentage, for example, the tool considers that requirements are fulfilled if the utility ratio is under the set value, but within 20 percentage units of it. Too small error limit value could possibly cause infinite loops when there are no such profiles available that result in a utility ratio between the upper and lower limit. This occurs if the smaller profile is too weak and the next bigger one falls below the lower limit. This on the other hand results in the need of setting the error limit large enough which then again may result in selection of too robust profiles. This phenomenon is best seen within the 5-field wide ESP test case. The tool selects a much larger profile (HEA 400) than the existing product has even though, the calculation with HEA 320 only results in slight exceedance in the 80 % set limit for

the utility ratio. HEA 340 would be more than sufficient but it never gets selected, because the tool tries the HEA 400 profile first and finds that it falls within the error limits. This issue could be addressed either by including a dynamic error limit which would change depending on the iteration loops or by just bearing in mind that this issue could arise and therefore checking the neighboring profiles for adequacy if the tool selects a profile with really low utility ratio.

Generally, the validation test provided great results. The selections made by the dimensioning tool do not seem to be always larger nor always smaller than in the existing products. This suggests that the differences are related to the uncertainties in the loading values rather than incorrect dimensioning calculation. The fact that the tool reached such level of similarity in selections compared to references indicates that the dimensioning calculations can be carried out surprisingly well even with minimal knowledge of the actual loading data.

5.4.3 Solve time

The key factors affecting solve time are the number of elements per member the user chooses to use, number of different loading combinations the user wants to analyze and number of fields in the casing being analyzed. The effect is most clearly seen when using the 'Select structure' mode with multiple loading combinations, since the program loops through all the portals of all the loading cases by nature even though one might be clearly more critical than others might.

To incorporate data about the effects different decisions have on solve time, the times are logged with different solving parameters. The number of elements per member is set to 20 in accordance to the analysis carried out in Chapter 5.2.5. The solve times are presented in Figure 49.

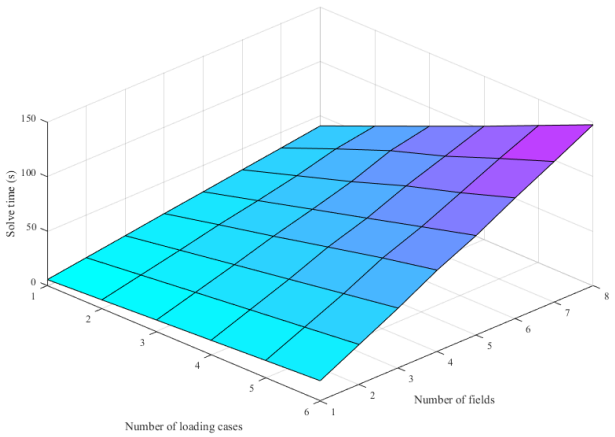

Figure 49: The effect of field amount and number of different loading cases to the solve time

It is evident that increasing either of the parameters increases the solving time. Similarly behaving solve times occur with the ‘Select structure –mode’, since the workflow is practically the same as with the ‘Check structure –mode’ but iterative.

While generally, a solve time of 160 seconds for 6 fields and 6 loading combinations is completely acceptable for a program that can be even run on the background, there is room for optimization. The main bottleneck is the platform itself. The problem with Excel is that combining sheet operations and VBA causes unavoidable inefficiency. The sheet operations involved in calculating the resulting loads and geometry are constantly updating on the background while the solver runs. They could be turned completely off programmatically but that is not an option since we need some of them when looping. This is an application problem unavoidable due to the approach used. The only available option to even remotely keep using Excel and avoid the dragging caused by the sheet operations would be carrying out all the operations using VBA. This would result in a drastic increase in required amount of coding and would most likely make Excel obsolete for the task.

Another significant aspect of optimization would be defining rules for the reasoning used when searching for the most critical members. In its current form, the tool analyses every portal loaded with all the possible loading combinations. In addition to this, the cross-section classes and reduced loading limits are analyzed individually for each element according to its respective loading state. While this is inefficient resource-wise, it is a fail proof method of assuring that the most critical element is eventually found and analyzed within all the structural members. To make the dimensioning tool work faster there could be a much more sophisticated algorithm to deduce which portal and loading combination is the most loaded one. With this information, the solver could be run for the single most critical combination only solving for the most critical frame portal.

6. CONCLUSIONS

This thesis project resulted in a configurator tool for the preliminary design of an ESP casing. The tool is able to calculate the loading the casing is opposed to in accordance to Eurocodes with only minimal input from the user. The user-interface for loading inputs is configured in such manner that the tool can suggest or automatically calculate values for the inputs user doesn't have. This is done while still allowing the user to use arbitrary input values should he wish to do so.

With the loading state analyzed, the tool successfully utilizes an approach of dividing the 3D casing structure to planar portal frames and uses 6-degree-of-freedom Euler-Bernoulli beam elements to solve the structure's response to loading. The selected platform motivated us to look into alternatives to the direct inverse which was largely inefficient when using Excel. It was found that the set of linear equations related to the finite element model can be solved drastically faster by utilizing so-called Cholesky decomposition algorithm.

When the structure's response has been solved, the tool uses limit state design approaches provided by the Eurocode to calculate the design resistance values for different parts of the structure. Different nominal resistance values are reduced according to cross-section class of the member as well as excessive shear and axial loads. These design resistance values are then compared to the occurring loads in order to compute the utility ratios.

The tool has two solving approaches, one selecting a structure according to user defined maximum utility ratio and another checking the user provided structure against the loading taking place. The 'Select structure' -mode utilizes a simple binary search algorithm which proved to be drastically faster than the originally selected naïve iteration.

The end-product was benchmarked extensively with different structure configurations and member profile selection to find any inconsistencies compared to commercial software (ANSYS and Ftool). The FEM-solver proved to operate accurately when benchmarked with an average difference of 3 % in ultimate load values. The tool in general proved to select structures similar to ones designed by actual engineers. The variation can be considered surprisingly small given that the loading circumstances were unclear and most of the loads were based on approximations using historical data and estimates of the possible loading taking place.

The benchmarking results kept in mind, the project proved to be very successful in fulfilling the initial need for automated design tool for the casing structure.

7. DISCUSSION AND FUTURE WORK

Whereas existing configurators often focus on product properties and linearly scale different dimensions to fit the needs of mass-customization in industrial applications. This thesis project provides an overview on product configurators incorporating structural analysis. From company's point-of-view, this is a first step towards automatized mass-customization.

Similar to most of development projects, the primary focus keeps shifting throughout the life cycle of the project. Within this project, the initial problem placement kept evolving, as the author grew more aware of the expanse of the design situation. The original tool specification proved to include conflicting property requirements, which made this project both interesting as well as challenging. The surprisingly complex nature of the design process should have been thoroughly mapped before any tool development took place.

Initially, the platform used, MS Excel, was selected to bring easy access to all the users and furthermore to make use of the author's earlier experience with said platform. The versatility of MS Excel with its easy interconnecting with other software is a major advantage, but the lack of computing capabilities of actual calculation software limited the use of complex solving methodologies such as non-linear models. Excel is a versatile tool when it comes to spreadsheet operations, but it is not made to handle long, streamlined calculation processes. Moreover, the programming process of solvers, user-interfaces and result visualization would have been drastically easier with ready-made mathematical toolboxes available in, for example, MATLAB. Keeping this in mind, Excel is however easily accessed. It has great interconnectivity with other software and it is more than suitable for preliminary design processes such as this one, if the approximate nature of the calculations is acknowledged.

Another major difficulty faced was the different knowledge levels of intended user-groups. The attempt to serve both the sales team and design engineers with the calculation tool proved to be tricky, because the tool had to have an example or suggestion for most of the values used in the design. The user interface had to be formulated so, that there is not much room for error and the tool was as clear and usable as possible. In practice this meant that numerous layers of data-validation had to be added to the user-forms making up the main user interface. All in all, the number of lines of VBA-code added up to 6869 lines. The distribution of the amount of code required for different task is shown in Figure 50.

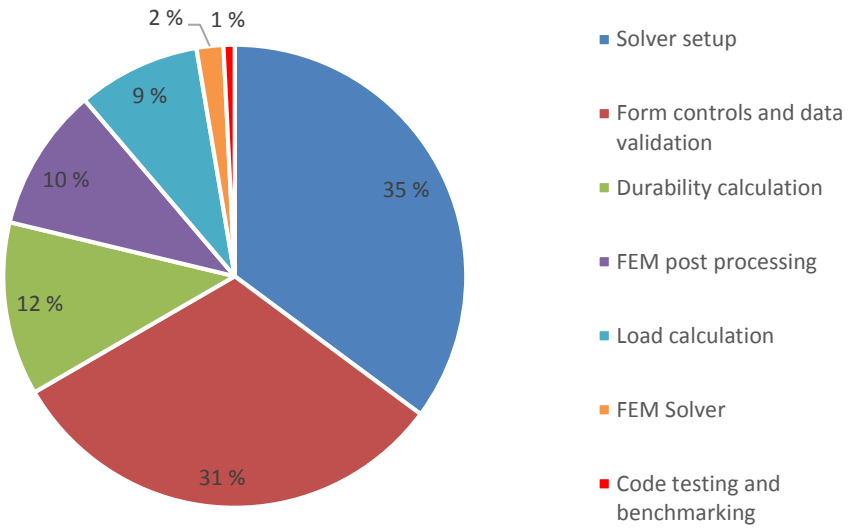

Figure 50: Distribution of code required to achieve different tool functions

Most remarkably, the pie chart shows that almost one third of all the code was related to controlling the user-forms which meant basically moving data around from the worksheet to the form and back in right places while simultaneously restricting user from inputting wrong kind of values. While this is something one cannot avoid with other platforms either, it is surprising that such a large amount of coding work went to something, that has practically nothing to do with the dimensioning task. It is to be noted, that the grand total of almost 7000 lines is by no means made by a professional software developer, so there is likely much room for improvement. But even with efficient coding, the distribution should remain similar to what is shown here.

Future similar projects should include an early-on scope declaration with comprehensive analysis of computational power needed to use the design approaches selected. The early phases should also include accurate listing of different structural details included in the calculation scope and the selected approach on designing them. Moreover, the group in charge of developing the tool should be cross-disciplinary to utilize the most knowledge of both the structural engineering point of view and computational approaches.

From a future perspective, regardless of the used platform, the next step would be incorporating the third dimension in the mathematical model to be able to estimate the structure's response to multiaxial loading comprehensively and its behavior in transverse direction. The reason this model does not include the depth dimension of the planar primary structures is the beam-element's inability to effectively model shell elements. Large portion of the casing's transversal durability is due to the wall plates and therefore no accurate calculations can be carried out without incorporating them. Another benefit of adding the third dimension would be the ability to model the whole casing structure to reach a comprehensive representation of the structures behavior. The currently infinitely stiff

foundation of the casing could have stiffness properties based on the primary support structure underneath it.

After adding the third dimension to the structure models, the dynamic behavior of the structure and loading should also be studied. This would most enhance the seismic analysis, which is largely neglected with the static approaches due to the dynamic nature of said loading type. The evaluation of each of the loading type could easily be a subject to a complete new master's thesis. The effect of special circumstances such as environment and location, to the size of the loading could be further studied to acquire more accurate evaluation of the loading. A large proportion of the automatic structure mass analysis is based on historical mass data. This evaluation could be more accurate if the system was analyzed as a complete structure instead of a section.

The used linear calculation method does not allow us to exploit the plastic range of members under loading. Incorporating non-linear analysis and external, ready-made FEM-software to allow the local stresses to exceed the yield limit would likely provide the company with lighter solutions. On the other hand, utilizing the plastic deformations in building like structures, which pose a risk to humans in the event of collapse, is generally riskier than using only the elastic range. All these future work suggestions should however be always evaluated with the cost and benefits in mind. If we reach a minutely lighter solution with an analysis tool that took years to develop, the benefits diminish.

8. REFERENCES

[1] G. S. Mill and W. O. Milligan, "Electrostatic precipitator" *AccessScience*, McGraw-Hill Education, 2014.

[2] SFS-EN 1993-1-1 Eurocode 3: Design of steel structures, Part 1-1: General rules and rules for buildings. Helsinki: Finnish Standards Association, 2006, p. 99.

[3] T. Salmi & K. Kuula, Rakenteiden Mekaniikka, Tampere: Pressus Oy, 2012, p. 463.

[4] A. Williams, Structural Analysis In Theory and Practice, Burlington: Elsevier Inc, 2009, p. 617.

[5] K.-J. Bathe, Finite Element Procedures, New Jersey: Prentice Hall, 1996, p. 1039.

[6] O. A. Bauchau and J. I. Craig, "Euler-Bernoulli beam theory" in *Structural Analysis*, Springer Netherlands, 2009, pp. 173-221.

[7] H. Marjamäki, "Teknillinen mekaniikka ja optimointi" 2012. [Online]. Available: http://webhotel2.tut.fi/mec_tme/mec_2430/palkki.pdf..

[8] K.-J. Bathe, Numerical Methods in Finite Element Analysis, New Jersey: Prentice Hall, 1976, p. 528.

[9] N. Willems and W. M. Lucas, Matrix analysis for structural engineer, Englewood Cliffs, NJ.: Prentice-Hall, 1968, p. 364.

[10] D. J. Dawe, Matrix and finite element displacement analysis of structures, Oxford: Clarendon Press XVIII, 1984, p. 565.

[11] O. C. Zienkiewicz, The Finite Element Method in Engineering Science, London: McGraw Hill, 1971, p. 521.

[12] J. E. Gentle, "LU and LDU Factorizations," in *Matrix Algebra Theory, Computations and Applications in Statistics*, 1st ed., G. Casell, S. Fienberg and I. Olkin, Eds., Springer Science+Business Media LLC, 2007, pp. 186-188.

[13] C. Haddad, "Cholesky Factorization," in *Encyclopedia of Optimization*, 2nd ed., A. F. Christodoulos and M. P. Panos, Eds., Springer US, 2009, pp. 374-376.

[14] T. H. Cormen, C. E. Leiserson, R. L. Rivest and C. Stein, Introduction to algorithms, 3rd ed., Cambridge: The MIT Press, 2009, p. 1292.

[15] R. Hunger, "Floating Point Operations in Matrix-Vector Calculus," Technische Universität München, Munich, 2007, p. 16.

[16] S. Pohjolainen, J. Multisilta, K. Suomela, P. Häkkinen, S. Mäki-Turja, O. Perttula and K. Korhonen, "LU-hajotelma nauhamatriiseille," 1997. [Online]. Available: http://matriisi.ee.tut.fi/matrix/.

[17] SFS-EN 1990 Eurocode: Basis of structural design. Helsinki: Finnish Standards Association SFS, 2006.

[18] SFS-EN 1991-1-1 Eurocode 1: Actions on structures. Part 1-1: General actions. Densities, self-weight, imposed loads for buildings. Helsinki: Finnish Standards Association SFS 2002, p. 45.

[19] SFS-EN 1991-1-3 Eurocode 1: Actions on structures. Part 1-3: General actions. Snow loads. Helsinki: Finnish Standards Association SFS, 2003, p 57.

[20] P. Ongelin and I. Valkonen, Hitsatut profiilit EN 1993 -käsikirja, Keuruu: Otavan Kirjapaino Oy, 2010, p. 610.

[21] SFS-EN 1993-1-5 Eurocode 3. Design of steel structures. Part 1-5: Plated structural elements. Helsinki: Finnish Standards Association SFS, 2006, p. 54.

[22] T. Salmi and S. Pajunen, Lujuusoppi, Tampere: Pressus Oy, 2010, p. 462.

[23] SFS-EN 1993-1-2 Eurocode 3: Design of steel structures. Part 1-2: General rules. Structural fire design. Helsinki: Finnish Standards Association SFS, 2005, p. 81.

[24] SFS-EN 1991-1-4 Eurocode 1: Actions on structures. Part 1-4: General actions. Wind actions. Helsinki, Finnish Standards Association SFS, 2011, p. 255.

[25] J. Jalkanen, J. Tuori and E. Hömmö, "Teräsrakenteiden maanjäristysmitoitus," Helsinki, 2013, p. 24.

[26] SFS-EN 1998-1 Eurocode 8: Design of structures for earthquake resistance. Part 1: General rules, seismic actions and rules for buildings. Helsinki: Finnish Standards Association, 2005, p. 230.

[27] N. S. Armouti, Earthquake Engineering: Theory and Implementation with the 2015 International Building Code, New York: McGraw-Hill Education, 2015, p. 544.

[28] J. Tuori, Seismic analysis methods in structural design, Tampere: Tampere University of Technology, 2015, p. 88.

[29] A. Haug, L. Hvam and N. H. Mortensen, "Definition and evaluation of product configurator development strategies" *Computers in Industry*, 2012, pp. 471-481.

[30] D. Sabin and R. Weigel, "Product Configuration Frameworks - A Survey," *IEEE Intelligent Systems*, vol. 13, no. 4, 1998. pp. 42-49.

APPENDIX A – CHOLESKY DECOMPOSITION ALGORITHM IN VISUAL BASIC FOR APPLICATIONS (VBA)

```
Sub Cholesky()
'Deactivate screen updating to create neater outlook and to save resources
Application.ScreenUpdating = False
'Declare variables
Dim a() As Double, L() As Double, sum As Double, sum2 As Double, m As Long, i As Long, j As Long
Dim k As Long, Mat As Range, Order As Double
'Set the order to be one smaller than the size of the global stiffness matrix since the indexing
starts at 0 in VBA
Order = ThisWorkbook.Worksheets("Main").Range("Ksize") - 1
Worksheets("Global Stiffness matrix").Activate
'Populate the mat array from the worksheet
Set Mat = ThisWorkbook.Sheets("Global Stiffness matrix").Range(Cells(1, 1), Cells(Order + 1,
Order + 1))
Worksheets("Main").Activate
'Ensure matrix is square
If Mat.Rows.Count <> Mat.Columns.Count Then
    MsgBox ("Correlation matrix is not square")
    Exit Sub
End If
m = Mat.Rows.Count
'Change the array sizes according to the size of the global stiffness matrix
ReDim a(0 To m - 1, 0 To m - 1)
ReDim L(0 To m - 1, 0 To m - 1)
For i = 0 To m - 1
    For j = 0 To m - 1
        a(i, j) = Mat(i + 1, j + 1).Value2
        L(i, j) = 0 'Set the values above the diagonal to 0
    Next j
Next i
'Carry out the cholesky algorithm
L(0, 0) = Sqr(a(0, 0))
L(1, 0) = a(1, 0) / L(0, 0)
L(1, 1) = Sqr(a(1, 1) - L(1, 0) * L(1, 0))
For i = 2 To m - 1
    sum2 = 0
    For k = 0 To i - 1
        sum = 0
        For j = 0 To k
            sum = sum + L(i, j) * L(k, j)
        Next j
        L(i, k) = (a(i, k) - sum) / L(k, k)
        sum2 = sum2 + L(i, k) * L(i, k)
    Next k
    L(i, i) = Sqr(a(i, i) - sum2)
Next i
'Return the matrix to the workbook for further use
Worksheets("LLT").Activate
ThisWorkbook.Sheets("LLT").Range(Cells(1, 1), Cells(Order + 1, Order + 1)) = L
Worksheets("Main").Activate
'Move to the solver sub
Call SolveEqn
Application.ScreenUpdating = True
End Sub
```

APPENDIX B – THE LINEAR SUBSTITUTION ALGORITHM IN VISUAL BASIC FOR APPLICATIONS (VBA)

```
Sub SolveEqn()
'Declaring variables
Dim L() As Double
Dim Order As Integer
'Set order to one index smaller than the global stiffness matrix since the indexing starts at 0
Order = ThisWorkbook.Worksheets("Main").Range("Ksize") - 1
'Resize the arrays accordingly
ReDim L(Order, Order)
Dim b() As Double
ReDim b(Order)
Dim w() As Double
ReDim w(Order)
For i = 0 To Order
For u = 0 To Order
L(i, u) = ThisWorkbook.Sheets("LLT").Range("A1")(i + 1, u + 1)
Next u
Next i
For i = 0 To Order
b(i) = ThisWorkbook.Sheets("Main").Range("ForceVector")(i + 1)
Next i
Dim wTemp As Double
'Forward substitution
w(0) = b(0) / L(0, 0)
For i = 1 To Order
wTemp = 0
For u = 0 To i - 1
wTemp = wTemp - (L(i, u) * w(u))
Next u
w(i) = (b(i) + wTemp) / L(i, i)
Next i
'Backward substitution
Dim LT() As Double
ReDim LT(Order, Order)
For i = 0 To Order
For u = 0 To Order
LT(u, i) = L(i, u)
Next u
Next i
Dim x() As Double
ReDim x(Order)
x(Order) = w(Order) / LT(Order, Order)
For i = Order - 1 To 0 Step -1
wTemp = 0
For u = Order To i + 1 Step -1
wTemp = wTemp - (LT(i, u) * x(u))
Next u
x(i) = (w(i) + wTemp) / LT(i, i)
Next i
'Return the deflection vector
For i = 0 To Order
ThisWorkbook.Sheets("Main").Range("DeflectionVector")(i + 1) = x(i)
Next i
End Sub
```

APPENDIX C: DETAILS ABOUT THE FEM BENCHMARKING

Structure details	**Case 1**	**Case 2**
Number of fields	4	4
Nominal length	4500	4000
Collecting plate width	500	500
Plate spacing	300	300
Nominal width	9600	15000
Nominal height	12500	12500
Penthouse height	5000	7000
Base elevation	5000	5000
Plate thickness	1,3	1,3
Loading details		
Temperature	200	C
Pressure	5000	Pa
Snow load		
Snow load on ground	2	kN/m
Topography	Normal	
Exposure coefficient	1	
Shape coefficient	0,8	
Wind load		
Basic wind velocity	24	m/s
Air density	1,293	kg/m3
Exposure coefficient	0,8/-0,5	
Terrain category	1	
Approximate loads		
Casing roof	0,6	kN/m2
Penthouse roof	1	kN/m2
Walls and insulation	0,8	kN/m2
Inlet diffuser	0,5	kN/m2
Inlet funnel	1,1	kN/m2
Outlet diffuser	0,2	kN/m2
Outlet funnel	0,7	kN/m2
T/R-Unit	3500	kg
Live load		
Platform load on roof	2,5	
Platform ratio	80	
Ash density	300	kg/m3
Ash film thickness	5	mm

APPENDIX D – MAXIMUM ERROR OF INTERNAL LOAD VALUES COMPARED TO RESPECTIVE RESISTANCE VALUE

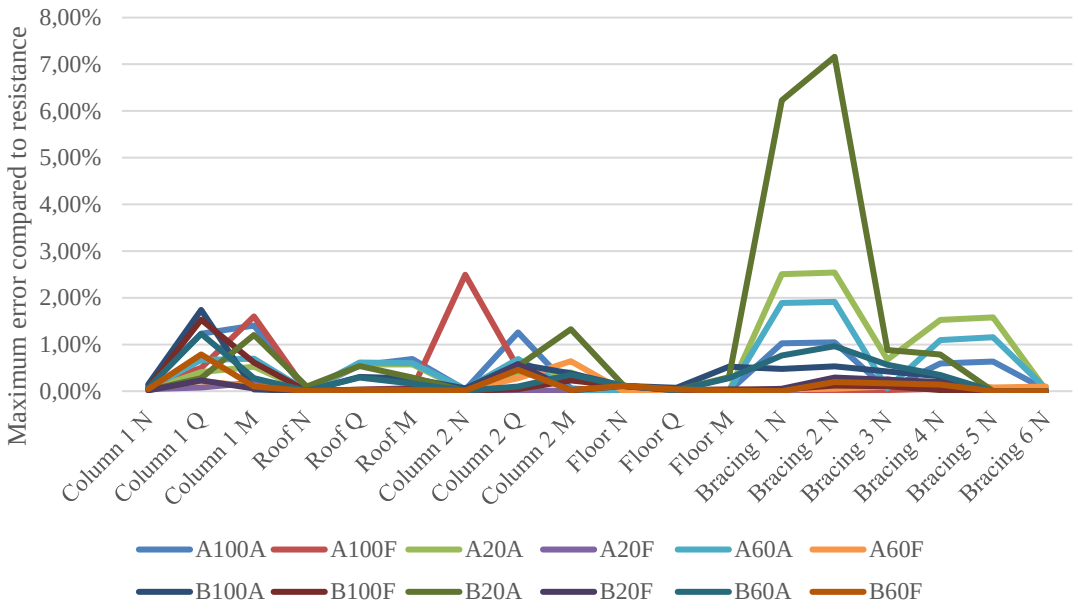

Figure 51: Relative error of internal loads